2021-08

Effects of a Pharmacological Activator of Ca2+-activated K+ Channels (KCa2/3) on Recovery from Acute Myocardial Infarction in Mice

Kim, Taeyeob

UNIVERSITY OF CALGARY

Effects of a Pharmacological Activator of Ca^{2+}-activated K^+ Channels ($K_{Ca}2/3$) on Recovery from Acute Myocardial Infarction in Mice

by

Taeyeob Kim

A THESIS

SUBMITTED TO THE FACULTY OF GRADUATE STUDIES

IN PARTIAL FULFILMENT OF THE REQUIREMENTS FOR THE

DEGREE OF MASTER OF SCIENCE

GRADUATE PROGRAM IN CARDIOVASCULAR AND RESPIRATORY SCIENCES

CALGARY, ALBERTA

AUGUST, 2021

Abstract

The goal of this project is to investigate the potential cardio-protective effects of a small molecule activator of endothelial $K_{Ca}2.3$ and $K_{Ca}3.1$ channel activity (i.e. SKA-31). Recent studies from our group have demonstrated that acute SKA-31 treatment improved agonist-evoked vasodilation in resistance arteries from multiple vascular beds and species, and this effect remains robust in arteries from Type 2 Diabetic tissues. Prolonged administration of SKA-31 to aged male rats also improved both their cardiac and vascular functions. In my research, I have hypothesized that enhancement of endothelial function by *in vivo* SKA-31 administration would improve recovery of the heart following an acute injury, such as myocardial infarction (MI). Experimentally, male mice (12-15 weeks of age, C57BL/6 strain) were subjected to surgical ligation of the left-anterior descending coronary artery to establish an acute MI. Sham surgeries involved all the same surgical procedures, except for the coronary ligation. Within 48 h post-surgery, MI and sham surgery mice were treated orally with either vehicle or 10 mg/kg of SKA-31 daily for 6 weeks. Echocardiography, Pressure-Volume (P-V) loop measurements and histological analysis were implemented to assess cardiac performance and structure, respectively, in each of the four treatment groups.

Myocardial damage in MI mice was confirmed by histological staining. Echocardiographic assessment of cardiac function 4 weeks post-surgery revealed that Ejection Fraction (EF), Fractional Shortening (FS), end systolic volume (ESV) and end diastolic volume (EDV) were similar in sham animals treated with either vehicle or SKA-31. In contrast, the MI animals treated with vehicle displayed ~50% decreases in EF and FS, and significantly larger values for ESV and EDV, compared with sham-treated mice. In addition, the MI animals displayed elevated EDPVR values of ~0.7 compared to ~0.3 observed in sham animals. This

finding indicates that the left ventricular wall is stiffer following infarction and strongly suggests the presence of diastolic dysfunction. However, no significant changes in other diastolic parameters, such as dP/dt_{min} and Tau, were detected in MI groups compared to the sham groups. These functional and structural parameters thus confirm the presence of sustained cardiac dysfunction in the MI mice. Treatment of MI mice with SKA-31 did not lead to improvements in EF, FS, ESV or EDV compared with vehicle treated MI animals. The results of my study show that a pharmacological intervention designed to enhance endothelial function did not significantly improve cardiac function in the setting of an acute injury. A potential confounding factor in this study is the possible effect of SKA-31 on the robust cardio-immunological responses in the post-MI heart, due to the expression of KCa3.1 channels within pro-inflammatory immune cells such as monocytes, neutrophils and macrophages.

Preface

This work was supported by research funding to Andrew P. Braun from the Canadian Institutes of Health Research and the Natural Sciences and Engineering Research Council of Canada. The experimental animal protocols used in this proposed study have been approved by the University of Calgary Animal Care Committee. Well-established and standardized experimental procedures have been used in this project with respect to the materials and equipment to ensure reproducibility.

Acknowledgements

I would like to begin by thanking my lab members, Dr. Ramesh C. Mishra, and Mr. O. Daniel Vera for their support throughout this project. I wish to show my sincere appreciation to Dr. Ramesh C. Mishra who helped me arrange and utilize the supplies needed in this project. Furthermore, I am also very thankful to Drs. Justin F. Deniset and Robert A. Rose who provided valuable advice and suggestions which synergistically helped me grow as a scientific researcher. Also, I am thankful to Dr. Yong-Xiang Chen for his support with histological analysis in this project. I wish to thank my supervisory committee members, Drs. Darrell D. Belke, Henry J. Duff and Vaibhav Patel for their time commitment and feedback. I would especially like to thank Dr. Darrell D. Belke for spending countless hours teaching me the invaluable skill sets involved in experimental and translational research. My deepest gratitude goes to Dr. Andrew P. Braun who has shown exceptional mentorship and has put in a tremendous amount of work into my project. Every time when I was encountered with challenges in my project, Dr. Braun provided insightful suggestions that allowed me to move forward with the project. I am very thankful to have his guidance and teaching throughout the study.

Dedications

My thesis is dedicated to my family, Cho Rog (Chloe) Kim, Joo Yeun Lee and Ki Moon Kim and my friends, Jungwoo (Brian) Woo and Hyunwoo (Henry) Ahn. All of these people have provided a tremendous amount of support throughout my study and I would not be where I am now without them.

Table of Contents

List of Tables

List of Figures

List of Abbreviations

AMI – Acute Myocardial Infarction

ANOVA – One-way Analysis of Variance

ANF – Atrial Natriuretic Factor

APD – Action Potential Duration

BD – Bowel Disease

BK_{Ca} - Large-conductance Ca^{2+}-activated K^+ channel

BPM – Beats Per Minute

$[Ca^{2+}]_i$- Intracellular Ca^{2+}Concentration

CABG – Coronary Artery Bypass Grafting

CCL – CC-chemokine Ligand

CCR – CC-chemokine Receptor

CHF – Congestive Heart Failure

CO – Cardiac Output

CRAC - Ca^{2+}-Release Activated Channel

CVD – Cardiovascular Disease

DAG – Di-Acyl Glycerol

DAMPs – Death-Associated Molecular Patterns

DCs – Dendritic Cells

dP/dt_{max} – Maximum Derivative of Change in Pressure Rise Over Time

dP/dt_{min} – Maximum Derivative of Change in Pressure Fall Over Time

EC – Excitation-Contraction

ECG – Electrocardiogram

ECM – Extracellular Matrix

EDH – Endothelial Derived Hyperpolarization

EDHF – Endothelial Derived Hyperpolarizing Factor

EDRF – Endothelial Derived Relaxing Factor

EDPVR – End-Diastolic Pressure Volume Relationship

EDV – End-Diastolic Volume

EF – Ejection Fraction

EKV – ECG-gated Kilohertz Visualization

eNOS – endothelial Nitric Oxide Synthase

ER – Endoplasmic Reticulum

ESPVR – End-Systolic Pressure Volume Relationship

ESV – End-Systolic Volume

FS – Fractional Shortening

GPCR – G-protein Coupled Receptor

hESC-CMs - human Embryonic Stem Cell derived Cardiomyocytes

HF – Heart Failure

HFrEF – Hearth Failure with reduced Ejection Fraction

HR – Heart Rate

HSPCs – Haematopoietic Stem and Progenitor Cells

IK_{Ca} – Intermediate-conductance Ca^{2+}-activated K^+ channel

IP_3 – Inositol 1,4,5-Trisphosphate

KO – Knock-Out

LAD – Left Anterior Descending

Ly6C – Lymphocyte Antigen 6C

LV – Left Ventricle

MACE – Major Adverse Cardiovascular Event

MEGJ – Myo-Endothelial Gap Junction

MI – Myocardial Infarction

MMPs – Matrix Metalloproteinase

NO – Nitric Oxide

PCI – Percutaneous Coronary Intervention

P_{dev} – Developed Pressure

P_{es} – End-Systolic Pressure

P_{ed} – End-Diastolic Pressure

PIP_2 - Phosphatidyl Inositol 4,5-Biphosphate

PLC – Phospholipase C

PM – Plasma Membrane

PRSW – Pre-load Recruitable Stroke Work

P-V loop – Pressure-Volume loop

PVR – Peripheral Vascular Resistance

RBC – Red Blood Cell

RMP – Resting Membrane Potential

SERCA - Sarcoplasmic-Endoplasmic Reticulum Ca^{2+}-ATPase

SK_{Ca} – Small-conductance Ca^{2+}-activated K^+ channel

SMC – Smooth Muscle Cells

SOCE - Store-Operated Ca^{2+} Entry

STEMI – ST-segment Elevation Myocardial Infarction

SV – Stroke Volume

TGF-β – Transforming Growth Factor beta

TLRs – Toll-like Receptors

TM – Transmembrane

TNF-α – Tumor Necrosis Factor alpha

TRPM4 - Transient Receptor Potential Cation Channel Subfamily M, member 4

T2D – Type 2 Diabetes

VEGF – Vascular Endothelial Growth Factor

Vm – Membrane potential

VSMCs – Vascular Smooth Muscle Cells

Chapter 1: Introduction

1.1 Overview

Cardiovascular disease (CVD) was the leading cause of death in the United States in 2017 and accounted for almost 860,000 resident deaths in that same year (Virani et al., 2020). In addition, CVD accounted for 14% of total US health expenditure in 2014 to 2015, more than any major diagnostic group (Virani *et al.*, 2020). Among these CVDs, Myocardial Infarction (MI) and Heart Failure (HF) were the major culprit, with an estimated annual incidence of ~605,000 new attacks and ~200,000 recurrent attacks (Virani *et al.*, 2020). Considering the computation based analysis of data from the Atherosclerosis Risk in Communities (ARIC) study of the National Heart, Lung, and Blood Institute (NHLBI), it revealed that approximately every 40 seconds, an American will have an MI (Givertz and Mann, 2013). This trend of elevating incidences of MI is now expanding on a global scale where the burden of CVD and Acute Myocardial Infarction (AMI) has shifted to low- and middle-income countries, which now accounts for more than 80% of deaths from CVD worldwide. (Murray et al., 2015; Murray et al., 2012). In 2016, it was estimated that ~600,000 Canadians were living with Heart Failure (HF) and in 2013, 45,600 hospital admissions were reported for Acute Heart Failure (AHF). (Gupta et al., 2021). However, the Canadian Cardiovascular Society has stated that current surgical approaches (e.g., stents, coronary artery bypass grafts) to correct MI-related damage are not totally effective, as evidenced by the high hospital readmission rates observed in these patients (Tran et al., 2017). Therefore, this information indicates a necessity for more refined approaches to mitigate the initiation and progression of MI including more effective therapeutic interventions.

MI-associated injury in the heart is characterized by necrosis of heart tissue due to the prolonged occlusion of a coronary artery that normally delivers oxygenated blood and nutrients to myocardium. Compromised blood flow to a region also prevents the proper removal of metabolic waste products. This reduction in blood flow leads to significant impairments of myocardial contractility and blood pumping activity, leading to elevated stress within the heart and the cardiovascular (CV) system. The severe form of MI can lead to acute cardiac arrhythmia/arrest which may cause situations where patients cannot be resuscitated. Therefore, immediate medical interventions are necessary to prevent further progression of myocardial damage. Once a patient with an Acute Myocardial Infarction (AMI) is admitted to the emergency room, the medical staff typically obtain electrocardiographic recordings and initiate antithrombotic therapy (Anderson and Morrow, 2017). The primary goal of such interventions is to establish reperfusion of the ischemic myocardium that is in the process of becoming infarcted so that it allows for the reduction of overall infarct size (Anderson and Morrow, 2017). Furthermore, the prolonged duration of MI can eventually lead to Congestive Heart Failure (CHF), which is typically associated with increased peripheral sympathetic tone. This situation adds stress on the systemic vasculature by increasing peripheral vascular resistance (PVR) which negatively impacts the hemodynamics of the systemic circulation (Gschwend et al., 2003; Ledoux et al., 2003). The fact that the heart and the peripheral circulation form a closed loop system is important when considering how changes in PVR may affect cardiac health and performance and how improving vascular function may benefit the heart. I will return to this topic in later sections.

Therefore, it is important to keep it mind that the pathophysiological impact associated with MI is not just limited to its local cardiothoracic area, but rather it can affect overall

hemodynamics of the CV system. To establish an understanding and appreciation of this pathophysiology of MI, it is important to first review the physiology of CV system. The mammalian CV system is largely composed of 3 parts: (1) the heart acting as a pump (2) blood and (3) the vessels that mediate the blood flow. Since these components form a closed loop system, there is an intimate relationship between the heart (pump) and blood vessels (tubes/pipes). That is, the activity of the blood vessels (i.e. mainly the arteries) influences heart function and vice versa. Practically speaking, the primary mechanical activity of arteries consists of either constriction (vasoconstriction) or dilation (vasodilation). In conduit arteries (i.e. those with an internal diameter > 0.5 mm), vasoconstriction is mediated mainly by the activity of innervating sympathetic nerves. Conduit arteries are normally considered the larger vessels that deliver blood from the heart to individual tissue beds. Once blood reaches a given vascular bed in a tissue, such as skeletal muscle or the brain, it is carried by small resistance arteries that form the microcirculation within the tissue. These small arteries are largely responsible for regulating blood pressure within the body and exhibit intrinsic myogenic vasoconstriction. That is, these arteries develop myogenic tone in response to elevations in intraluminal pressure, which decreases their intraluminal diameter and the level of wall tension within the artery (Davis and Hill, 1999). Myogenic constriction is also important for controlling blood flow within vascular beds and the cellular mechanisms within the arterial smooth muscle responsible for this activity have been investigated in depth.

Whereas vasoconstriction is mediated by either the sympathetic nervous system or the vascular smooth muscle itself, vasodilation is regulated mainly by the vascular endothelium, a monolayer of cells that lines the vessel lumen and directly contacts the circulating blood. The endothelium can produce near maximal dilation of arteries by generating chemical and electrical

signals that act directly on the surrounding smooth muscle to cause rapid and robust relaxation. A more detailed description of these pathways is presented below. Impairment of the endothelium (i.e. endothelial dysfunction) is typically an early event observed in the progression of cardiovascular complications associated with CVDs such as hypertension, atherosclerosis, type 2 diabetes and stroke. It has been suggested that preventing/reversing endothelial dysfunction would lessen the morbidity and mortality associated with CVD.

With regards to the relationship between blood flow and tissue perfusion, this interaction is well described mathematically by *Poiseuille's Law*:

$$Q = \frac{\pi P r^4}{8\eta l}$$

Q = Blood flow
P = Intraluminal pressure
R = Intraluminal radius
η = Blood viscosity
l = Vessel length

which states that blood flow is directly proportional to the intraluminal pressure and radius of blood vessels. However, it is also evident that flow is very sensitive to changes in vessel radius, as indicated by its exponential relationship ($Q \propto r^4$). This situation implies that the regulation of a blood vessel's radius is very important for regulating blood flow and peripheral vascular resistance (PVR). For example, a modest 5% increase in arterial radius will lead to a 21.5% increase in vessel flow. Furthermore, blood flow and PVR are important parameters that influence heart function, due to the closed loop arrangement of these elements.

To enhance our mechanistic understanding of the relationship between blood flow and blood vessels, it is reasonable to briefly review the structure of vessels. Arteries are composed of

multiple layers that wrap around each other to form tube structures (Fig. 1). The luminal side where there is direct physical and chemical contact with blood circulation is covered with a single cell layer called endothelium and there is an overlying muscle layer composed of smooth muscle cells (SMC). The number of smooth muscle layers decreases as one moves down the vascular tree, with the aorta having typically 10-12 layers and arterioles (intraluminal diameter 20-30 microns) having only a single layer of smooth muscle. This endothelium-SMC complex is mainly responsible for the regulation of vascular tone, along with input from sympathetic nerves. Historically, it was the 1980's when Nitric Oxide (NO) was discovered to be the intrinsic substance in the vascular wall that mediates smooth muscle relaxation, leading to vasodilation (Furchgott and Zawadzki, 1980; Ignarro et al., 1987a; Ignarro et al., 1987b; Palmer et al., 1987). Since the NO is generated within the endothelium, it was termed Endothelium-Derived Relaxing Factor (EDRF). However, subsequent studies have identified NO-independent vasodilation, where vasodilation is mediated by electrical communication between endothelium and SMC. The underlying mechanism is the transduction of endothelium-generated hyperpolarization to the overlying SMC (Kuriyama and Suzuki, 1978). This communication occurs via physical connections between the two cell layers termed myoendothelial junctions (Mathew John et al., 2018; Sheng et al., 2009) and promotes smooth muscle relaxation by decreasing the voltage-dependent opening of L-type calcium channels. This phenomenon was initially thought to be due to an Endothelium-Derived Hyperpolarizing Factor (EDHF) (Busse et al., 2002). However, more recent evidence points to the importance of electrical signaling between the endothelium and vascular smooth muscle (i.e. endothelium-derived hyperpolarization, EDH) as the major signal for driving smooth muscle relaxation and vasodilation (Köhler et al., 2016; Vanhoutte et al., 2017). Physiologically, the most prominent signal required to activate both EDRF and EDH is

Figure 1.

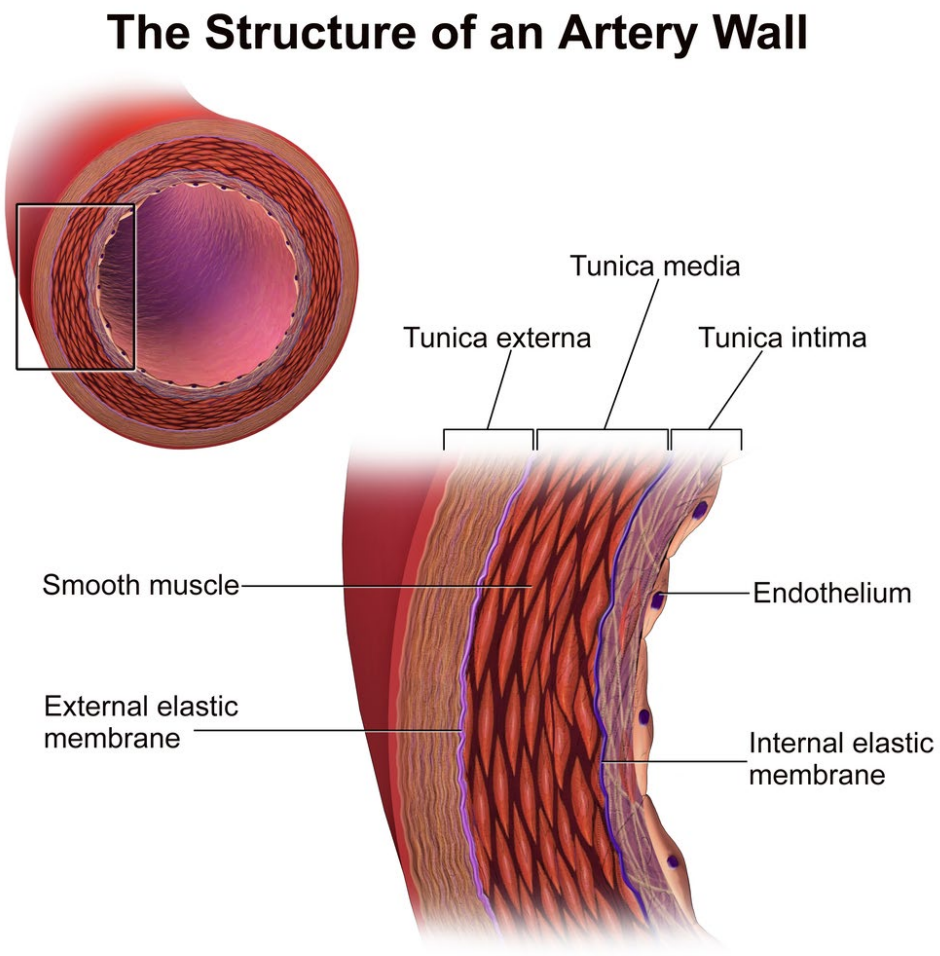

[Taken from: Artery [Internet]. En.wikipedia.org. 2020 [cited 30 May 2020]. Available from: https://en.wikipedia.org/wiki/Artery]

Figure 1. The arterial wall is composed of multiple layers or tunica. These layers are typically separated by elastic membranes or lamina. The functional unit is the endothelium-smooth muscle layer complex, which is the major regulator of the vascular myogenic tone that manipulates the diameter of the arteries. The endothelium is single cell layer and arteries are characterized by a smooth muscle layer that is 1-2 layers thick in small resistance arteries. As the diameter of arteries increase, so does the number of surrounding smooth muscle layers.

elevation of intracellular Ca^{2+}concentration ($[Ca^{2+}]_i$) in endothelium, which typically is accomplished by stimulus-evoked Ca^{2+}-release from Endoplasmic Reticulum (ER).

Once an agonist (vasorelaxant) binds to a calcium-mobilizing G-protein Coupled Receptor (GPCR) that is localized on the endothelial cell membrane, it induces conformational change, which recruits the heterotrimeric G-protein complex that further transduces the signal by activating its effector protein, Phospholipase C (PLC). The activated PLC then cleaves the bond between the phosphorus of inositol head group and glycerol, so it produces inositol triphosphate (IP_3) and Di-Acyl Glycerol (DAG). Subsequently, IP_3 binds to its specific receptor channels on the ER leading to a release of Ca^{2+}into the cytosol (Fig. 2) (Mathew John *et al.*, 2018). This cytosolic Ca^{2+} can activate endothelial Nitric Oxide Synthase (eNOS) that generates the gas molecule, NO, which can simply diffuse into the SMC and mediate vasodilation through the stimulation of soluble guanylyl cyclase, the production of cGMP from GTP and the activation of type I cGMP-dependent protein kinase, cGKI. However, the increase in endothelial $[Ca^{2+}]_i$, can also activate the small and intermediate conductance, Ca2+- activated K + channels in endothelium, commonly known as SKCa (K_{Ca}2.3) and IKCa (K_{Ca}3.1), respectively. Once activated, these channels mediate K^+ efflux that leads to endothelial membrane hyperpolarization and this electrical signalling can be transmitted to overlying SMC via Myo-Endothelial Gap Junctions (MEGJ), mediating hyperpolarization dependent vasodilation. Importantly, it has been reported that K_{Ca}2/3 channels are widespread in the mammalian vasculature and implicated in regulation of vascular tone and membrane potential of small resistance arteries (Edwards et al., 2010; Hasenau et al., 2011). Note that KCa2/3 are normally expressed only in vascular endothelium, although proliferative smooth muscle cells may express KCa3.1 channels to support their synthetic phenotype. Also, it has been reported that in

resistance arteries, vasorelaxation is more prominently driven by endothelial hyperpolarization rather than NO (Félétou and Vanhoutte, 2006). Since the resistance arteries are the major vessels that mediate tissue perfusion and represents the largest cross-sectional area within the peripheral circulation, it is possible to state that manipulation of such electrical events within the resistance arteries can trigger changes in blood pressure and overall hemodynamics of the systemic circulation. This situation also helps explain why resistance arteries play such a prominent role in blood pressure regulation.

As previously stated, the CV system is a closed system. Thus, the interrelationships between the heart and vessels in terms of their functionality are very important. Furthermore, the well-defined mathematical relationship, $\text{Blood Pressure (BP)} = \text{Cardiac Output} \times \text{Peripheral Vascular Resistance (PVR)}$, states that the BP has a direct proportionality with PVR. Furthermore, in accordance with *Poiseuille's Law,* the radius changes of the blood vessels, with the emphasis on the small resistance arteries, are the major regulators of blood flow and vascular resistance. This relationship is due mainly to the large cross-sectional area that resistance arteries occupy in the peripheral circulation versus conduit arteries. Therefore, it is possible to state that by manipulating the physical and chemical characteristics of the small resistance arteries, it can impact cardiac function and overall CV system performance.

Figure 2.

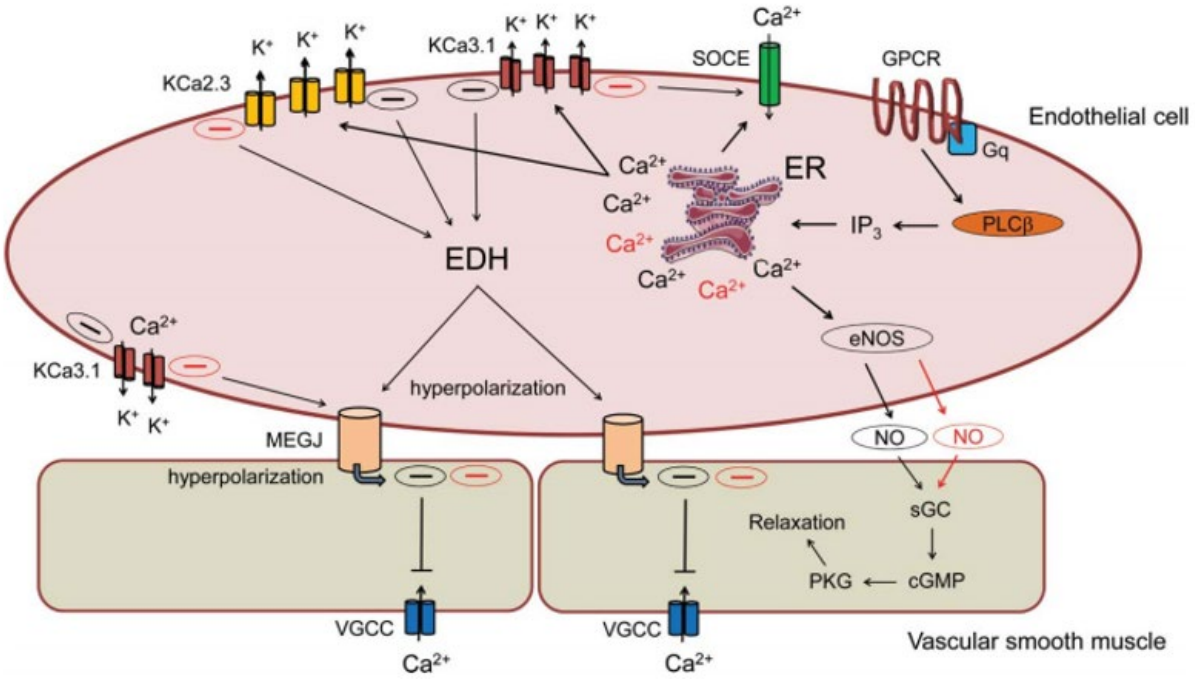

Figure 2. Cartoon depicting nitric oxide (NO) and hyperpolarization-dependent mechanisms contributing to agonist-induced vasodilation in resistance arteries. Simulation of endothelial GPCR/Gαq complexes by Ca^{2+}-mobilizing vasodilatory agonist promotes activation of PLC-β, the generation of IP_3 via phosphatidyl inositol 4,5-biphosphate (PIP_2) hydrolysis and the opening IP3 receptors/Ca^{2+} release channels on the endoplasmic reticulum (ER). ER Ca^{2+} release is sensed by STIM1, an EF-hand protein localized in the ER membrane that combined migrates and couples with the Ca^{2+} influx channel Orai1, leading to Store-Operated Ca^{2+} Entry (SOCE). The elevation of cytosolic Ca^{2+} by the latter effectors initiate endothelial-derived hyperpolarization (EDH) that can increase the electrical driving force for Ca^{2+} entry in endothelium and also transfer to the adjacent smooth muscle via myo-endothelial gap junctions (MEGJ) to reduce voltage-gated Ca^{2+} channel activity. The presence of SKA-31 or similar KCa channel positive modulators can pharmacologically "sensitize" $KCa_{2.3}$ and $KCa_{3.1}$ channel activation, thereby augmenting cell signaling mechanisms influenced by these channels, Key pathways that may be enhanced following KCa channel sensitization (i.e. generation and transfer of hyperpolarizing current, *de novo* NO generation) are highlighted with red shading.

[Taken from: Mathew John C, Khaddaj Mallat R, George G, Kim T, Mishra R, Braun A. Pharmacologic targeting of endothelial Ca2+-activated K+ channels: A strategy to improve cardiovascular function. Channels. 2018;12(1):126-136.]

1.2 Acute Myocardial Infarction

In clinical settings, the major aetiology of MI is due to an occlusion of a coronary artery that is associated with thrombus (e.g., rupture of atherosclerotic plaque) related events. Therefore, the animal model of MI in this project was established by surgically ligating the LAD coronary artery of mice which obstructs the normal coronary circulation. This manipulation leads to acute deprivation of myocardial oxygen and nutrients. The surgery mediated permanent coronary occlusion is a relevant animal model of acute ST-segment Elevation MI (STEMI) patients who do not receive timely or successful reperfusion of the injured myocardial tissue (Lindsey et al., 2018a). Furthermore, the permanent occlusion approach allows monitoring of long-term LV remodeling which makes it more suitable to be utilized in this project since one of the main aims of this project is to evaluate the effects of prolonged pharmacological intervention in response to acute myocardial injury. The major characteristics of infarcted myocardium are significant geometrical and physiological changes by wall thinning, increases in LV dimensions and volumes, and decreases in fractional shortening (FS) and ejection fraction (EF) (Lindsey *et al.*, 2018a).

1.3 Ca^{2+}-activated K^+ channels

The family of K_{Ca} (Ca^{2+}-activated K^+channel) channels was first described by G. Gardos in erythrocytes and reported to have significant roles in volume regulation of the erythrocytes (Gardos, 1958). Subsequently, the first electrophysiological profile of KCa channels was recorded and reported from molluscan neurons (Meech and Standen, 1974). Moreover, the introduction of patch-clamp technique allowed more extensive investigation of K_{Ca} channels and revealed that there are 3-subtypes: (1) large-conductance ($BK_{Ca}/K_{Ca}1$) (2) small-conductance ($SK_{Ca}/K_{Ca}2$) and (3) intermediate-conductance ($IK_{Ca}/K_{Ca}3$) Ca^{2+}-activated K^+channel. The

three types of channels have distinct voltage dependence, Ca^{2+} sensitivity, pharmacology, and conductance (Hille., 2007). Also, the cDNA profile of the K_{Ca} channels revealed that IK_{Ca} and SK_{Ca} channels share significantly similar amino acid sequences that are distant to the amino acid sequences of BK_{Ca} channel (Atkinson et al., 1991; Ishii et al., 1997; Joiner et al., 1997; Köhler et al., 1996; Vergara et al., 1998). Furthermore, each IK_{Ca} and SK_{Ca} channel subunit is comprised of 6 transmembrane (TM) spanning domains where BK_{Ca} channel subunits have 7 TM domains with an additional transmembrane segment which possesses the extracellular N-terminus (Meera et al., 1997). This proteomic difference is also corelated to the distinct biophysics of the channels in terms of their intracellular Ca^{2+}sensitivity and corresponding channel opening. Each holo-K_{Ca} channel type is an assembly of four similar subunits and may contain accessory subunits. For example, BK_{Ca} channels typically co-assemble with a beta or gamma subunit that can affect the voltage or Ca^{2+} sensitivity of gating. For all subtypes of K_{Ca} channels, the rise in intracellular Ca^{2+}concentration ($[Ca^{2+}]_i$) is the major signal for channel opening and it is sensed by the intracellular C-terminus. However, for BK_{Ca} channels, the Ca^{2+} ions can directly bind to the domains within the C-terminus (Schreiber et al., 1999), but for IK_{Ca} and SK_{Ca} channels, there is a permanently bound calmodulin on the C-terminus of each subunit that acts as a cytosolic Ca^{2+}-sensor (Hille., 2007) (Keen et al., 1999). Also, it is important to recognize that $K_{Ca}1$ channels are the products of KCNMA1 gene expression where $K_{Ca}2$ and $K_{Ca}3$ channels are products of KCNN gene expression. Overall, the $K_{Ca}2$ and 3 channels share similar genetic lineage, structure and biophysics that are distant to the $K_{Ca}1$ channel. This difference in gene expression pattern can also be associated with the distinct localization of channel expression in different tissues. In terms of artery, the $K_{Ca}1$ channel is predominantly expressed in vascular smooth muscle cells (VSMCs) where K_{Ca} 2/3 channels are poorly expressed on VSMCs. On the other hand, the K_{Ca}

2/3 channels are robustly expressed on vascular endothelial cells where $K_{Ca}1$ channel is poorly expressed on endothelial cells (Félétou, 2009; Köhler *et al.*, 2016). Moreover, the $K_{Ca}2/3$ channel subunits do not contain an arginine-rich S4-voltage sensor transmembrane domain which is usually found in other K^+channels such as K_V and $K_{Ca}1$ channels (Köhler *et al.*, 2016). This implies that the channel is not voltage dependent, which has been confirmed by electrophysiological recordings. However, if there is significant and maintained elevation of $[Ca^{2+}]_i$, the channel can produce robust and lasting hyperpolarization values near the K^+equilibrium potential (~-89 mV) (Köhler *et al.*, 2016). The activation of channels can occur with >100 nM of $[Ca^{2+}]_i$ with the EC_{50} value of 250-900 nM (Köhler *et al.*, 2016). Also, it is important to recognize the difference in conductance values between $K_{Ca}2$ and $K_{Ca}3$ channel. Once $K_{Ca}2$ channels are activated, they efflux K^+ with a single channel conductance of 5-10 pS whereas $K_{Ca}3$ channels efflux $K^+$with a conductance in the range of 30-40 pS (Köhler *et al.*, 2016). Furthermore, the subcellular expression pattern of $K_{Ca}2$ and $K_{Ca}3$ channels appear to differ within the vascular endothelium, which can have important physiological implications. The biochemical approach of membrane fractionation revealed that $K_{Ca}2.3$ proteins are found mainly at intercellular contacts within the endothelial monolayer as well as in caveolin-1 rich membrane fractions. On the other hand, K_{Ca} 3.1 channel protein appears to be localized mainly in areas of the cell membrane that are near the ER Ca^{2+}stores and at sites where endothelial cells and smooth muscle cells form myoendothelial gap-junctional contacts through holes in the internal elastic lamina (Köhler *et al.*, 2016). These observations suggest that (1) $K_{Ca}2.3$ is more sensitive to rises in intracellular Ca^{2+}that are introduced from extracellular spaces via co-localized mechano-sensitive or receptor-operated channels such as TRP types. $K_{Ca}2.3$ may thus be more sensitive to shear stress as a stimulus to evoke endothelial activation (2) $K_{Ca}3.1$

channels are more sensitive to the intracellular Ca^{2+} that is released from ER stores with the upstream signal from GPCR signaling, which can be activated by vasodilatory agonists such as acetylcholine, bradykinin, ATP, etc. Overall, these spatial and biophysical properties of K_{Ca} 2/3 channels suggest that they are mainly involved in EDH and relay of hyperpolarization to neighboring endothelial and smooth muscle cells. Also, Edwards et al have suggested that endothelial $K_{Ca}2$ channels are co-localized with K_{IR}, $K_{Ca}3$ and $Na^{+}/K^{+} - ATPases$ within caveolae. Once intracelllular K^{+}effluxes into the external caveolar space by the $K_{Ca}2$ channel, it increases the overall concentration/density of the K^{+} ions within the caveolae from ~ 5 mM to 15 mM, which can activate the K_{IR} channel. In other words, the initial hyperpolarization triggered by $K_{Ca}2$ channels can be further relayed and amplified by activation of endothelial K_{IR} channel (Edwards *et al.*, 2010). Thus, this information suggests that EDH can be a multi-channel response and a multi-step phenomenon. These overall characteristics of the channels should be kept in mind as we consider the data from my project.

1.4 SKA-31

The cellular pathway of hyperpolarization dependent vasodilation has been suggested to represent a novel drug target in the treatment of CV disease (Köhler *et al.*, 2016). Also, the fact that such a vasodilatory pathway and PVR are prominent in the context of small resistance arteries further provides significance to their therapeutic potential. By using the FDA-approved neuroprotectant agent, riluzole as a chemical template for rational drug design, Wulff and co-investigators synthesized a novel series of small molecules intended as activators of small- and/or intermediate-conductance, calcium-activated K+ channels (i.e., KCa2/3 channels). Among these molecules was SKA-31, which displays selectivity as a $K_{ca}2/3$ channels activator with an EC_{50} ~0.3 μM for $K_{ca}3.1$ channels and EC_{50} ~2 μM for $K_{ca}2.3$ channels

(Sankaranarayanan et al., 2009). This group also reported that SKA-31 displays 100-1000-fold selectivity over various other Na+, Ca2+ and K+ channels, which is very important for interpretation of SKA-31 actions in both in vitro and in vivo preparations. Based on its demonstrated potency, its improved target selectivity and more desirable pharmacokinetic profile (see Discussion), SKA-31 appears to be better suited for experimental studies in complex tissues and organisms compared with first generation K_{Ca} channel activators, such as DC-EBIO and NS309.

As described previously, when a vasorelaxant hormone targets Ca^{2+}-mobilizing GPCRs in the endothelium (e.g., acetylcholine acting upon muscarinic receptors), it leads to robust Ca^{2+}-release from ER and elevation of $[Ca^{2+}]_i$ that target $K_{ca}2/3$ channels on the plasma membrane (PM) and activates them. Once these channels are activated, they mediate K^+-efflux and membrane hyperpolarization that can be transferred from endothelial cells into the vascular smooth muscle layer via MEGJ. Thus, pharmacological enhancement of K_{Ca} channel activities can affect the regulation of vascular contractility by endothelium-dependent vasodilatory hormones. SKA-31 and similar K_{Ca} channel activators are reported to sensitize and activate these channels, which is associated with inhibition of myogenic tone, vasodilation, and increased agonist-evoked NO production (Dalsgaard et al., 2010; Sheng *et al.*, 2009). Endothelial dysfunction is a condition associated with elevated states of vasoconstriction, a decrease in myogenic responsiveness and reduced NO bioavailability (Deanfield et al., 2007). Therefore, the anticipated effects of SKA-31 at levels of intact resistance arteries and vascular beds could involve enhancement of endothelial health and improved myogenic responsiveness. Furthermore, as background experimental evidence, there are supporting data sets obtained by a wide range of experiments, from single cell patch clamp studies to large animal trials. These results have

demonstrated that acute treatment with SKA-31 enhances the electrical conductance of $K_{ca}2/3$ channels and physiologically, improves coronary flow and decreases systemic vascular resistance in rodents and large animal models (Mishra et al., 2013; Mishra et al., 2016; Sankaranarayanan *et al.*, 2009) (Fig. 3 and 4). With such promising background results, I chose SKA-31 as a pharmacological tool in this project to investigate the potential therapeutic benefit of endothelium-derived hyperpolarization in the setting of acute MI.

1.5 Hypothesis

Recent studies from the Braun laboratory have demonstrated that pharmacological enhancement of vascular endothelial function in settings such as aging and type 2 diabetes (T2D) is able to augment coronary flow and improve cardiac function (John et al., 2020; Mishra *et al.*, 2013). Based on such data and our well-established understanding of the CV system, I was able to develop an overarching scientific hypothesis for my research project. Specifically, I hypothesized that **"enhancement of endothelial function as a primary target would secondarily improve cardiac performance, which would prove beneficial in the setting of an acute injury, such as MI".** Endothelial function is often impaired in conditions such as T2D and aging, which represent situations of chronic, low level injury. However, it is unknown if pharmacological augmentation of endothelial function may provide similar benefit in the setting of acute injury, given the different circumstances of tissue injury. It is thus evident that my project represents a completely novel investigation into this area of inquiry.

The level of contractility in the peripheral arterial circulation significantly changes following a MI, as evidenced by increases in PVR and vasoconstriction. Furthermore, pharmacological interventions are often used clinically to enhance the coronary circulation in the

setting of an acute MI, and this practice provides additional rationale for my project. Thus, acute MI is a reasonable model to test the proposed hypothesis.

Figure 3.

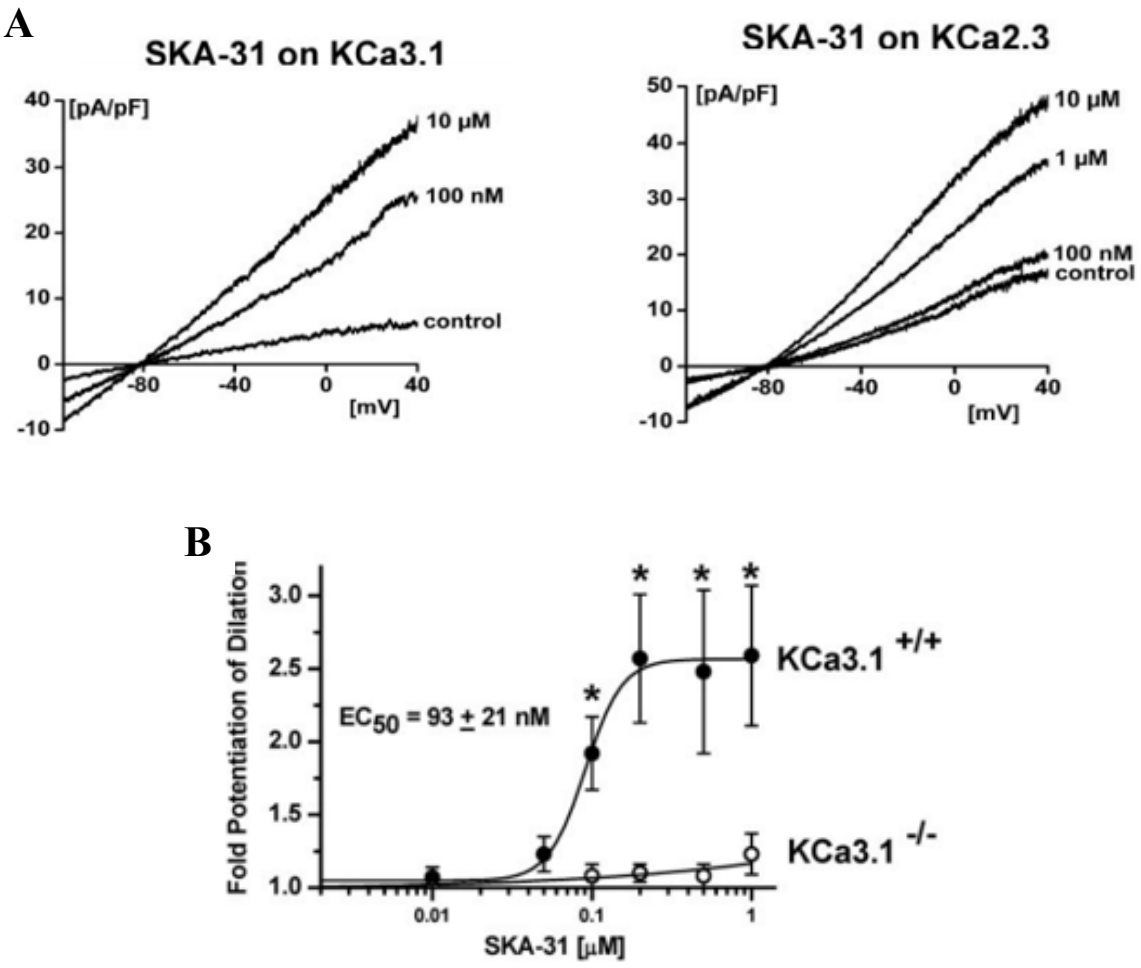

Figure 3. [A] Electrophysiological studies demonstrate that SKA-31 can directly activate the opening of KCa 2/3 channels in a concentration dependent manner. The mouse carotid artery endothelial cell was utilized in these experiments. Mouse carotid artery dilation was also stimulated in the presence of SKA-31. **[B]** The significant decrease in dilation due to absence of KCa3.1 channel by gene knock out further reinforces the selectivity of the drug.

[Taken from: Sankaranarayanan, A., Raman, G., Busch, C., Schultz, T., Zimin, P.I., Hoyer, J., Köhler, R., and Wulff, H. (2009). Naphtho[1,2-d]thiazol-2-ylamine (SKA-31), a new activator of KCa2 and KCa3.1 potassium channels, potentiates the endothelium-derived hyperpolarizing factor response and lowers blood pressure. Mol Pharmacol *75*, 281-295. 10.1124/mol.108.051425.]

Figure 4.

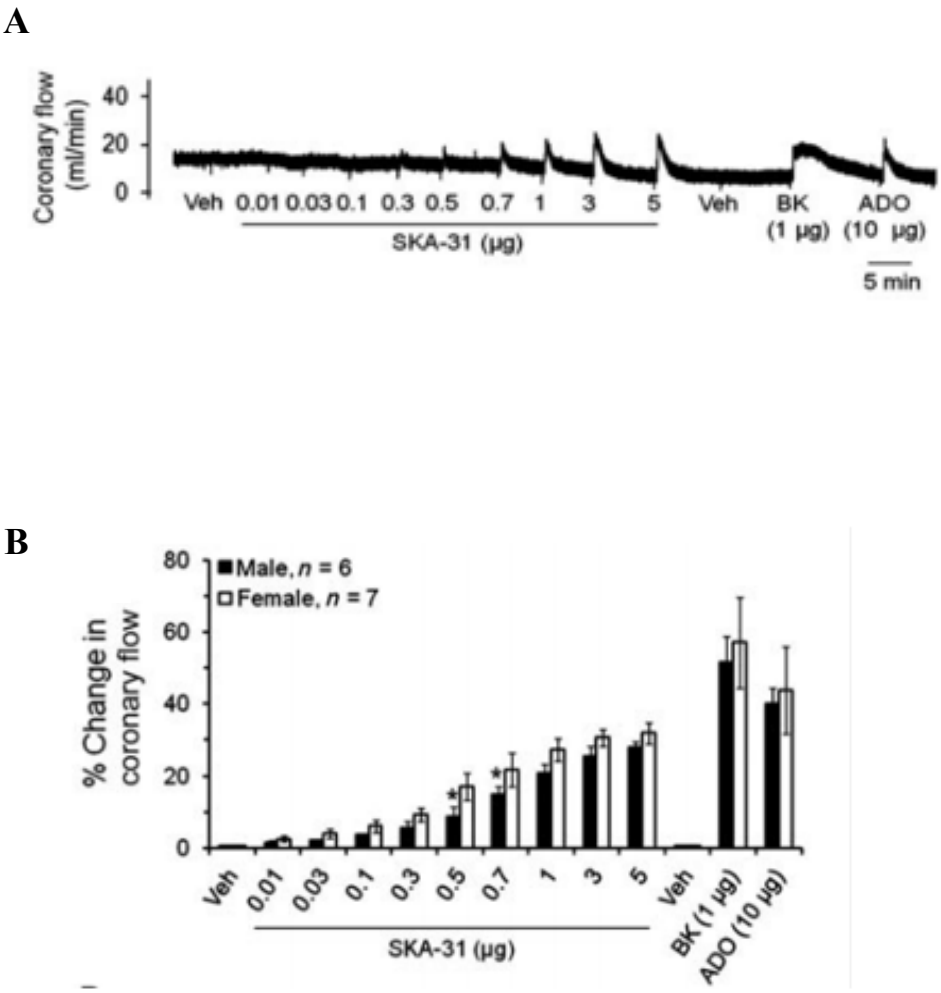

Figure 4. Acute bolus application of SKA-31 increases total coronary flow in Langendorff-perfused rat hearts in a dosage dependent manner. The experiments were performed in both male and female rats and similar effects were observed in both sexes.

[Mishra, R.C., Belke, D., Wulff, H., and Braun, A.P. (2013). SKA-31, a novel activator of SK(Ca) and IK(Ca) channels, increases coronary flow in male and female rat hearts. Cardiovasc Res *97*, 339-348. 10.1093/cvr/cvs326.]

Chapter 2: Materials and Methods

2.1 Experimental animals & treatment

The goal of this study was to investigate potential cardio-protective effects of prolonged SKA-31 administration in the setting of an acute myocardial injury. Thus, to critically evaluate the corresponding drug effects, male mice (12-15 weeks of age, C57B1/6 strain) were used as an animal model in this project. The experimental approaches to measure cardiac functional parameters are well established in mice (Pacher et al., 2008) and the relative ease with which one can observe animal health *in vivo* further increases feasibility of the approaches. Another advantage of mice is the tremendous number of genetically engineered models available for experimental use. Creation of such models is now routine, and they can be invaluable for manipulating select proteins or pathways for which pharmacological tools may not exist and doing so in a prolonged manner. I have also chosen to focus my experiments on male mice to avoid the cyclical sex hormone fluctuations found in female animals due to estrous related events. Also, historically, a majority of clinical and experimental cardiovascular investigations have utilized cells and tissue samples obtained from male subjects. This latter point may thus allow us to compare more directly the results obtained from my current study to these previous investigations. However, as indicated by previous reports, several cardiovascular disease risk factors that are unique to women have emerged that require attention. (Garcia et al., 2016). In fact, a potential next phase of this project could be to undertake an evaluation of SKA-31 effects in female mice with acute myocardial injury. In terms of experimental groups, there are 4 groups in this project: (1) control group undergoing sham surgery with vehicle treatment, (2) Sham surgery group with SKA-31 treatment, (3) Acute injury group with surgically induced ligation of coronary artery to create a myocardial infarction (MI); this group is treated with drug vehicle, (4) MI group with SKA-31 treatment (Fig. 5). The functional measurements obtained from sham

surgery groups with treatment of either vehicle or SKA-31 establish the baseline, which can serve as reference points.

Figure 5.

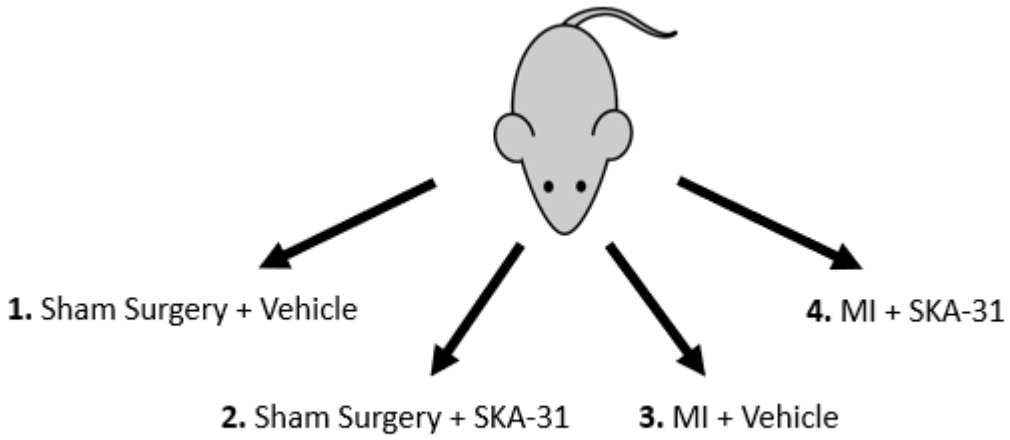

Figure 5. The 4 different experimental groups proposed for my experiments. (1) sham surgery with vehicle treatment, (2) sham surgery with SKA-31 administration, (3) acute injury model of MI via ligation of coronary artery with vehicle treatment, (4) MI model with SKA-31 treatment.

to which the parallel MI groups can be compared. Therefore, the effects that are induced by SKA-31 can be effectively observed in a controlled manner.

All procedures for animal treatment and care were conducted in accordance with the Guide for the Care and Use of Laboratory Animals of the National Institutes of Health (Grundy, 2015), and were reviewed and approved by the University of Calgary Animal Care Committee (Protocol #AC18-0056). The mice were obtained from the Jackson Laboratory (Bar Harbor, ME USA) and housed under standard conditions with regulated temperature (i.e. 22℃) and humidity and on a 12h/12h light/dark cycle. The mice were fed with certified standard chow diet and tap water ad libitum. Also, the animals were monitored by veterinarians and trained technicians throughout the study to detect any signs of disease such as weight loss and opportunistic infection. Mice were euthanized under isoflurane anesthesia by opening the diaphragm to access and excise the heart after the completion of P-V loop analysis. Tissues and organs were collected according to the experimental protocols.

2.2 Surgical approach to establish MI in mice

To introduce the MI, a well-established surgical approach was used to permanently ligate the Left Anterior Descending (LAD) coronary artery (Tzahor and Poss, 2017) (Fig. 6). With the support from Dr. Darrell Belke in the Libin Institute's Cardiovascular Phenotyping core facility, University of Calgary Cumming School of Medicine, the coronary artery ligation was implemented. During the procedure, mice were initially anesthetized by 4% isoflurane with oxygen as the carrier gas, intubated and ventilated using a VentElite Small Animal Ventilator (Harvard Apparatus). During the surgical procedure, anesthesia is maintained with 2% isoflurane. The thoracic area was shaved and cleaned with ethanol and betadine prior to a left

Figure 6.

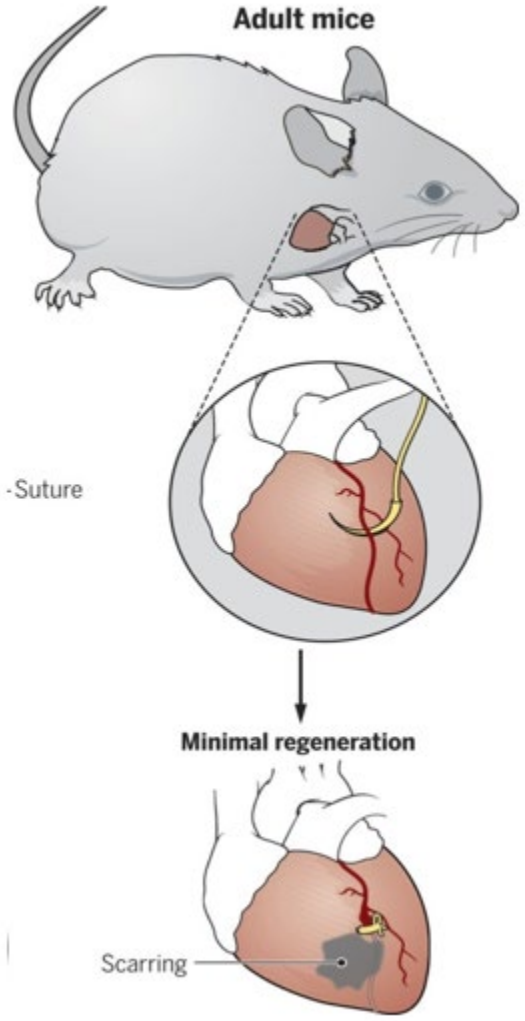

[Taken from: Tzahor E, Poss K. Cardiac regeneration strategies: Staying young at heart. Science. 017;356(6342):1035-1039.]

Figure 6. Surgical approach adopted to ligate the left anterior descending coronary artery. The ligation would permanently block coronary blood flow to a portion of the left ventricle, leading to ischemic and hypoxic conditions in the myocardium that result in scarring and tissue damage (indicated by the grey area).

thoracotomy in the fourth intercostal space. Once the left ventricle is detected, the pericardium is removed, and LAD coronary artery is ligated with monofilament 8-0 suture (Ethicon). The placement of suture ~1 mm distal to the left atrium generates infarct sizes ranging from 35-60% of total LV (Lindsey *et al.*, 2018a). Subsequently, the intercostal space and skin are closed with a 5-0 Vicryl suture (Ethicon) and the air in the thoracic cavity is evacuated by using a pleural catheter. All the same steps are used for the sham operation, except the LAD ligation is omitted. However, after the removal of pericardium, the area where the 8-0 suture is usually placed during the MI operation is poked 2-3 times with fine forceps. An important consideration in this procedure is that the LAD artery in mice is buried within the ventricular wall, which makes it surgically very difficult to place a suture ligation in precisely the same location in all mice. As a result, the sizes of resulting infarct in the LV wall are expected to vary, which will influence the extent of cardiovascular dysfunction in mice and possibly the effects of SKA-31 to promote recovery. This variable has been integrated into the process of analyzing and interpreting the functional and histological results from my four treatment groups of mice.

2.3 Echocardiography

Doppler echocardiography was carried out by using a Vevo 3100 FUJIFILM Visual Sonics instrument, and it has been implemented in anesthetized mice to evaluate overall cardiac performance and left ventricular wall thickness/dimensions. The practical aspect with this technique is that such measurements can be repeated, that is, it can be implemented at different time points following the initial surgical intervention in mice. Thus, cardiac function of both MI and sham surgery mice with either vehicle or SKA-31 treatment was measured at 2 weeks and 4 weeks post-surgery. This approach allowed me to monitor the development and progression of MI-related cardiovascular dysfunction and recovery. Also, any effects induced by SKA-31

treatment were also being evaluated. The mice were initially anesthetized with 4% isoflurane with oxygen as a carrier gas then the transthoracic echocardiography has been performed under light anesthesia (1.5-2% isoflurane). The mice were placed on a heated pad (37°C) with incorporated ECG tracing panels. Prior to the animal placement, the ECG-recording gel was placed on the metal panels and once the animal was positioned, its paws were attached to the panels to obtain ECG recordings. Subsequently, the hair removal gel was applied to the thoracic area then wiped off with a Kimwipe tissue after ~1 min. The thoracic area was cleaned again with 75% alcohol which was followed by application of Aquasonic ultrasound transmission gel (Parker Laboratories INC. Fairfiled, New Jersey USA). First, the left atrial view was obtained to evaluate left atrial performance such as contraction, relaxation, and to observe any potential anatomical changes. Subsequently, the M-mode (short axis view) echocardiography was implemented (5-7 trials/recording episode) to evaluate left ventricular wall thickness, Ejection Fraction (EF), Fractional Shortening (FS) and Heart Rate (HR) (Fig. 7). In addition, this procedure was followed by B-mode (long axis view) echocardiography to obtain a longitudinal view of LV (Fig. 8). The ECG-gated Kilohertz Visualization (EKV) was implemented on the B-Mode imaging to assess End-Systolic Volume (ESV), End-Diastolic Volume (EDV), Stroke Volume (SV), and Cardiac Output (CO). Representative images of M-mode and B-mode analysis of each experimental group are illustrated in the Appendix. Lastly, the color (10 – 15 trials/recording episode) and tissue (10 – 15 trials) Doppler echocardiography was implemented to evaluate the mitral valve physiology.

Figure 7.

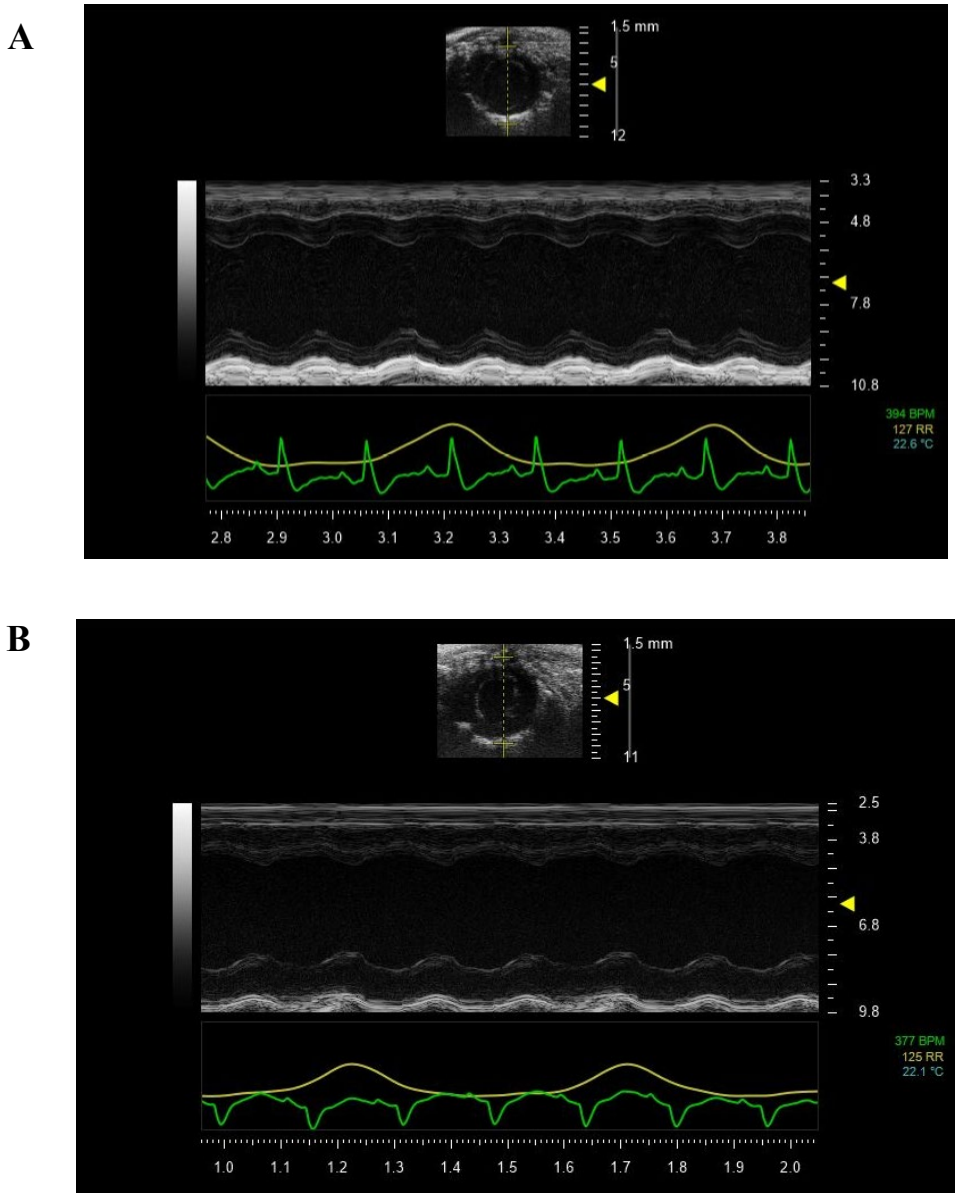

Figure 7. The short axis view of the left ventricle as recorded by echocardiography. These representative images were taken at 2 weeks following either sham or MI surgery. **[A]** In this example, the mouse underwent sham surgery, and the relatively clean patterns of anterior and posterior side of left ventricular wall are readily observable. Also, the accompanying ECG (lower trace) is normal with clear layout of the PQRST complex. **[B]** This mouse underwent MI surgery and the echocardiographic image illustrates a relatively diminished anterior wall thickness at both systole and diastole. The QRS complex of the ECG is inverted (lower trace).

Figure 8.

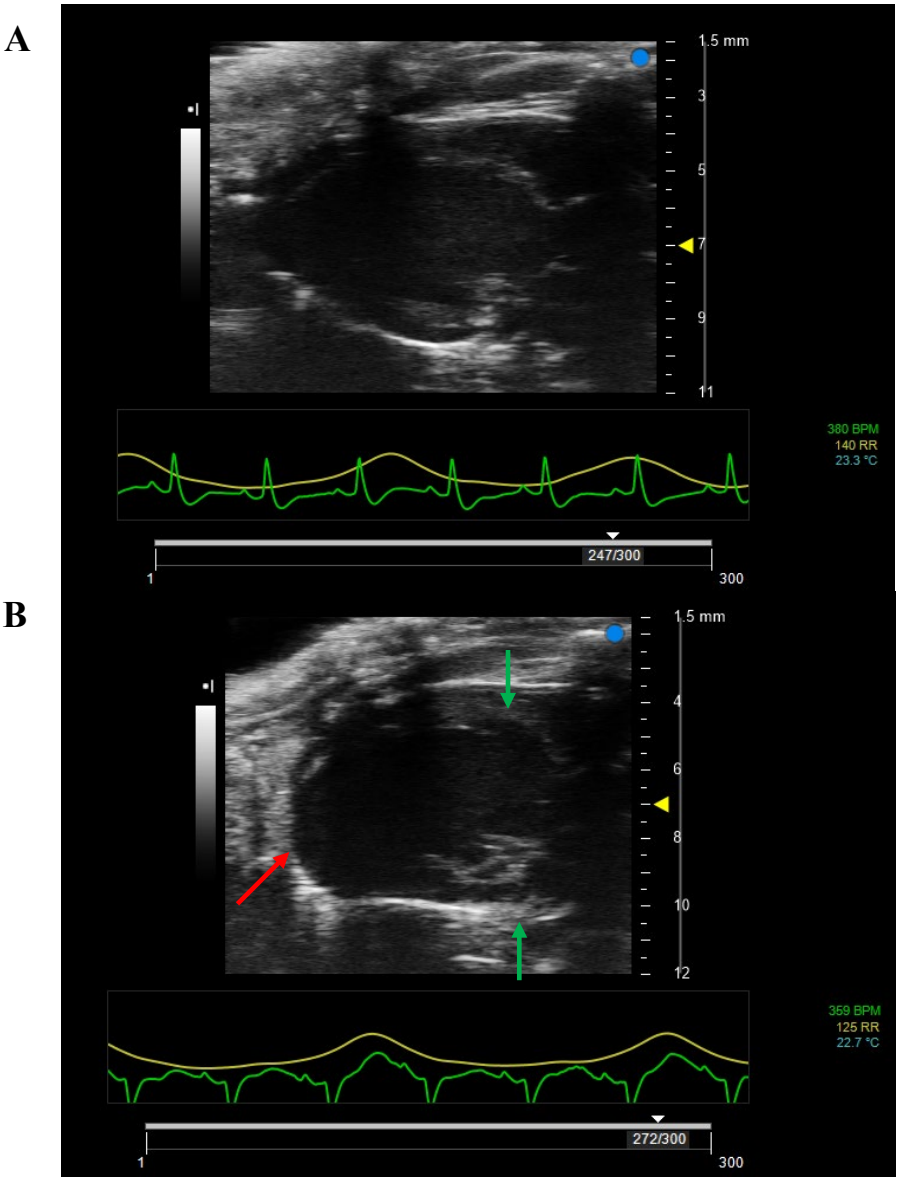

Figure 8. The long axis view of the left ventricle. These representative images were taken at 4 weeks following either sham or MI surgery. **[A]** This mouse underwent sham surgery and one can see the uniform layout of myocardium from base to apex [**B]** This mouse underwent MI surgery and the image illustrates a slight increase in anterior and posterior wall thickness (green arrows, indicating potential hypertrophy of the remaining viable myocardium). Also, the apex of the left ventricle shows a thinning/absence of the of viable myocardium, implying no muscle movement (red arrow). These images of sham and MI surgery mice long axis views were taken prior to the P wave of ECG.

2.4 Pressure-Volume loop analysis

At 6-7 weeks post-surgery, an invasive left ventricular pressure-volume (P-V) loop analysis was implemented. It is the preferred method to obtain robust, quantitative information with regards to ventricular load volume and the interaction of heart and vasculature (Pacher *et al.*, 2008). Pressure-volume loop analysis is somewhat superior to echocardiography in that it provides direct measures of ventricular contractility that are independent of cardiac pre-load and after-load. These factors can impact echocardiographic measures of cardiac function and cannot be readily determined in a non-invasive setting. During the procedure for P-V loop analysis, the mice were initially anesthetized by 4% isoflurane with oxygen as carrier gas then maintained the anesthesia with 2% isoflurane via intubation and ventilation by using a VentElite Small Animal Ventilator, Harvard Apparatus. A micro-catheter (Millar Instruments, Model Number: PVR-1045, Length: 3.5 cm, Tip F Size: 1F, Electrode Spacing: 4.5 mm) that can measure the impedance and pressure is inserted into the left ventricle via right carotid artery. The measurements are performed in a chronological order (1) Baseline pressure and volume measurements with ventilator on, (2) Baseline pressure and volume measurements with ventilator off, (3) Abdominal occlusion of the vena cava to manipulate afterloads and preloads to determine the End-Systolic Pressure Volume Relationship (ESPVR) and End-Diastolic Pressure Volume Relationship (EDPVR). Once all the measurements are completed, a parallel conductance value is obtained by injecting hypertonic saline via the jugular vein. Finally, blood is withdrawn from the animal at the end of the measurements to calibrate the conductance catheter. The animals are then euthanized by excision of the heart, and additional tissues are collected for histopathological analysis.

2.5 Histological Analyses of Select Tissues

Following euthanasia, the heart, brain, liver, spleen, kidney, and aorta have been harvested. They were washed and rinsed of blood with ice cold 1X PBS then fixed in 4% (w/v) paraformaldehyde overnight. Following adequate fixation, tissues were prepared for sectioning and staining in collaboration with the Libin Institute Histopathology Core facility (supervised by Dr. Y. Chen). The organs were dehydrated and embedded in paraffin wax, and then cut into 5-micron thick sections using a microtome. However, the hearts underwent additional steps to evaluate the infarct/fibrosis size. The pictures of whole heart were taken under 1.25x magnification. Subsequently, the heart was cut into 3 separate transverse sections (1) base segment containing aortic arch (2) middle segment (3) heart apex. This approach allowed evaluation of infarct size at different zones of the myocardium.

Tissue sections were then stained using hematoxylin and eosin (H&E) to visualize structural elements and allow morphometric measurements of cellular and tissue dimensions. The staining of non-target organs (e.g. brain) will allow me to assess potential toxic effects of prolonged SKA-31 administration in my treatment groups. Sections of the myocardial left ventricle have also been stained with picrosirius red (i.e. a collagen stain) to visualize connective tissue and fibrotic regions associated with the site of injury. Stained tissue sections were visualized using an Olympus BX53 fluorescence-equipped microscope at 1.25x magnification. The areas with collagen deposition were identified as bright yellow or orange coloured tissue under polarizing illumination. The size of infarct/fibrosis was determined using the following formula:

$$\% \, Infarction = \frac{Infarct \; Size}{LV \; Free \; wall} \times 100$$

The LV free wall was obtained by [Total LV wall – LV endocardial area] and infarct size was obtained by summation of area that displayed bright yellow or orange coloured region under polarizing illumination. The histological data analysis was implemented with the aid of ImageJ software.

2.6 Quantification and Statistical Analysis

Once the images are obtained from echocardiography, they are analyzed with Vevo LAB 3.1.0 software, FUJIFILM Visual Sonics. The images are collected from short and long axis views, which provide the left ventricular anterior and posterior wall thickness, EF, FS, ESV and EDV. Furthermore, the color and tissue doppler imaging were also performed to obtain mitral valve functions, which can provide blood flow velocity during E and A waves. This information can indicate the diastolic function of the left ventricle (e.g. wall stiffness). The measurements with the short axis view were implemented by exploring the region marked by the placement of probe at the LV papillary muscle, which indicates the center of LV. This approach was applied to all groups of animals to maintain the consistency and uniformity of the data analysis. In each trial, 5 – 10 cardiac cycles were chosen to evaluate and calculate the cardiac function indicators such as EF and FS by connecting the points of systole and diastole using Vevo LAB 3.1.0 software. The data obtained by long axis view were ESV, EDV, SV and CO and these measures were attained by manually tracing the LV myocardial wall from aorta to apex with the EKV mode.

The data obtained from P-V loop analysis were analyzed by using Labchart software (AD Instruments, Colorado, USA). Careful calibration of pressure and volume measurements have been undertaken to obtain precise information of ESPVR, EDPVR, EF, dP/dt max, dP/dt min and Tau. The load-dependent parameters such as EF, ESV, EDV, P_{es}, P_{ed}, P_{dev}, dP/dt_{max},

dP/dt_{min} and Tau were measured from baseline measurement by selecting 35-50 P-V loops; mal-shaped P-V loops recorded from an animal taking a breath were manually excluded (Fig. 9). The load-independent parameters such as ESPVR, EDPVR and PRSW were measured by manipulating the venous return by temporary occlusion of the abdominal vena cava. On the Labchart software with the P-V loop tracings, the regions where both pressure and volume simultaneously drop were selected (20-30 P-V loops) for the analysis using this occlusion technique (Figure. 10). Also, the mal-shaped P-V loops from an animal taking a breath were manually excluded. The representative images of P-V loop tracings recorded from each experimental group are illustrated in the Appendix.

Functional measurements obtained from the four main experimental groups in my study (i.e. sham surgery + vehicle, sham surgery + SKA-31 treatment, MI surgery + vehicle and MI surgery + SKA-31) have been analyzed statistically by two-way analysis of variance (ANOVA) followed by a Tukey post-hoc test. This approach thus allowed me to evaluate the impact of the two main independent variables in this project, (1) presence of MI and, (2) SKA-31 treatment on measurements of cardiac function and structure. All data in this thesis are reported as average values +/- standard deviation. When mentioned, N values represent the number of animals used for a given measurement. Primary endpoints to be evaluated include the effect of surgical procedure on cardiovascular performance and the potential impact of drug treatment on these same parameters in sham and MI surgery groups (Group 1: n = 6, Group 2: n = 6, Group 3: n = 8, Group 4: n = 10). Both echocardiographic and P-V loop analysis were done on multiple trials/replicates. For example, the short axis view obtained from one animal was recorded using 5-7 trials with analysis of 5-10 cardiac cycles in each window. Thus, analysis of 25-70 cardiac cycles was performed for a single animal. In addition, the EKV mediated B-mode measurement

allows the software to calculate an average from an entire ECG tracing and myocardial contraction/relaxation series. Therefore, the data analysis was implemented to minimize the potential variability. Furthermore, the histological analysis was also carried out on 2-3 sections/replicates per tissue to minimize the variability.

To estimate the minimal number of animals per group to detect meaningful differences, I have performed a preliminary power calculation using SigmaPlot software. By setting the number of groups to 4 and the level of statistical significance (alpha) to 0.05, the level of power is estimated to be >0.8 for a minimal group size of 7 animals when the amount of variance (i.e. anticipated standard deviation of residuals) is arbitrarily set to 50% of the minimum detectable difference in means between two groups (e.g. detectable difference in means = 40, SD of residuals = 20). A lower amount of variance leads to increased statistical power.

Figure 9.

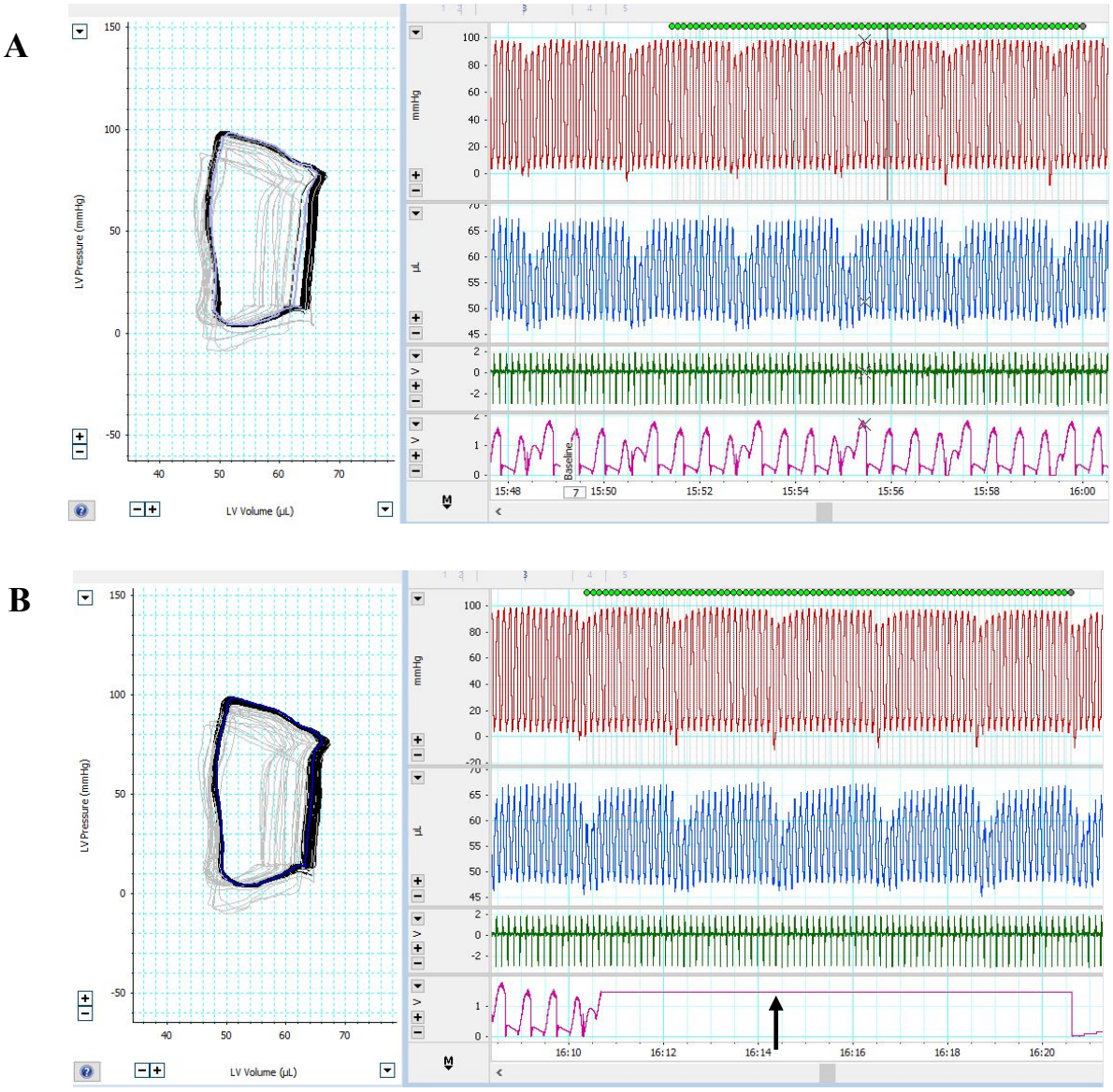

Figure 9. Baseline measurements of cardiac performance obtained from pressure-volume (P-V) loop analysis. In these representative screen capture plots, the red trace in the top panel indicates left ventricular (LV) pressure, the blue trace below indicates LV volume, the green trace indicates ECG and the pink trace indicates ventilatory activity. [**A]** The baseline measurements of cardiac performance with the ventilator on. [**B]** The baseline measurements with ventilator off as indicated by the flat pink line (black arrow).

Figure 10.

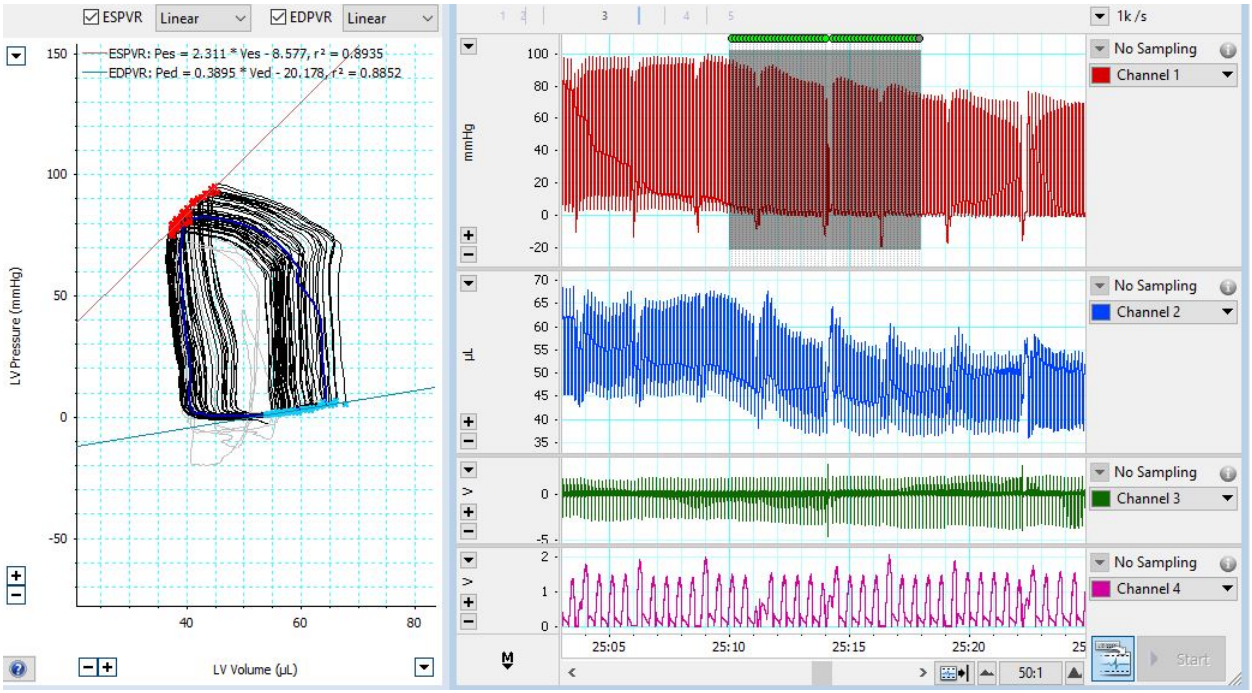

Figure 10. A typical measurement of ESPVR and EDPVR following occlusion of the abdominal vena cava; this intervention manipulates the preload and afterload of the heart. The pattern of tracings and color coding shown in this screen capture shot are similar to those described in the legend for Figure 9. The specific region of data where both pressure and volume drop simultaneously, as indicated by the shading in the top panel, was selected for the measurement.

Lastly, the data obtained from echocardiography and P-V loop analysis have been analyzed in a blinded fashion by three independent individuals. (1) Taeyeob Kim in Dr. Andrew Braun's Laboratory, University of Calgary Cumming School of Medicine (2) Dr. Ramesh Mishra in Dr. Andrew Braun's Laboratory, University of Calgary Cumming School of Medicine (3) Dr. Darrell Belke in the Libin Institute Cardiovascular Phenotyping core facility, University of Calgary Cumming School of Medicine. The independent measurements carried out by these three individuals for a given parameter were then averaged to obtain a single value. In the event that an individual measurement was noticeably different from the other two, the analysis was revisited to determine the nature of the variance and corrections were made, if warranted. This post-hoc procedure generally avoided inclusion of any erroneous measurements in the final average values reported in this thesis. This strategy of blinded and independent analysis of functional measurements thus provided a more rigorous evaluation of cardiac function that minimized experimental bias and enhanced the overall reliability of the data.

Chapter 3: Results

3.1 Surgical induction of MI in mice significantly decreased the LV function

Echocardiography is now commonly used to measure different aspects of cardiac architecture and physiology in rodents (Lindsey et al., 2018b). The major parameters that are commonly used to evaluate systolic function are EF and FS (Lindsey *et al.*, 2018b).Theses parameters are obtained by using M-mode echocardiography. As illustrated in Figure 11, the MI groups (Groups 3 and 4) show significant reduction in EF and FS which clearly indicates that systolic function of LV has been significantly diminished. The mice that received sham surgery display EF values of ~50% and FS value of ~25% but mice that received MI surgery display EF value of ~30% and FS value of ~15% at both 2- and 4-weeks post-surgery. Moreover, there is a

noticeable trend that can be found in the MI groups 3 and 4. The EF and FS values of group 3 are **30.55%** ± 6.42 and **14.21%** ± 3.26 at 2 weeks post-surgery and **25.84%** ± 5.79 and **11.97%** ± 2.90 at 4 weeks post-surgery, respectively (means ± SD). The EF and FS values of group 4 are **23.41%** ± 4.95 and **10.82%** ± 2.52 at 2 weeks post-surgery and **22.56%** ± 6.54 and **10.51%** ± 3.17 at 4 weeks post-surgery, respectively (Table. 1). Thus, there is a trend of decreased EF and FS in MI group with SKA-31 treatment at 2- and 4-weeks post-surgery. However, this is not a statistically significant difference. Nonetheless, it is important to recognize this trend since it can potentially have meaningful physiological implications.

Figure 11.

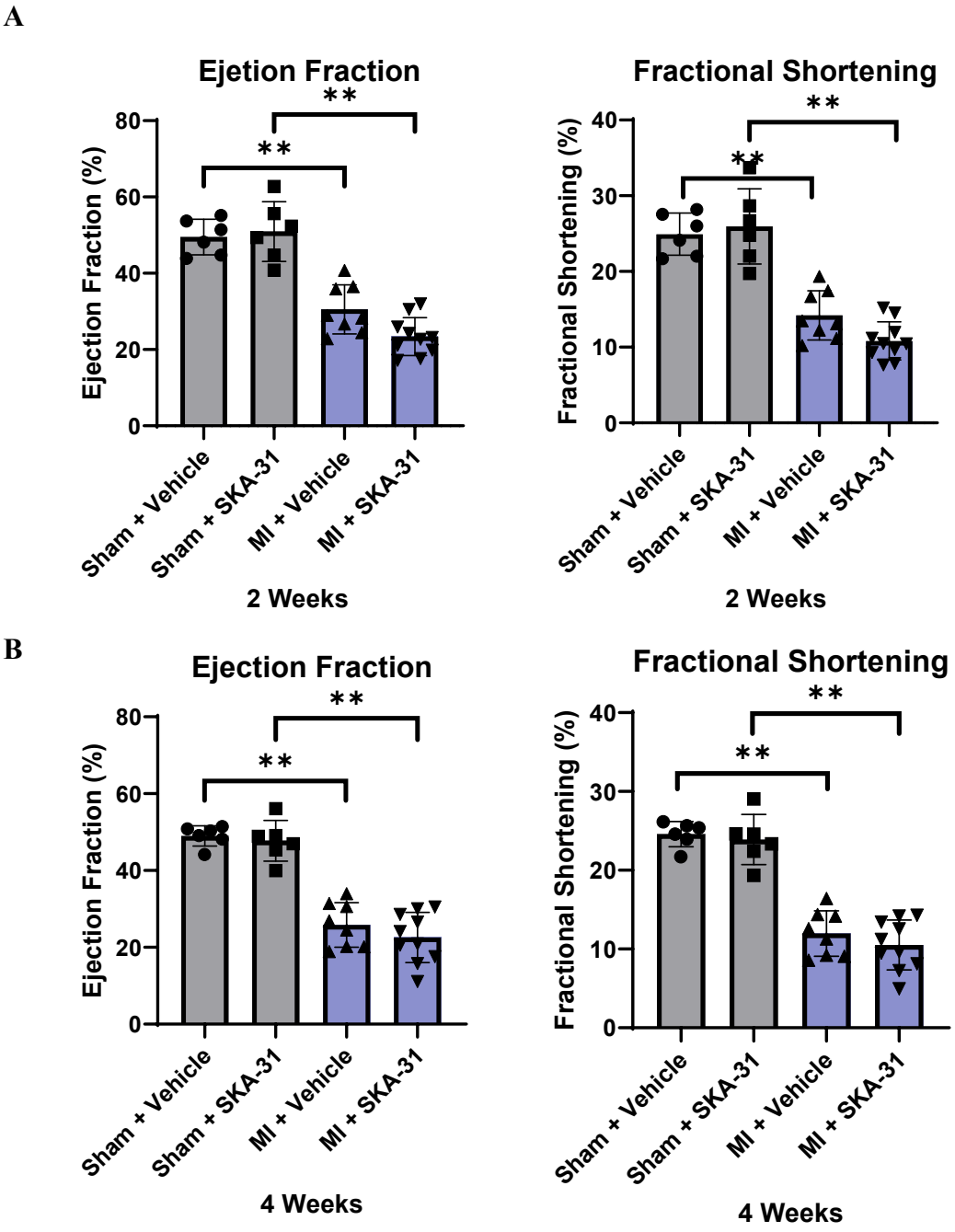

Figure 11. Echocardiographic (M-mode) measurement of LV EF (Ejection Fraction) and FS (Fractional Shortening). [**A]** 2-weeks post-surgery (Sham/MI) measurement [**B]** 4-weeks post-surgery (Sham/MI) measurement. Data presented as mean ± SD, n = 6-10. ** = $p<0.0001$, two-way ANOVA and Tukey post-hoc test.

Table 1.

A

Parameters Measured	Sham + Vehicle (n=6)	Sham + SKA-31 (n=6)	MI + Vehicle (n=8)	MI + SKA-31 (n=10)
EF (%)	49.51 ± 4.66	50.95 ± 7.82	30.55 ± 6.42**	23.41 ± 4.95##
FS (%)	24.93 ± 2.77	25.93 ± 4.97	14.21 ± 3.26**	10.82 ± 2.52 ##
ESV (µL)	41.55 ± 6.86	37.20 ± 9.07	67.45 ± 23.48	79.85 ± 24.86 #
EDV (µL)	71.43 ± 6.47	70.67 ± 5.95	96.91 ± 24.71*	117.8 ± 27.43 #
HR (BPM)	402.4 ± 38.26	412.8 ± 25.65	416.5 ± 54.71	391.2 ± 55.80

B

Parameters Measured	Sham + Vehicle (n=6)	Sham + SKA-31 (n=6)	MI + Vehicle (n=8)	MI + SKA-31 (n=10)
EF (%)	49.00 ± 2.64	47.74 ± 5.23	25.84 ± 5.79**	22.56 ± 6.54 ##
FS (%)	24.58 ± 1.61	23.89 ± 3.18	11.97 ± 2.90**	10.51 ± 3.17 ##
ESV (µL)	38.68 ± 3.00	37.41 ± 6.44	77.78 ± 29.57*	95.24 ± 31.48 #
EDV (µL)	71.08 ± 3.74	70.35 ± 10.23	109.4 ± 25.93*	121.8 ± 32.29 #
HR (BPM)	425.7 ± 27.79	402.3 ± 19.76	419.4 ± 37.11	396.0 ± 33.64

Table 1. (Echocardiography) Functional and structural parameters measured following 2-weeks **[A]** and 4-weeks **[B]** post treatment with vehicle/SKA-31 in sham and MI operated mice. Data are presented as means ± SD calculated from 6-10 animals. * = $p<0.05$, ** = $p<0.0001$ between groups 1 and 3, two-way ANOVA and Tukey post-hoc test. # = $p<0.05$, ## = $p<0.0001$ between groups 2 and 4. **EF** – Ejection Fraction; **FS** – Fractional Shortening; **ESV** – End-Systolic Volume; **EDV** – End-Diastolic Volume; **HR** – Heart Rate

It is also important to take a note of how these parameters are determined and which specific information with regards to LV that they convey. By carefully studying the mathematical formulae of EF and FS, it is possible to obtain more insight into the measurements. Both Vevo LAB 3.1.0 software (Echocardiography) and Labchart software (P-V loop analysis) use the following formulae to calculate EF and FS:

$$EF = \frac{EDV-ESV}{EDV} \times 100\% \quad FS = \frac{(LVIDd-LVIDs)}{LVIDd} \times 100\%.$$

Thus, the EF is an indicator of LV volume changes while FS is an indicator of LV diameter changes. In other words, EF interprets the 3-dimensional changes of LV chamber while FS interprets 2-dimensional changes. Furthermore, the FS can be used to interpret the contraction and relaxation behavior of a single cardiomyocyte which is associated with length-tension relationship of the Frank-Starling mechanism (Andersen and Vik-Mo, 1982). As a result, both parameters are currently and widely used by cardiovascular scientists to evaluate overall cardiac function, thus, it is noteworthy to remind ourselves what each parameter represents.

The structural aspect of left ventricle also needs to be rigorously evaluated. This assessment was implemented by examining left ventricular volume changes during systole and diastole. By using the B-mode echocardiography, measurement of LV volume changes in each cardiac cycle was performed. Mice in group 3 display ESV and EDV values of **67.45 µL** ± 23.48 and **96.91 µL** ± 24.71 at 2 weeks post-surgery and **77.78 µL** ± 29.57 and **109.40 µL** ± 25.93 at 4 weeks post-surgery, respectively and mice in group 4 display ESV and EDV values of **79.85 µL** ± 24.86 and **117.8 µL** ± 27.43 at 2 weeks post-surgery and **95.24 µL** ± 31.48 and **121.8 µL** ± 32.29 at 4 weeks post-surgery, respectively (Figure 12, Table 1). In contrast to mice in groups 3 and 4 that received MI surgery, mice in the sham surgery groups (i.e. groups 1 and 2) showed

Figure 12.

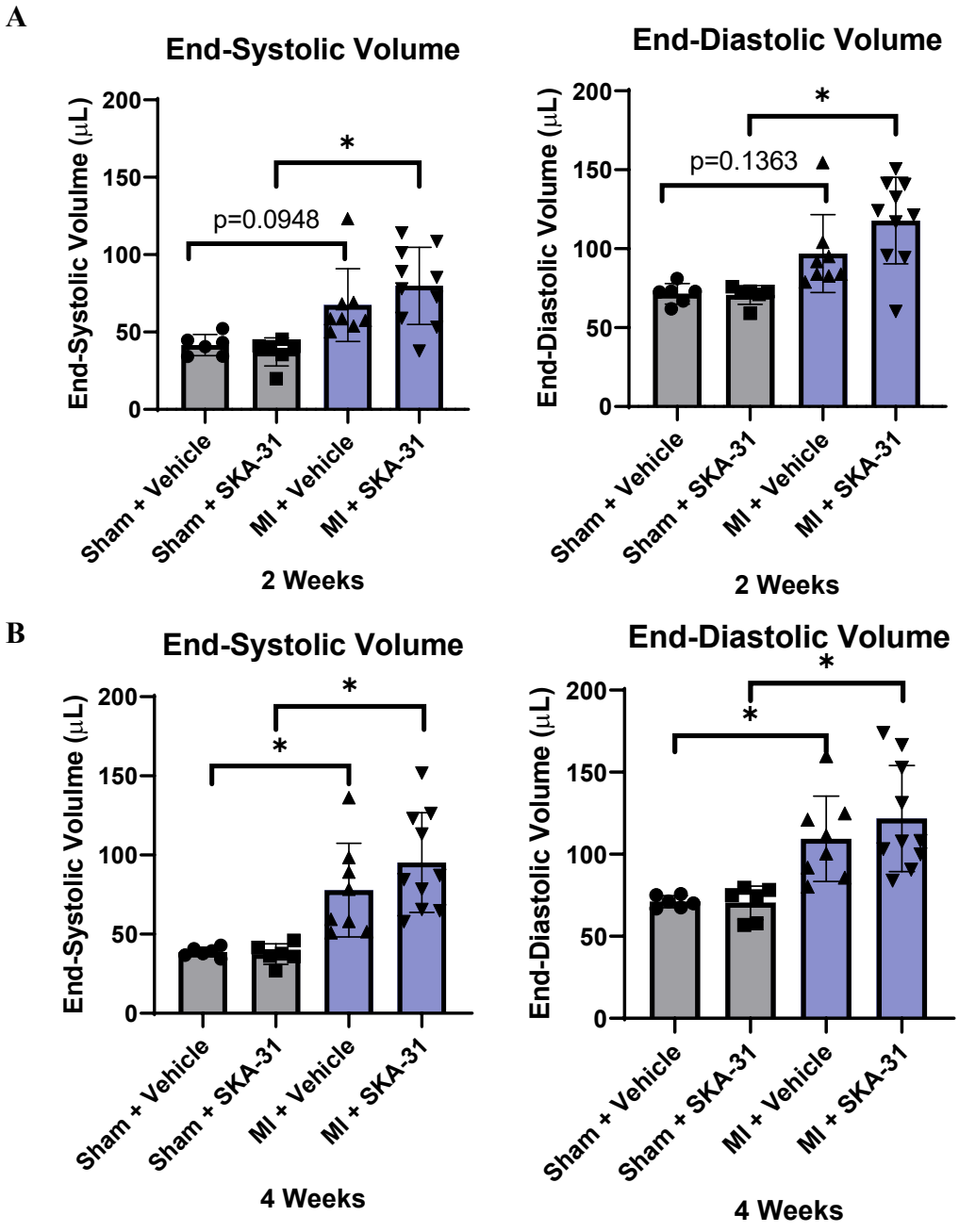

Figure 12. Echocardiographic (B-mode) measurement of LV ESV (End-Systolic Volume) and EDV (End-Diastolic Volume). **[A]** 2-weeks post-surgery (Sham/MI) measurement **[B]** 4-weeks post-surgery (Sham/MI) measurement. Data presented as mean ± SD, n = 6-10. * = $p<0.05$, two-way ANOVA and Tukey post-hoc test.

ESV and EDV values of ~40μL and ~70μL, respectively (Table 1). These values are significantly less than those observed in the MI surgery groups, which showed ESV and EDV values of ~70μL and ~110μL, respectively. However, as previously indicated, there is also an interesting trend that can be found between group 3 and group 4 at both 2- and 4-weeks post-surgery. Compared to group 3, mice in group 4 display slightly elevated values of ESV and EDV. Again, there is no statistically significant difference between groups 3 and 4, but it is important to pay attention to this trend and consider these observations in the overall interpretation of the data.

Overall, the experimental data clearly indicate that MI injury was induced by surgical ligation of LAD artery which triggered left ventricular volume enlargement and decreased systolic function of the LV. These overall significant functional and structural LV modifications observed in this study are consistent with previously reported investigations which defines infarction as geometrical and physiological changes by wall thinning, increases in LV dimensions and volumes, and decreases in FS and EF (Gao et al., 2010a; Gao et al., 2000; Lindsey *et al.*, 2018a). Thus, the surgical approach that is used in this project certainly established the MI model in our adult male mice.

3.2 SKA-31 treatment did not induce significant impact on sham-operated mice

Identical cardiac function assessments were implemented with mice undergoing sham surgery (Group 1 and Group 2). By carefully examining the pattern of the data, it is possible to notice that there is no significant difference between group 1 (Sham + Vehicle) and group 2 (Sham + SKA-31) in terms of EF and FS (Figure. 11). The EF and FS values of group 1 are **49.51%** ± 4.66 and **24.93%** ± 2.77 at 2 weeks post-surgery and **49.00%** ± 2.64 and **24.58%** ± 1.61 at 4 weeks post-surgery, respectively (mean +/- SD). The EF and FS values of group 2 are

50.95% ± 7.82 and **25.93%** ± 4.97 at 2 weeks post-surgery and **47.74%** ± 5.28 and **23.89%** ± 3.18 at 4 weeks post-surgery, respectively (Figure 11, Table 1). Therefore, the SKA-31 treatment utilized in the sham surgery group did not affect the overall systolic function of heart.

In addition to the assessment of systolic function of LV, structural evaluations were implemented in sham-operated mice. At 2 weeks post-surgery, mice in group 1 displayed values of End-Systolic Volume (ESV) and End-Diastolic Volume (EDV) of **41.55 µL** ± 6.86 and **71.43 µL** ± 6.47 at 2 weeks post-surgery and **38.68 µL** ± 3.00 and **71.08 µL** ± 3.74 at 4 weeks post-surgery, respectively. Mice in group 2 display values of ESV and EDV of **37.20 µL** ± 9.07 and **70.69 µL** ± 5.95 at 2 weeks post-surgery and **37.43 µL** ± 6.44 and **70.35 µL** ± 10.23 at 4 weeks post-surgery, respectively (Figure 12, Table 1). Thus, again, the SKA-31 treatment in the sham surgery group did not significantly affect the left ventricular volume values compared to the sham surgery group that received the drug vehicle treatment.

These echocardiographic measurements were implemented at two different time-points: 2- and 4-weeks post-surgery. The 2-week time point was used to confirm the successful establishment of MI by evaluating (1) electrocardiogram (ECG) measurement by Vevo 3100 FUJIFILM Visual Sonics instrument (2) M-mode echocardiography (absence of systolic and diastolic movement of LV wall) (Figure. 7) (3) B-mode echocardiography (sagittal view of left ventricle) (Figure. 8). Furthermore, this 2-week time point acted as a mid-point evaluation of cardiac function which also allowed monitoring of the overall impact of SKA-31 treatment during the initial stage of pharmacological intervention. In addition, the second echocardiographic measurements at 4 weeks post surgery were implemented to assess overall impacts of long-term administration of SKA-31.

3.3 Left Ventricle undergoes robust compensatory events after the onset of MI

In addition to the echocardiographic measurements, P-V loop analysis was implemented at 6 weeks post-surgery as a terminal procedure. The primary purpose of P-V loop analysis was to obtain information with regards to pressure aspects and contractility of the left ventricle. Also, this invasive technique provided quantitative measurements of both left ventricular volume and pressure. The major parameters that were evaluated include: EF, ESV, EDV, P_{es}, P_{ed}, P_{dev}, dP/dt_{max}, dP/dt_{min}, Tau, ESPVR, EDPVR and PRSW (Table. 2). The parameters of EF, ESV, EDV, P_{es}, P_{ed}, P_{dev}, dP/dt_{max}, dP/dt_{min} and Tau were measured during baseline measurements with the presence of mechanical ventilation (Figure. 9). As illustrated in Figure 13, the overall patterns of EF, ESV and EDV are comparable to the values obtained via echocardiography. Thus, these findings indicate that the measurements that were implemented via echocardiography and P-V loop analysis are consistent and act as a further confirmation of the precision and reliability of our measurements. However, the left ventricular pressure measurements illustrate a somewhat different pattern. At the end of the 6-week study period, there was no identifiable difference among all 4 groups. As illustrated in Figure 14A, mice in both the sham surgery and MI surgery groups showed ESP values of ~80-90 mmHg and EDP values of ~10-13 mmHg. However, the elevation of EDP in group 4 compared to the rest of groups needs to be recognized. The modest and statistically insignificant elevation of EDP observed in group 4 could be associated with (1) imperfect relaxation of left ventricle (Leite-Moreira, 2006) (Opie., 1991) (2) severe LV wall thinning which creates a blood reservoir that has not been ejected properly during the systole, which can lead to a pressure overload within left ventricle. However, there is no statistically significant difference between EDP values in groups 3 and 4. Moreover, the P_{dev} is ~80% for all 4 groups (Figure. 14B). This fact can indicate

Figure 13.

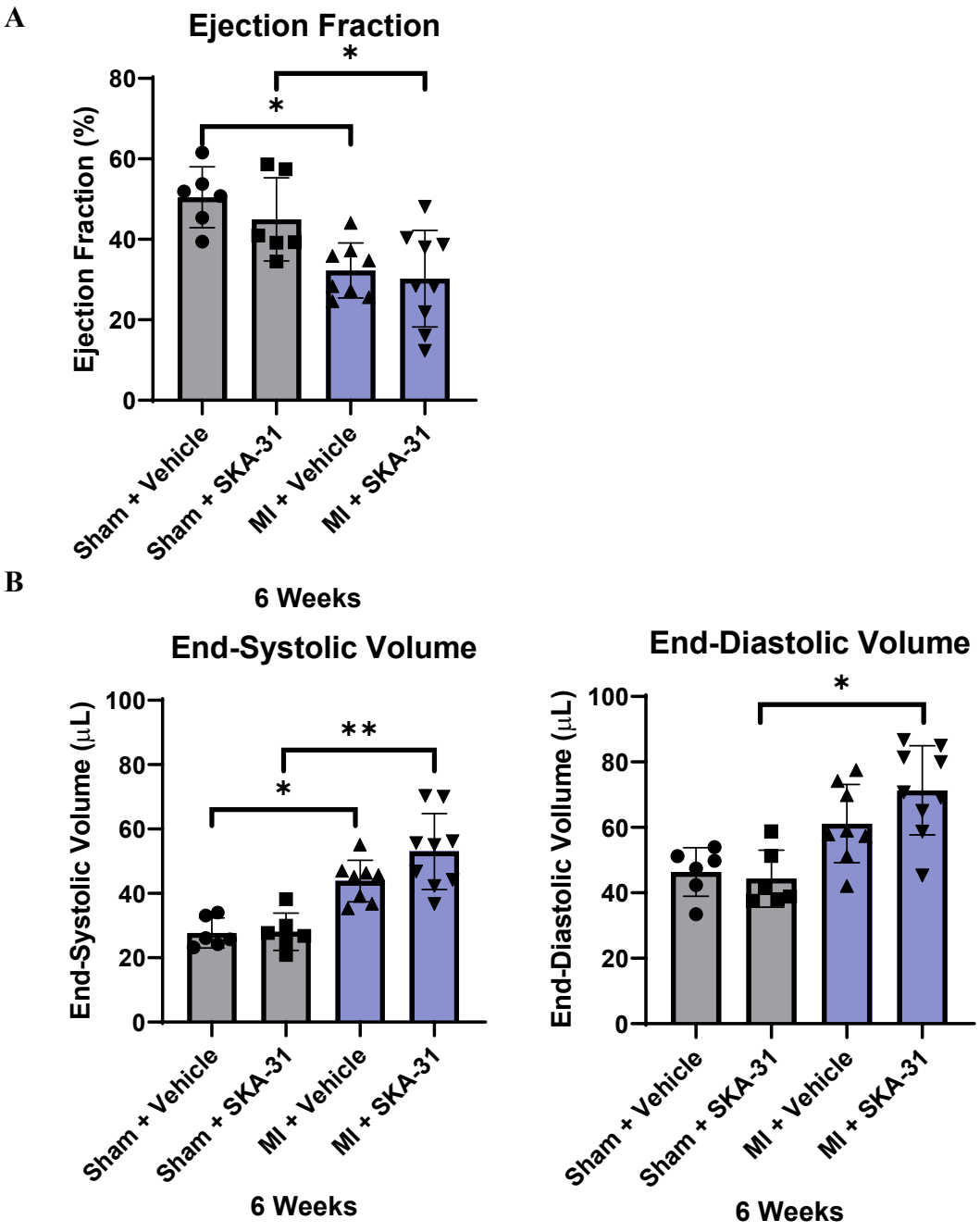

Figure 13. P-V loop measurement of LV **[A]** EF (Ejection Fraction), **[B]** ESV (End-Systolic Volume) and EDV (End-Diastolic Volume) at 6-weeks post-surgery (Sham/MI) measurement. Data presented as mean ± SD, n = 6-10. *=$p<0.05$, **=$p<0.0001$, two-way ANOVA and Tukey post-hoc test.

Table 2.

Parameters Measured	Sham + Vehicle (n=6)	Sham + SKA-31 (n=6)	MI + Vehicle (n=8)	MI + SKA-31 (n=10)
EF (%)	50.46 ± 7.55	44.99 ± 10.34	32.24 ± 6.83*	30.23 ± 11.99#
ESV (µL)	27.72 ± 4.68	28.08 ± 5.83	43.85 ± 6.47*	53.01 ± 11.76 ##
EDV (µL)	46.38 ± 7.42	44.35 ± 8.73	61.16 ± 11.98	71.32 ± 13.61 #
P_{es}(mmHg)	83.93 ± 15.77	86.81 ± 14.87	91.09 ± 11.58	98.67 ± 4.33
P_{ed} (mmHg)	10.25 ± 5.52	9.30 ± 4.01	9.46 ± 3.89	13.37 ± 4.87
P_{dev} (mmHg)	83.00 ± 12.50	87.71 ± 12.62	87.59 ± 13.22	92.62 ± 5.99
dP/dt_{max} (mmHg/s)	6299 ± 1546	6381 ± 2303	6906 ± 1911	6563 ± 1209
dP/dt_{min} (mmHg/s)	-5014 ± 1414	-5526 ± 1698	-5578 ± 1943	-5209 ± 1062
Tau (ms)	9.10 ± 2.21	8.22 ± 1.30	9.42 ± 2.97	10.93 ± 2.52
ESPVR (Slope)	3.19 ± 0.84	3.64 ± 0.74	3.33 ± 1.31	3.63 ± 1.53
EDPVR (Slope)	0.35 ± 0.08	0.35 ± 0.09	0.65 ± 0.21	0.56 ± 0.32
PRSW (mmHg × µL)	50.27 ± 14.00	50.35 ± 11.57	50.58 ± 15.91	66.98 ± 16.81
HR (BPM)	451.9 ± 69.97	458.7 ± 77.92	460.5 ± 26.95	475.2 ± 52.20

Table 2. (Pressure-Volume loop analysis) Functional and structural parameters measured following 6-weeks post treatment with vehicle/SKA-31 in sham and MI operated mice. Data are presented as means ± SD calculated from 6-10 animals. * = $p<0.05$, ** = $p<0.0001$ between groups 1 and 3, two-way ANOVA and Tukey post-hoc test. # = $p<0.05$, ## = $p<0.0001$ between groups 2 and 4.

EF – Ejection Fraction; **ESV** – End-Systolic Volume; **EDV** – End-Diastolic Volume; $\boldsymbol{P_{es}}$ – End-Systolic Pressure; $\boldsymbol{P_{ed}}$ – End-Diastolic Pressure; $\boldsymbol{P_{dev}}$ – Developed Pressure; **ESPVR** – End-Systolic Pressure Volume Relationship; **EDPVR** – End-Diastolic Pressure Volume Relationship; **PRSW** – Preload Recruitable Stroke Work; **HR** – Heart Rate

Figure 14.

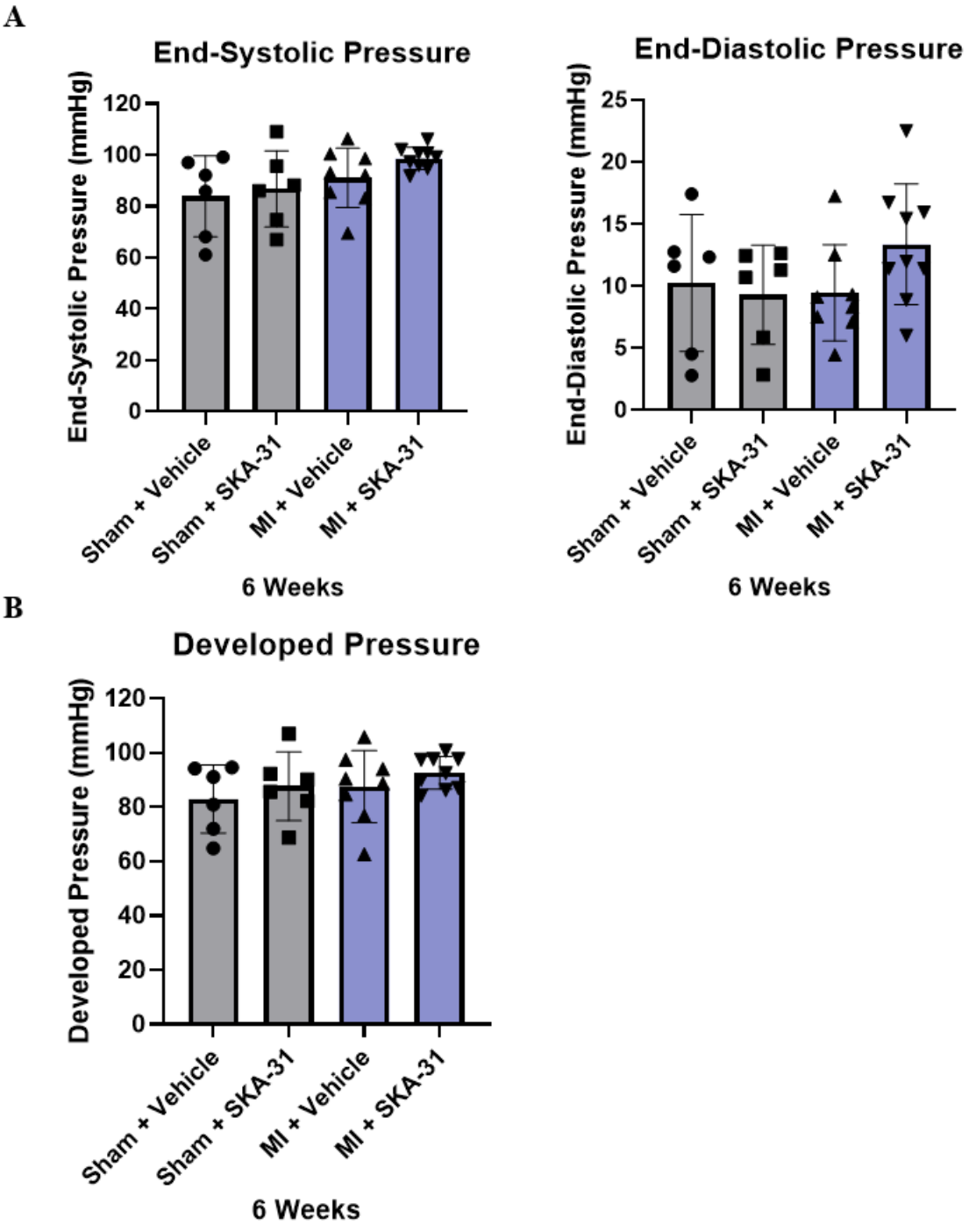

Figure 14. P-V loop measurement of LV **[A]** End-Systolic Pressure and End-Diastolic Pressure **[B]** Developed Pressure at 6-weeks post-surgery (Sham/MI) measurement. Data presented as mean ± SD, n = 6-10. No statistically significant differences were found among the 4 groups.

that (1) SKA-31 treatment did not affect the pressure aspects of LV function in mice that underwent either sham or MI surgery (2) the pressure changes during systole and diastole are not significantly impacted by the prior induction of an acute MI injury, due to subsequent robust compensatory mechanisms such as hypertrophy and adaptive LV remodeling that occurred by the 6-week time point. Moreover, the parameters that indicate information with regards to real-time left ventricular dynamics were measured: dP/dt_{max} and dP/dt_{min}. The dP/dt_{max} indicates the maximum derivative of change in pressure rise over time, whereas dP/dt_{min} indicates the maximum derivative of change in pressure fall over time. In other words, the dP/dt measurements implies information with regards to the cardiomyocyte's intracellular Ca^{2+}dynamics. The value of dP/dt_{max} can be interpreted as the rate of cytosolic Ca^{2+}elevation and binding to the myofilament protein Troponin C, which triggers the cardiomyocyte to contract. The value of dP/dt_{min} can be interpreted as the rate of Ca^{2+}unbinding from Troponin C, due to the sequestration of cytosolic free calcium by Sarcoplasmic-Endoplasmic Reticulum Ca^{2+}-ATPase (SERCA) and extrusion via the NCX. Therefore, dP/dt_{max} value can indicate overall rate of Excitation-Contraction (EC) coupling of cardiomyocytes and Ca^{2+} sensitivity of myofilaments. Furthermore, the time constant of isovolumic relaxation (Tau) was measured. This is also another common parameter evaluated via P-V loop analysis that conveys information with regards to isovolumic relaxation (diastolic function) of LV.

As illustrated in the Figure 15 A, B and C, there is no statistically significant difference among all 4 groups. In all 4 groups, the dP/dt_{max} value is ~6000 mmHg/s and dP/dt_{min} value is ~-5000 mmHg/s. Also, the Tau value is ~10ms in all 4 groups (Figure. 15C). However, interestingly, the similar trend of elevated Tau value was detected from mice in group 4. This

potentially indicates that left ventricle requires more time to relax during isovolumic relaxation. Though, it is not a statistically significant difference.

Figure 15.

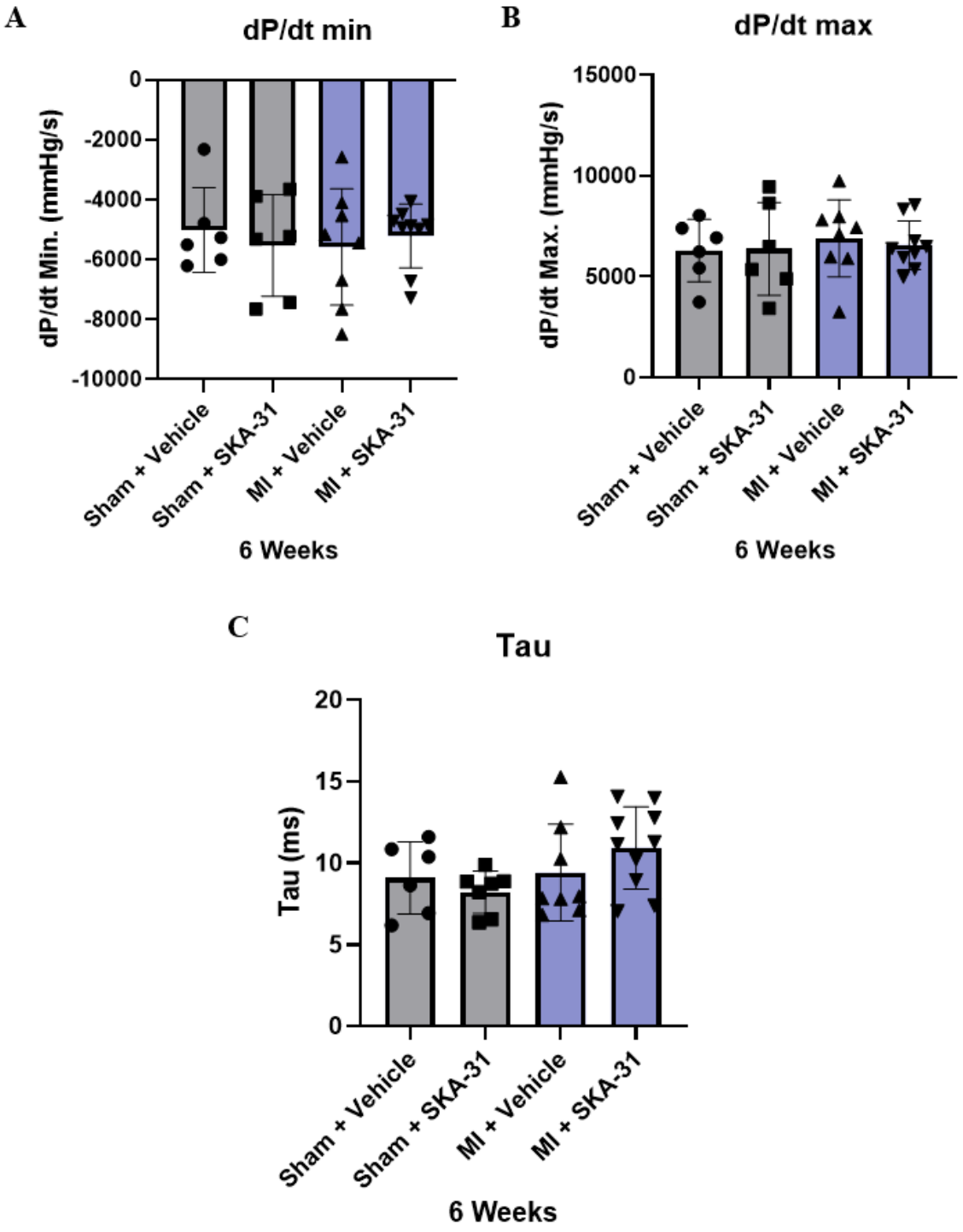

Figure 15. P-V loop measurement of LV **[A]** dP/dt_{max} **[B]** dP/dt_{min} **[C]** Tau at 6-weeks post-surgery (Sham/MI) measurement. Data presented as mean ± SD, n = 6-10. No statistically significant differences were found among the 4 groups.

Overall, the obtained data using P-V loop analyses indicate that (1) the presence of MI in the mice (i.e. group 3) did not have a significant impact on pressure changes in the LV during systole and diastole (2) SKA-31 treatment did not affect the systolic and diastolic function of LV in both sham and MI groups.

3.4 MI is associated with increase in LV wall stiffness and diastolic dysfunction

The other measurements that are routinely carried out by P-V loop analysis are the load-independent measurements, which were obtained by temporarily occluding the abdominal vena cava, which decreases the venous return to the heart. This manoeuvre allows for measurements of myocardial performance that are independent of loading conditions, which conveys information of left ventricular contractility and compliance. The parameters evaluated by this approach include: ESPVR, EDPVR and PRSW. The slope of ESPVR and EDPVR are obtained via linear relationships that derive from connecting multiple points of End-Systolic Pressure/Volume and End-Diastolic Pressure/Volume during temporary abdominal vena cava occlusion (Figure. 10).

As illustrated in Figure 16 A, B, and C, the slope of ESPVR is ~3 in all 4 groups along with PRSW values of ~50 $mmHg \times \mu L$ in all 4 groups. This further reinforces the idea that there is no significant impact of SKA-31 on systolic function of LV in both sham and MI group mice. However, there is noticeable trend found in the EDPVR measurements. In sham surgery groups, the slope of the EDPVR is ~0.3, but in the MI surgery groups, the EDPVR slope is ~0.7. The elevation of EDPVR slope indicates that the infarcted left ventricle shows decreased compliance, which shifted the End-Diastolic Pressure/Volume curve upward and to the left. This indicates that the LV with infarction is stiff and demonstrates diastolic dysfunction. However,

Figure 16.

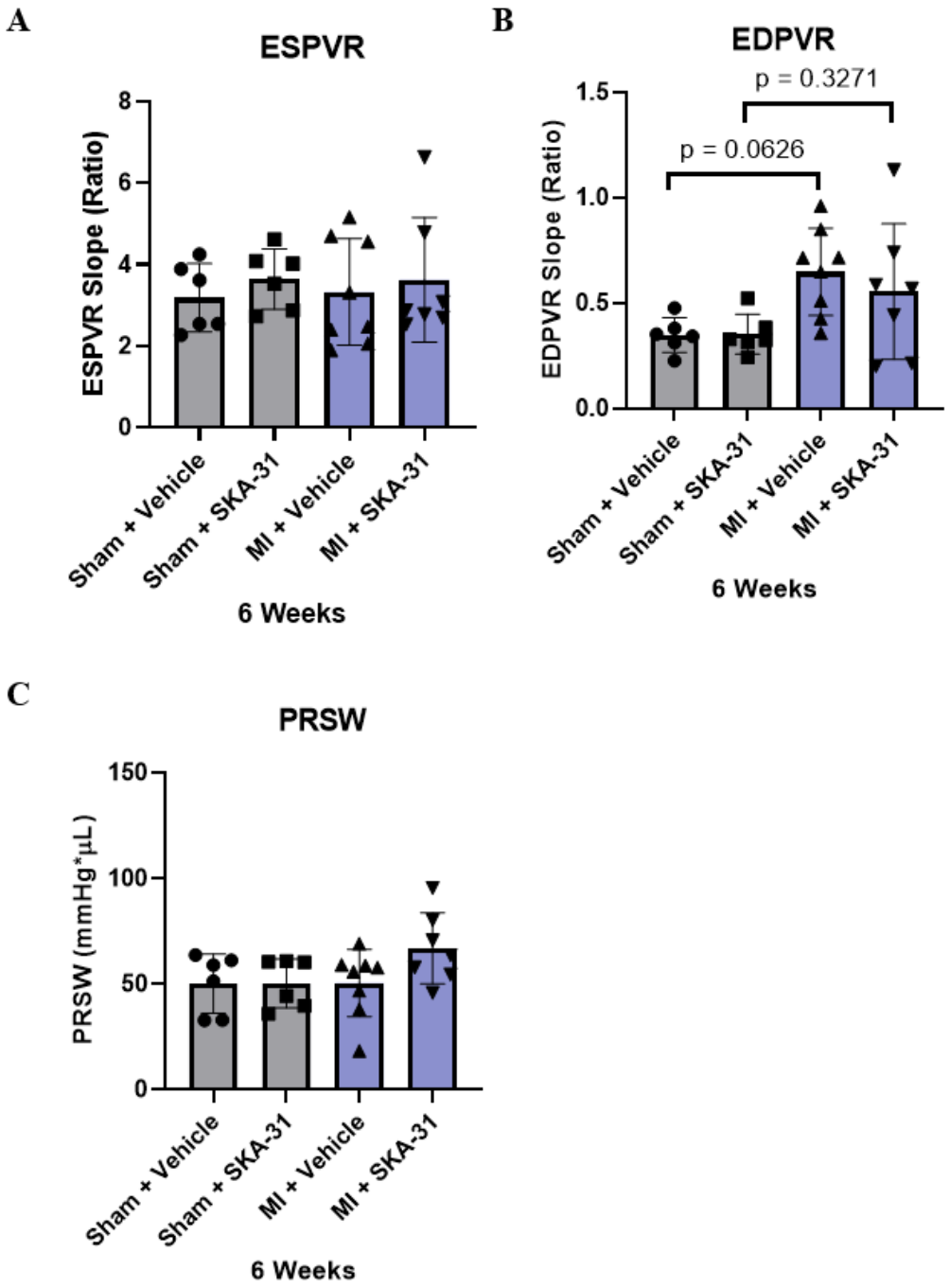

Figure 16. P-V loop measurement of LV **[A]** ESPVR (End-Systolic Pressure Volume Relationship) **[B]** EDPVR (End-Diastolic Pressure Volume Relationship), p = 0.0626 between group 1 and 3, p = 0.3271 between group 2 and 4, two-way ANOVA **[C]** PRSW (Preload Recruitable Stroke Work) at 6-weeks post-surgery (Sham/MI) measurement. Data presented as mean ± SD, n = 6-10. No statistically significant difference found among the 4 groups.

there is no significant difference between groups 1&2 and groups 3&4, which indicates that there are no significant effects of SKA-31 treatment in both the Sham and MI operated mice. Furthermore, over the ~6 week time course of my study, neither SKA-31 treatment nor establishment of MI in mice affected animal growth/body weight (please see the Appendix: Figure S13-S14).

3.5 Heart rate remained constant in all 4 groups

In addition to functional and structural parameters, the heart rate of mice was measured via both echocardiography and P-V loop analysis. Heart rate is an important parameter since it is one of the major determinants of overall cardiovascular homeostasis as evidenced by the mathematical relationship of

$$Cardiac\ Output = Heart\ Rate\ \times Stroke\ Volume$$

Also, the heart rate is positively correlated with EF and FS therefore, it needs to be stably maintained to precisely assess the left ventricular performance (Lindsey *et al.*, 2018b). As illustrated in Figure 17, the heart rate is stable and consistent among the 4 groups with values of ~400-420 beats per minute (BPM) at 2-, 4- and 6-weeks post-surgery. A heart rate of >400 BPM is reported to be within the physiological range of murine heart rate under isoflurane anesthesia (Lindsey *et al.*, 2018b). Also, it is important to avoid a heartrate that is >650 BPM suggesting activation of autonomic nervous system and <400 BPM suggesting deep anesthesia which overall can negatively influence the interpretation of cardiac function (Lindsey *et al.*, 2018b). However, as illustrated in Figure 17 A, B and C, the experimentally obtained heart rates via both echocardiography and P-V loop analysis at 2-, 4-, and 6-weeks post surgery do not depict any statistically significant differences among all 4 groups. This observation suggests that SKA-31 treatment did not affect the heart rate in either the sham or MI operated mice.

Figure 17.

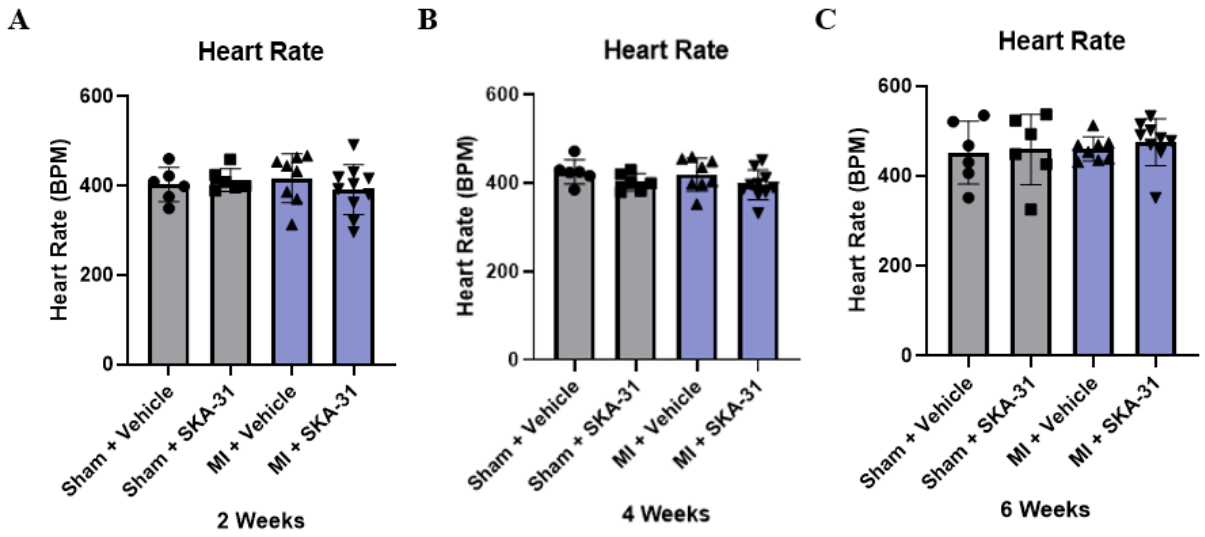

Figure 17. Echocardiographic measurement of HR (Heart Rate) (M-mode) **[A]** at 2-weeks post-surgery (Sham/MI) measurement [**B]** at 4-weeks post-surgery (Sham/MI) measurement **[C]** P-V loop measurement of HR at 6-weeks post-surgery (Sham/MI). Data presented as mean ± SD, n = 6-10.

3.6 Cardiac fibrosis is associated with the onset of MI

Lastly, histological analysis (i.e. H & E and PSR staining) was implemented to assess the size of the surgically induced infarction and subsequent fibrosis in the LV at 6-7 weeks following the initial surgical procedure. The size of the infarct was measured using two different regions of the LV: the mid-myocardium and apical myocardium. As illustrated in Figures 18 and 20, no unusual fibrosis was observed in the sham surgery mice receiving either drug vehicle or SKA-31 treatment. However, noticeable fibrosis was observed in the MI surgery mice that received either vehicle or SKA-31 treatment (i.e. groups 3 and 4) (Figures 19 and 20). In the mid-myocardium of the LV, the group 3 mice showed ~8% infarction and the group 4 showed ~15% infarction. In apical region of the LV, both group 3 and group 4 mice showed ~30% infarction. These observations indicate that the extent of fibrosis in the mid-myocardium showed an elevated value in group 4 compared to group 3, however, the difference was not statistically significant. Somewhat unexpectedly, I also did not observe a statistically greater amount of fibrosis in mid-myocardium in the MI surgery mice treated with vehicle compared with sham mice treated with vehicle (groups 1 & 3, $P = 0.5123$). Even though the change in fibrosis was >5-fold, there was considerable scatter in the data that obscured this difference (see Figure 20). However, in the case of the sham surgery and MI surgery mice treated with SKA-31 (i.e., groups 2 & 4), I did note a statistically greater amount of fibrosis in the mid-myocardium of MI surgery mice ($P = 0.0290$). However, there is no statistical difference in the extent of fibrosis in the mid-myocardium between groups 3 and 4.

In the case of the apical myocardium, I did observe a greater level of tissue fibrosis in MI surgery mice receiving vehicle treatment compared to sham surgery for mice treated with vehicle (groups 1 & 3, Figure 20). A similar situation was observed when comparing MI surgery mice to

sham surgery mice treated with SKA-31. No statistically significant differences in the extent of fibrosis in the apical myocardium were observed between the sham surgery mice receiving either vehicle or SKA-31 treatments (i.e. groups 1 & 2). I also did not find any differences in the extent of fibrosis in MI surgery mice receiving either treatment regimen (groups 3 & 4).

Figure 18.

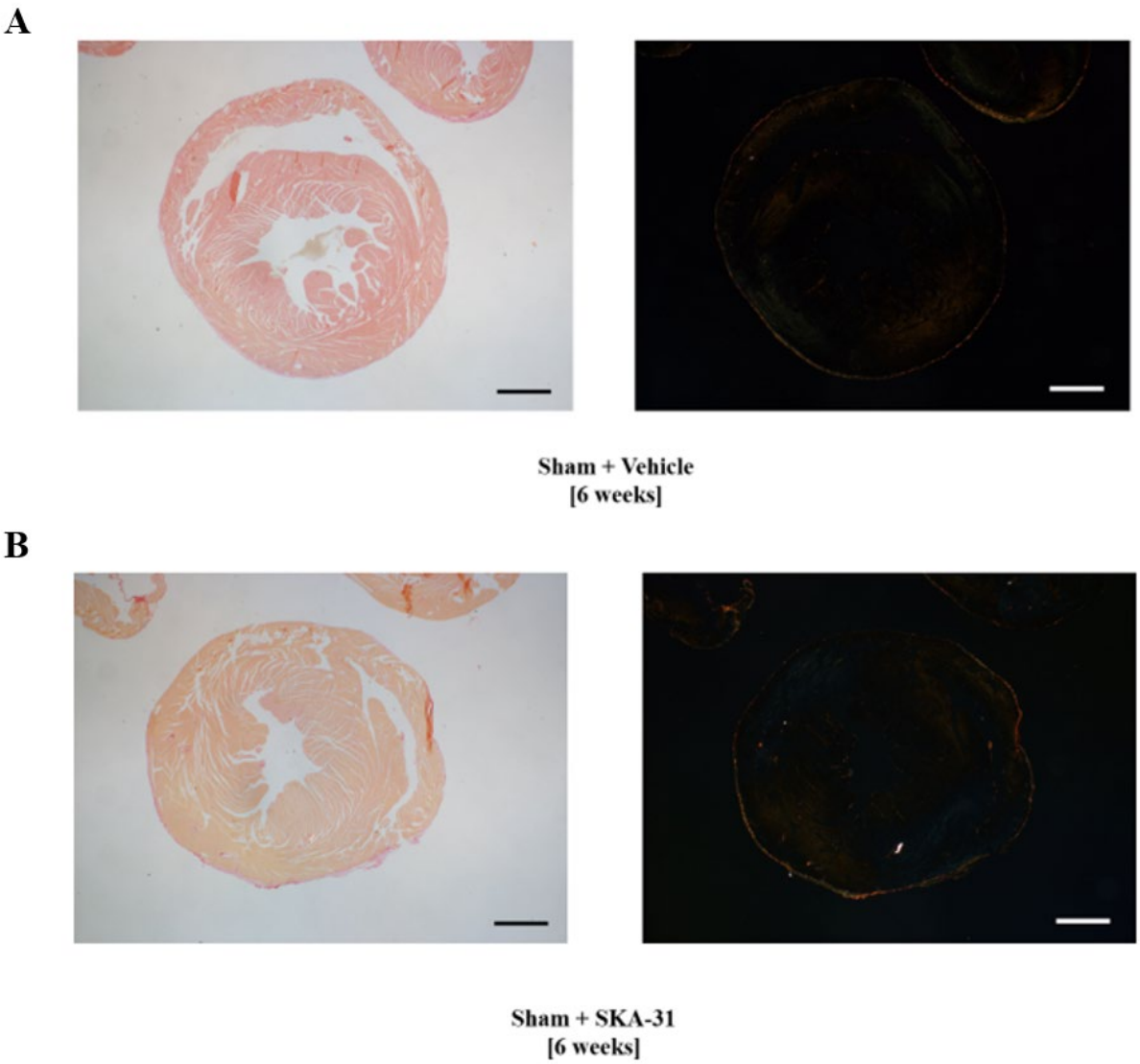

Figure 18. Sham Groups (Group 1 and Group 2) Representative images of mouse heart LV with PSR staining. Both images were taken at 1.25x magnification. The image in panel **[A]** was taken under bright field conditions and the image in panel **[B]** was taken with polarzied fluorescent light. The illuminated regions in the polarized light image indicate fibrosis. Scale bars = 1 mm

Figure 19.

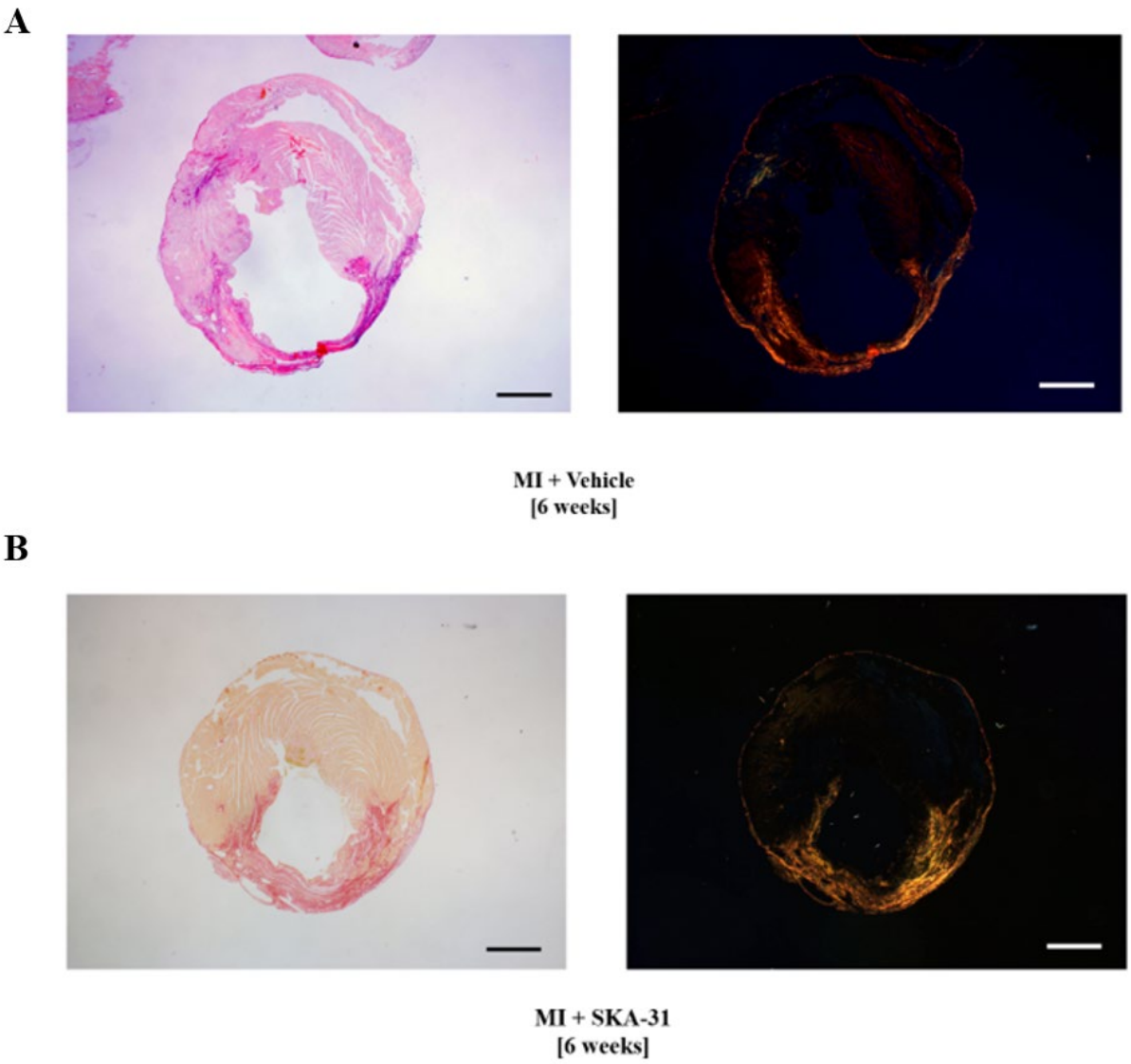

Figure 19. MI Groups (Group 3 and Group 4) Representative images of mouse heart LV with PSR staining. Both images were taken at 1.25x magnification. The image in panel **[A]** was taken under bright field conditions and the image in panel **[B]** was taken with polarzied fluorescent light. The illuminated regions in image **[B]** indicate the region of fibrosis, which implies the infarction area. Scale bars = 1 mm

Figure 20.

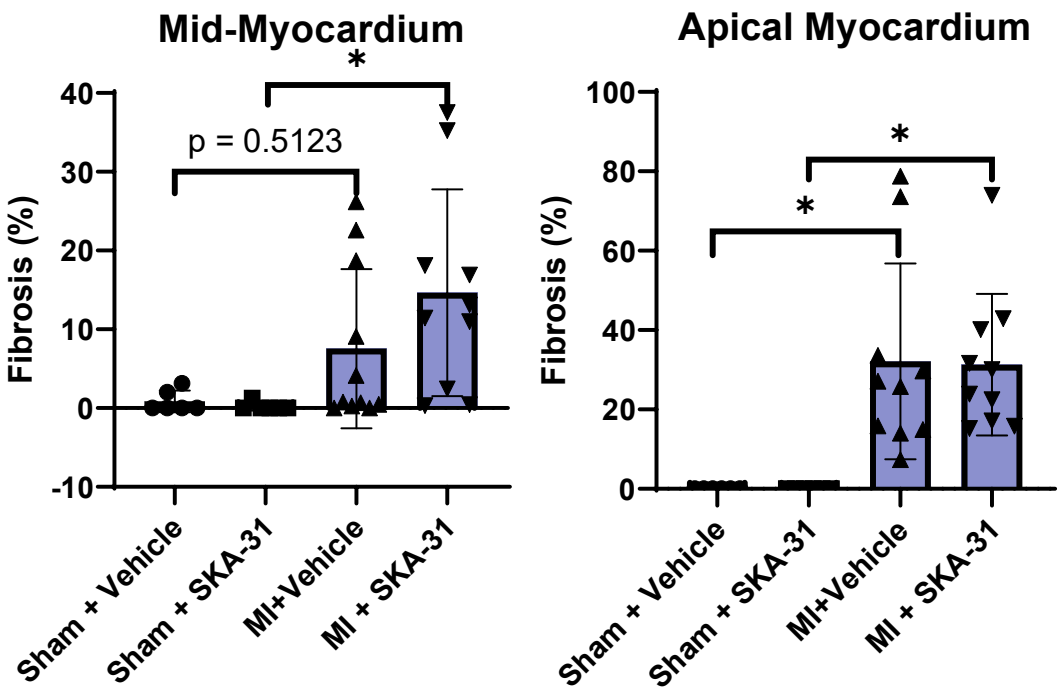

Figure 20. Histological assessment of mouse heart LV. The size of the infarct was measured from transverse sections of LV at mid-myocardium and apical myocardium at 6 weeks post-surgery (Sham/MI) measurement. Data presented as mean ± SD, n = 6-10. * = $p<0.05$, two-way ANOVA and Tukey post-hoc test.

3.7 Plasma concentration of SKA-31

To evaluate that the daily ingestion of SKA-31 led to pharmacologically relevant levels of drug in the circulation, I measured the steady-state concentration of SKA-31 in plasma samples prepared from mice administered SKA-31 either by oral gavage or feeding using a formulation of SKA-31 in condensed milk. In a group of male C57BL/6 mice (12-14 weeks of age, n = 5) administered SKA-31 (10 mg/kg) daily via oral gavage, blood samples were collected on Day 1, 3 and 7 to evaluate the level of SKA-31 within the blood plasma. A second group of 5 male C57BL/6 mice (12-14 weeks of age) ingested SKA-31 (10 mg/kg) daily in a mixture with condensed milk; total volume of ~200 µL consisting of 50 µL of SKA-31 mixture and 150 µL of condensed milk. The blood samples from this group were collected on Day 8 (Table. 3). The mice that received SKA-31 by oral gavage demonstrated average plasma concentration of 400 – 540 nM and and mice that ingested SKA-31 in a mixture with condensed milk displayed a steady-state SKA-31 plasma concentration of ~360 nM. The interval between the final SKA-31 administration and blood sample collection was approximately 20 hours. These data indicate that the steady state plasma concentrations of SKA-31 achieved by these two methods are comparable. In addition, as described in the Introduction section, SKA-31 displays selectivity for $K_{ca}2/3$ channels with an EC_{50} ~0.3 µM for $K_{ca}3.1$ channels and EC_{50} ~2 µM for $K_{ca}2.3$ channels (Sankaranarayanan *et al.*, 2009). Thus, the established steady state plasma concentration of 350 – 540 nM was likely sufficient to sensitize endothelial $K_{ca}2/3$ channels in vivo.

Table 3.

Mouse	Day 1 Concentration (nM)	Day 3 Concentration (nM)	Day 7 Concentration (nM)	Day 8 Concentration (nM)
M1 Oral Gavage	652	467	852	N/A
M2 Oral Gavage	639	246	228	N/A
M3 Oral Gavage	385	209	290	N/A
M4 Oral Gavage	251	1048	400	N/A
M5 Oral Gavage	558	747	227	N/A
M6 SKA-31 with Condensed Milk	N/A	N/A	N/A	251
M7 SKA-31 with Condensed Milk	N/A	N/A	N/A	328
M8 SKA-31 with Condensed Milk	N/A	N/A	N/A	459
M9 SKA-31 with Condensed Milk	N/A	N/A	N/A	356
M10 SKA-31 with Condensed Milk	N/A	N/A	N/A	405
Mean	497nM ± 174	543nM ± 354	400nM ± 263	360nM ± 79

Table 3. Plasma concentration of SKA-31 after 7 days of administration. M1-M5 mice received 10 mg/kg SKA-31 daily via oral gavage and blood samples were collected on Day 1, 3 and 7. M6-10 mice ingested 10 mg/kg SKA-31 daily as a mixture in condensed milk (total volume of 200 µL = 50 µL SKA-31 + 150 µL condensed milk) and blood samples were collected on Day 8.

Chapter 4: Discussion

The positive prognosis of MI patients is highly correlated with immediate and successful long-term restoration of coronary blood flow to the injured myocardium. Thus, when a patient with an acute MI (AMI) is admitted to the hospital, medical staff often attempt to vasodilate the coronary arteries and improve the overall hemodynamics of the systemic circulation (Anderson and Morrow, 2017). Subsequent procedures such as Percutaneous Coronary Intervention (PCI) or Coronary Artery Bypass Grafting (CABG) can be implemented to improve coronary hemodynamics by dilating a stenosed artery or to establish bypass circulation to an ischemic zone, respectively. The decision to proceed with these invasive procedures can be made by examining the severity of the infarction and confirming which coronary branch is blocked via coronary angiography (Anderson and Morrow, 2017). Furthermore, many pharmacological interventions to mitigate the severity of MI involve attempts to dilate the coronary arteries and arteries of systemic circulation (Holt and Pang, 2019). In the case of AMI, coronary spasm can occur as a means to fulfill the metabolic demand of the ischemic myocardium and prolonged duration of MI can lead to heart failure, which is associated with increase in PVR and vascular myogenic tone (Gschwend *et al.*, 2003; Ledoux *et al.*, 2003; Sambuceti et al., 1997). Therefore, it is important to emphasize that these attempts to vasodilate the arteries need to be implemented as soon as AMI is established (Anderson and Morrow, 2017; Sambuceti *et al.*, 1997). The primary purpose of vasodilation is to increase blood perfusion to the damaged area to promote tissue healing and reduce the amount of stress put on the myocardium by lessening PVR (i.e., afterload). Thus, in this project, the pharmacological intervention of SKA-31 administration was introduced at 24-48 hours post-surgery as a novel strategy to mitigate the progression of MI-related injury. The primary intent of systemic administration of SKA-31 treatment was to sensitize vascular endothelial K_{Ca}2.x and K_{Ca} 3.1 channels, which participate directly in

endothelium-dependent vasodilation via membrane hyperpolarization and nitric oxide signaling and contribute to the overall health of the endothelium. These actions may thus promote more adaptive vascular myogenic responses when encountered in the context of a major adverse cardiovascular event (MACE), such a myocardial infarction.

As mentioned in the Introduction, the functional effects of the K_{Ca} channel activator SKA-31 have been observed in both cellular and tissue level experiments. Also, Mishra et al. reported previously that SKA-31 triggered vasodilation of the intact rat coronary circulation in a dosage dependent manner, which was observed via *ex vivo* experiments (i.e., Langendorff-style perfusion of isolated hearts). Thus, the anticipated effects of prolonged *in vivo* SKA-31 treatment immediately following the onset of MI are that this intervention would promote myocardial healing and enhance overall cardiovascular hemodynamics. Furthermore, since it is an *in vivo* treatment, it is important to recognize that SKA-31 may affect other cell and tissue types outside the vascular endothelium that express the same K_{Ca} channels. With regards to the pharmacodynamics and pharmacokinetic profile of the drug, Sankaranarayanan et al. reported that when SKA-31 was acutely administered intraperitoneally to rats (male, 9 – 11 weeks of age) with the dosage of 10 mg/kg, the total SKA-31 plasma concentration peaked at 2 h after the application with the value of 20.83 ± 1.45 μM and displayed a half-life of ~12h. Therefore, it is possible to state that SKA-31 represents a potentially valuable pharmacological tool that possesses desired pharmacokinetic properties of a moderately long half-life and a low plasma protein binding property (Sankaranarayanan *et al.*, 2009). Moreover, it is important to recognize the different EC_{50} values of SKA-31 between K_{Ca}2.x and K_{Ca} 3.1 channels. SKA-31 displays approximately 10-fold greater potency for K_{Ca}3.1 channels with the EC_{50} value of ~0.3 μM compared to EC_{50} value of ~2 μM for K_{Ca}2.3 channels (John et al., 2018). Thus, the K_{Ca}3.1

channels are more sensitive to SKA-31 and we would anticipate that this channel type may be enhanced to a greater extent following in vivo SKA-31 administration.

4.1 Prolonged in vivo SKA-31 treatment did not impact the cardiac function of sham operated mice

As illustrated in Figures 11, 12, 13, 14, 15, 16, 17, and 20, it is possible to state that there is no significant impact on cardiovascular function in sham surgery mice treated daily for 6-7 weeks with 10 mg/kg SKA-31 (i.e., group 2) or drug vehicle (group 1). Both systolic and diastolic functions of mice in group 2 are comparable to the measurements observed in group 1. As described in the Materials and Methods section, the sham surgery shared all the same surgical procedures as the MI operation except for the LAD coronary ligation. Also, the entire procedures and steps involved in measuring cardiac function via echocardiography and P-V loop analysis were identical in all 4 treatment groups. Therefore, it is possible to state that the SKA-31 treatment had no obvious effects on cardiovascular performance in mice that received the sham surgery. In previous investigations, our group has rigorously evaluated the effects of SKA-31 on different species, sex, vascular beds, and disease model animals. The pathological models include T2DM, hypertension and aging, which all share the endothelial dysfunction as a comorbidity (John *et al.*, 2020; Khaddaj-Mallat et al., 2018; Khaddaj Mallat et al., 2019; Mishra *et al.*, 2013; Mishra et al., 2021; Mishra *et al.*, 2016; Mishra et al., 2014). However, all the control groups from these investigations did not exhibit unusual or unexpected responses to either acute or prolonged SKA-31 administration. To carefully interpret this data, first, it is important to recognize the dosages that have been utilized in these investigations. As described in Results section of this thesis and the report from Sankaranarayanan et al, the dosage of 10 mg/kg/day establishes a steady-state level of SKA-31 in blood plasma that is enough to sensitize the K_{Ca} 2/3 channels (i.e. ~360 nM). In other words, the minimal dosage of SKA-31 was

intentionally used in the previous investigations to make the targeted endothelial K_{Ca} channels more sensitive or responsive to the upstream signal only when the primary stimulus is present, rather than activating the channels directly. This "priming" strategy was utilized to minimize direct activation of the endothelium by SKA-31, which might lead to unwanted side-effects. For example, the hyper-activation of $K_{Ca}2/3$ channels could lead to over-lasting hyperpolarization of the endothelium-SMC complex that can trigger an undesired decrease in PVR and BP, which can disturb normal organ perfusion. Furthermore, it is also important to consider the physiological and pathophysiological conditions of the overall cardiovascular system in sham surgery mice. In the control/sham groups of the previous investigations, along with this current study, the animals did not exhibit noticeable changes in their cardiovascular parameters (John *et al.*, 2020; Khaddaj-Mallat *et al.*, 2018; Khaddaj Mallat *et al.*, 2019; Mishra *et al.*, 2013; Mishra *et al.*, 2021; Mishra *et al.*, 2016; Mishra *et al.*, 2014). As cardiac function in these animals was already normal and blood vessels did not have significant progression of endothelial dysfunction, it is reasonable to anticipate that with the minimal dosage of the SKA-31, there should not be a significant impact of the drug in healthy mice. By using the experimental evidence from previous investigations as a reference, it is possible to state that the SKA-31 administration in sham groups of this project also had no significant impact since the overall cardiovascular system was relatively healthy. This is also evidenced by the fact that there was no statistically significant difference between group 1 and group 2 in both systolic and diastolic functions of heart.

4.2 Prolonged in vivo SKA-31 treatment did not significantly impact the cardiac function of mice with MI

By evaluating the data obtained from (1) ECG (2) M-mode echocardiography (3) B-mode echocardiography (4) P-V loop analysis and (5) histological analysis, it is possible to state that surgical ligation of LAD coronary artery successfully established MI in mice. The systolic and

diastolic functions of LV that underwent MI surgery displayed significant impairment that is consistent with the anticipation and results published from previous investigations of MI model mice (Gao *et al.*, 2010a; Gao *et al.*, 2000; Lindsey *et al.*, 2018a). In this project, to rigorously assess the hypothesis, the mice in group 3 (i.e., MI surgery + vehicle treatment) are very important since they serve as a baseline that forms the foundation to critically analyze the effects of SKA-31 under the conditions of MI injury. Therefore, multiple steps provided confirmation of the successful establishment of MI by independently analyzing the 5 categories mentioned above. The MI mice in this project exhibited (1) ECG with inverted QRS complex or ST-segment elevation (Figure 7B) (2) absence of inotropic and lusitropic movement of either anterior or posterior wall of LV (Figure 8B) (3) absence of LV movement in apex (distal to the ligation) (Figure 8B) (4) Significant decrease in EF and increase in ESV, EDV and EDPVR (Figures 11, 12 and 13) (5) ≥30% fibrosis (Figures 19 and 20). The same assessments were applied to group 4 as well. Thus, with the basis of the experimental evidence, it is possible to state that group 3 formed the robust MI group in this project that acted as a baseline for assessing effects mediated by SKA-31 in mice with MI-dependent injury.

As mentioned in Section 3.1 of the Results chapter, the overall pattern of the cardiac function and structure indicators such as EF, FS, ESV and EDV did not generate statistically significant differences between groups 3 and 4. However, there are some noticeable trends observed in group 4 that need to be recognized. Both EF and FS of group 4 are relatively more depressed compared with group 3 at both 2- and 4-weeks post-surgery (Table. 1). Furthermore, by carefully interpreting the data, it is possible to recognize that there is no noticeable difference in EF and FS of group 4 between 2 weeks (EF: **23.41%** ± 4.95, FS: **10.82%** ± 2.52) and 4 weeks (EF: **22.56%** ± 6.54, FS: **10.51%** ± 3.17) post-surgery that were measured by echocardiography.

On the other hand, the EF and FS parameters of group 3 showed a decreasing trend from 2 weeks (EF: **30.55%** ± 6.42, FS: **14.21%** ± 3.26) to 4 weeks (EF: **25.84%** ± 5.79, FS: **11.97%** ± 2.90) post-surgery. Also, the EF and FS values of group 4 are lower at both 2- and 4-weeks post-surgery compared to the values seen in group 3, although none of these differences were statistically significant. This pattern of data could potentially indicate that systolic function of LV was further compromised by SKA-31 treatment in group 4. Such aggravation in group 4 appears to be already established at 2 weeks post-surgery since EF and FS values are lower at 2 weeks compared to the group 3. Also, this lower value was static and maintained as seen in the data from subsequent echocardiographic measurements. A similar trend was observed from structural aspects of LV. The ESV and EDV of group 4 mice are both elevated compared to group 3 at both 2- and 4-weeks post-surgery. The ESV and EDV of group 3 display values of ESV: **67.45µL** ± 23.48 and EDV: **96.91µL** ± 24.71 whereas group 4 values are ESV: **79.85µL** ± 24.86 and EDV: **117.8µL** ± 27.43 at 2 weeks post-surgery. At 4 weeks post-surgery, group 3 displays value of ESV: **77.78µL** ± 29.57 and EDV: **109.4µL** ± 25.93 where group 4 displays value of ESV: **95.24µL** ± 31.48 and EDV: **121.8µL** ± 32.29. Although the values for a given parameter between groups 3 and 4 were not statistically different, these values suggest that volume enlargement was augmented with the SKA-31 administration at both 2 weeks and 4 weeks post-surgery. In other words, the early SKA-31 treatment that was implemented within 48 hours post-surgery may have impaired the recovery of overall cardiac function in terms of both functional (EF and FS) and structural (ESV and EDV) aspects.

From the P-V loop analysis, the parameters of EF, ESV and EDV were also measured. However, the trend of EF observed from the data obtained by P-V loop analysis was different from the trend seen in the data obtained by echocardiography. From P-V loop analysis, the mice

in group 3 demonstrated an average EF value of **32.24%** ± 6.83 and group 4 showed a EF value of **30.23%** ± 11.99 (Table. 2). Thus, it is possible to state that these two values are very compatible, 32% ≅ 30%. Based on these findings, the P-V loop analysis did not reveal a decreasing pattern in cardiac function between groups 3 and 4 similar to that observed from echocardiographic measurements. However, the overall trend of ESV and EDV values obtained by P-V loop analysis are comparable to the values obtained from echocardiography. The group 3 showed ESV: **43.85µL** ± 6.47 and EDV: **61.16µL** ± 11.98 where group 4 showed ESV: **53.01µL** ± 11.76 and EDV: **71.32µL** ± 13.61. Therefore, it is possible to notice that the mice that received SKA-31 treatment exhibited modestly elevated values of ESV and EDV. However, once again, the average values did not present statistically significant differences. Nonetheless, to thoroughly interpret the data, it is important to review the differences in the methodologies utilized between the echocardiography and P-V loop analysis. As mentioned in the Materials and Methods section, the cardiac function measurements carried out by echocardiography and P-V loop analysis were both under the influence of ~2% isoflurane. However, the major difference between the two techniques is the index of invasiveness. The echocardiography does not require any surgical procedures due to the technology of Doppler ultrasound probe that can penetrate the tissue and provide an image of the LV. On the other hand, the P-V loop analysis requires right carotid endarterectomy to retrogradely insert the micro-catheter (Length: 3.5 cm, Tip F Size: 1F, Electrode Spacing: 4.5 mm) into the LV chamber. As the catheter is required to be physically placed within the LV to measure volume changes (Figure. 21), this positioning of the catheter

Figure 21.

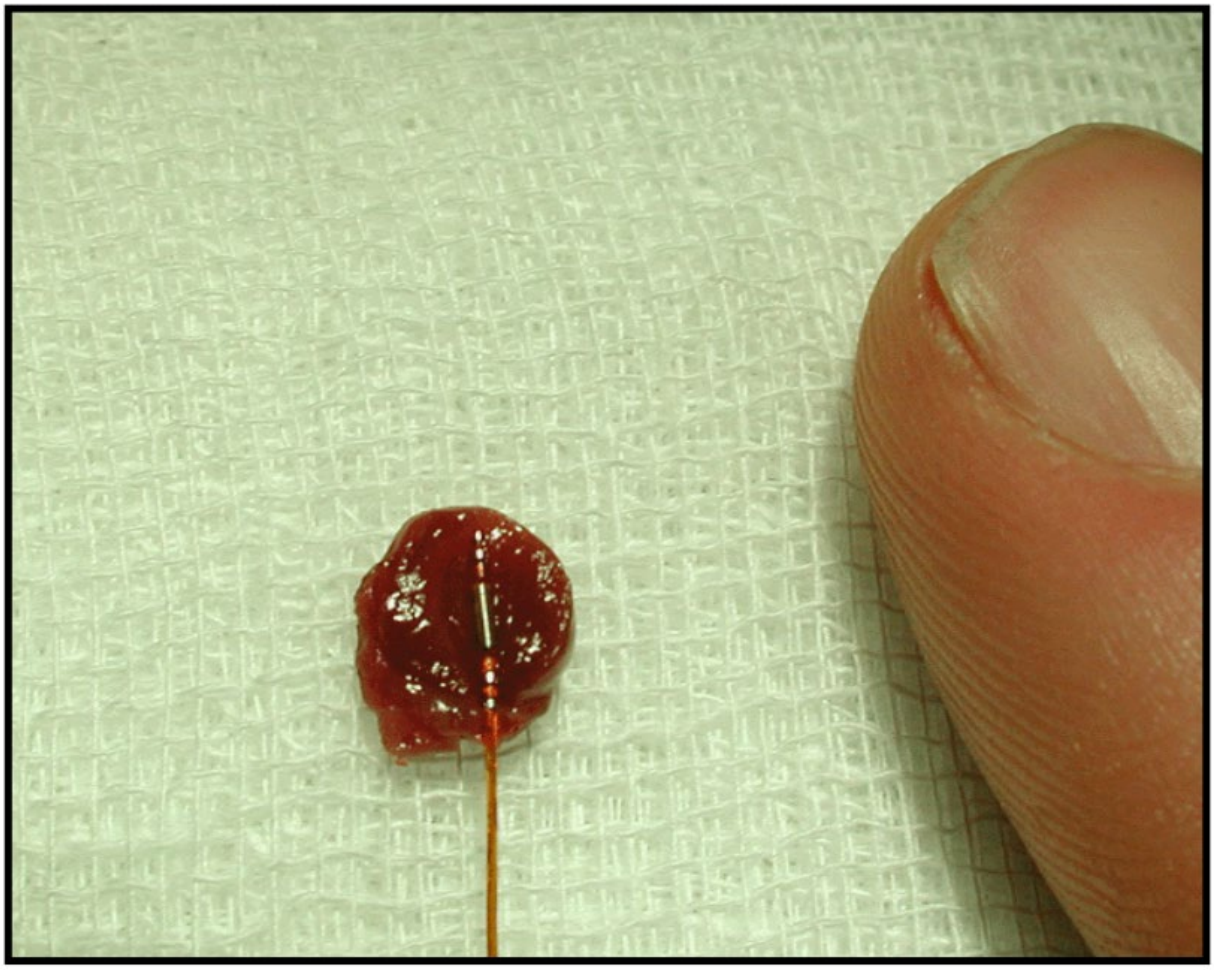

Figure 21. Presentation of the size of the Millar conductance-microcatheter. The catheter is positioned in the left ventricle from a longitudinally sliced murine heart. The tip of the catheter is placed in the apex of the heart, while the proximal part runs through the aortic valves. From top to bottom are seen two volume electrodes, the pressure sensor and at the bottom two volume electrodes. An index finger indicates the miniature size of the catheter.

[Taken from: Lips, D.J., van der Nagel, T., Steendijk, P., Palmen, M., Janssen, B.J., van Dantzig, J.M., de Windt, L.J., and Doevendans, P.A. (2004). Left ventricular pressure-volume measurements in mice: comparison of closed-chest versus open-chest approach. Basic Res Cardiol *99*, 351-359. 10.1007/s00395-004-0476-5.]

within the chamber could influence precise volume measurements. Lips et al. (2004) have suggested that the placement of the conductance-catheter may underestimate the true LV volume by a factor of 2-3. Volume measurements are calculated using the conductance function of the catheter (i.e., electric field between the current electrodes) with the formula:

$$V(t) = \rho L^2[G(t) - G^p]$$

$V(t)$ = left ventricular volume at time, t
ρ = mouse specific blood resistivity
L = distance between the sensor electrodes
G(t) = instantaneous conductance
G^p= parallel conductance,

When inserted into the LV chamber, the electric field of the conductance catheter may also detect the volumes of other structures (i.e., lungs and mediastinum) due to protrusion of the electric field into these structures. It is thus important to consider these data with the inclusion of this characteristic of P-V loop analysis. As described in the results section, the EF value is determined from the volume changes within the LV.

$$EF = \frac{EDV - ESV}{EDV} \times 100\%$$

Thus, due to the mentioned variables associated with the P-V loop catheter, the overall trend of EF observed from P-V loop analysis can be different from the trend observed from data obtained by echocardiography. Furthermore, by carefully looking at the values, the ESV and EDV values obtained by P-V loop analysis are less than the values obtained by echocardiography (Table. 4). Therefore, the underestimation of the volume measurements by conductance-catheter can be a logical reason why a discrepancy may be observed in EF, ESV, and EDV between echocardiography and P-V loop analysis.

Table 4.

MI + Vehicle (Group 3)	Echocardiography (2 weeks)	Echocardiography (4 weeks)	P-V Loop Analysis (6 weeks)
EF (%)	30.55 ± 6.42	25.84 ± 5.79	32.24 ± 6.83
ESV (μL)	67.45 ± 23.48	77.78 ± 29.57	43.85 ± 6.47*#
EDV (μL)	96.91 ± 24.71	109.4 ± 25.93	61.16 ± 11.98*#

MI + SKA-31 (Group 4)	Echocardiography (2 weeks)	Echocardiography (4 weeks)	P-V Loop Analysis (6 weeks)
EF (%)	23.41 ± 4.95	22.56 ± 6.54	30.23 ± 11.99
ESV (μL)	79.85 ± 24.86	95.24 ± 31.48	53.01 ± 11.76*#
EDV (μL)	117.8 ± 27.43	121.8 ± 32.29	71.32 ± 13.61*#

Table 4. Summary and comparison of the data obtained by echocardiography and P-V loop analysis in MI groups (Group 3 and Group 4). Data are presented as means ± SD calculated from 6-10 animals. * = $p<0.05$, between echocardiography (2 weeks) and P-V loop analysis (6 weeks). # = $p<0.05$, between echocardiography (4 weeks) and P-V loop analysis (6 weeks), Students' t-test.

Even though there are some limitations that are associated with P-V loop analysis, there is no doubt that such technique is a very useful strategy to obtain information with regards to the LV. The major strength of this approach is that it allows simultaneous measurement of LV pressure and volume *in vivo* under both load-dependent and -independent conditions (Pacher *et al.*, 2008; Shioura et al., 2007). In early stages of the P-V loop analysis, this technique was implemented mainly in larger animals and even in humans for the purpose of understanding left ventricular dynamics and diagnosis, respectively (Baan et al., 1984). However, as smaller animals started to be widely used in cardiovascular investigations, especially mice, the micro-catheter was developed. One of the major reasons why the P-V loop analysis in murine models started to be commonly used is that it allowed assessment of global cardiac function in genetically engineered murine models for studies of human diseases (Burkhoff et al., 2005; Pacher et al., 2004; Shioura *et al.*, 2007). Furthermore, with the pressure probe on the catheter, this technique allows the evaluation of pressure changes within the LV which is not possible with echocardiography. Thus, the major parameters of LV that were measured throughout P-V loop analysis in this project were P_{es}, P_{ed}, P_{dev}, dP/dt_{max}, dP/dt_{min}, Tau, ESPVR, EDPVR and PRSW. However, as described in the Results chapter, the overall trend observed from pressure aspects of LV function did not generate statistically significant differences among all 4 groups when measured 6-7 weeks post-surgery. The interpretation of the data from P-V loop analysis in this project needs to be done very carefully because immediately after the onset of MI, the LV rapidly initiates an adaptation process that is accompanied by robust left ventricular remodelling. In other words, the timing of P-V loop measurements is very important since the LV remodelling is a process that occurs over-time. Therefore, depending on when P-V loop analysis is performed relative to the stage of LV remodeling, it is possible that left ventricular

dynamics can be different, as suggested by my data. In this project, the P-V loop analysis was implemented at ~6 weeks post-surgery. The reason behind this decision is that P-V loop analysis acted as a terminal procedure due to its invasiveness. The 2nd echocardiographic measurements were conducted at 4 weeks post-surgery, so it was reasonable to provide enough time between the two procedures to minimize the potential confounding variables such as level of stress on the animal due to consecutive experiments and repeated exposure to the isoflurane. Moreover, Shioura et al reported that MI model mice (C57/BL6, male, 20-25g, n = 25) displayed significant cardiac function collapse starting after 6 weeks post-surgery using permanent LAD coronary artery ligation, which eventually led to HF at 10 weeks post-surgery (Shioura *et al.*, 2007).

In addition, Shioura et al investigated overall progression and impacts of MI on left ventricular function by implementing P-V loop analysis at different time points subsequent to the LAD coronary ligation: i.e. 2-, 4-, 6-, and 10-weeks post-MI. The overall pattern of P-V loop analysis at different time points post-infarction demonstrated right-shifted loops with decreased amplitude. This indicates LV volume is elevated with declined contractility. Shioura et al reported that LV with infarction initially displayed significant reduction in systolic function i.e., SW and ESPVR with the greatest decline at 2 weeks post to the MI and maintained the depressed value throughout the time-course of 10 weeks post to the infarction. This pattern of significant decline in systolic function was not observed in this study. However, interestingly, Shioura et al reported that a significant increase in ESV and EDV observed at 2 weeks post-MI (ESV: **91µL** ± 4, EDV: **109µL** ± 14) was reversed at 6 weeks post-MI (ESV: **61µL** ± 7, EDV: **78µL** ± 3) which is comparable with the values of the control group (ESV: **58µL** ± 8, EDV: **88µL** ± 14) (Shioura *et al.*, 2007). However, further enlarged volume values were observed at 10 weeks post-MI (ESV: **97µL** ± 6, EDV: **114µL** ± 25). This trend of restoration was generally observed at 4- and

6 weeks post-infarction. In other words, both systolic and diastolic function of LV displayed the greatest decline at 2 weeks post-MI but started to return towards normal values by 4 weeks post-MI with further restoration at 6 weeks post-MI. The cardiac indices that exhibited this pattern were P_{es}, P_{ed}, ESV, EDV, dP/dt_{max}, dP/dt_{min} and Tau. However, these indications of restored cardiac function were no longer observed at 10 weeks post-MI, but rather, appeared to be similar to the values observed at 2 weeks post-MI. The values obtained at 10 weeks post-MI basically indicated that LV is in its progression towards HF. Thus, it is possible to state that cardiac function measurement in LV with infarction is highly dependent upon timing. In this project, the P-V loop analysis was implemented at 6-7 weeks post to MI surgery, which appears to be a stage when the LV is in the phase of active cardiac restoration and re-modelling. These observations could help explain why I did not find a statistically significant difference in LV function between the sham and MI groups in this project at the 6-week time point using P-V loop analysis. In addition, Shioura et al suggested that this restoration of cardiac function at 4- and 6 weeks post-MI can be explained by different activities of MMPs and distinct temporal patterns of fetal gene expression such as β-MHC and atrial natriuretic factor (ANF). Their RT-PCR data revealed that β-MHC and ANF expression levels were significantly higher at 2 weeks post-MI, but restored back to baseline at 4- and 6-weeks post-MI. However, another significant rise of β-MHC expression at 10 weeks post-MI was also observed. Also, MMP2 showed significantly increased expression at 4- and 10 weeks post-MI, whereas MMP9 showed significantly increased expression at 4 weeks post-MI. These differential expression levels of certain genes can act as molecular biomarkers of ventricular remodeling that can potentially provide insight to determine the optimal timing of therapeutic intervention to maximize the beneficial effects.

4.3 MI triggers LV remodeling which is accompanied by robust immune responses

As illustrated and demonstrated by the experimental evidence from this project and Shioura et al, there is no doubt that the LV can undergo complex processes of adaptation. One of the major processes exhibited by the LV is compensatory hypertrophy as well as scar formation and stabilization, which occurs in rodents at 2- to 3-weeks post-MI (Jugdutt et al., 1996). These processes could partially explain why the MI mice in this project (i.e. group 3) did not show significant difference in LV function obtained by P-V loop analysis compared with sham surgery mice (group 1). However, it is important to consider what are the initial signals that are responsible for triggering compensatory hypertrophy and what are the molecular mechanisms that initiate myocardial tissue healing and scar formation/stabilization. To answer these inquiries, it is necessary to review what are the initial immediate responses of cardiomyocytes upon the ischemic insult.

The reduced O_2 availability to the working myocardium can trigger the switch from aerobic metabolism (efficient oxidative phosphorylation) to anaerobic metabolism (glycolysis) that significantly decreases the available ATP consumed by cardiomyocytes (Kübler and Spieckermann, 1970). In addition, the prolonged presence of ischemia can trigger myocardial necrosis, which can subsequently lead to formation of a fibrotic scar. The loss of cardiomyocytes and associated tissue fibrosis can provide a significant amount of stress on the remaining viable myocardium, which puts more stress on the systolic function of LV and triggers compensatory hypertrophy. Therefore, it is possible to recognize that O_2 deprivation leads to a series of events that are initiated by cell damage and overall tissue injury, which can trigger robust immune responses from innate immune system.

Recent investigations have revealed and identified that immune cells play important roles in post-MI events (Bajpai et al., 2019; DeLeon-Pennell et al., 2017; Deniset et al., 2019; Frangogiannis et al., 2007; Heidt et al., 2014; Hilgendorf et al., 2014; Mach et al., 1997; Nahrendorf et al., 2007; Sager et al., 2016; Swirski and Nahrendorf, 2018) First, it is important to recognize that heart is composed of diverse cell types. The inotropic and lusitropic function of the heart are not just mediated by cardiomyocytes. Muscle cells are structurally supported by the extracellular matrix (ECM) and associated cell types (e.g. fibroblasts) and there are endothelial cells that line the chambers, arteries, veins, and valves. Also, there are excitable cells (e.g. autonomic nerves) that coordinate and influence intrinsic cardiac excitability. Furthermore, the healthy adult mouse heart contains major leukocyte classes, such as neutrophils, B cells and T cells that exceed the ones found in skeletal muscle by 12-fold (Swirski and Nahrendorf, 2018). However, out of all the immune cell types, macrophages make up the largest population in the heart that are monocytes derived. Detailed surface marker profiling of cardiac macrophages showed that there are at least four subsets. All the cardiac macrophage sub-types uniformly express the surface markers $CD45^{+}$F4/80$^{+}CD11b^{+}CD64^{+}MERTK^{+}$ but they have a distinct expression pattern of MHC class II molecules: CC-chemokine receptor 2 (CCR2) and lymphocyte antigen 6C (Ly6C) (Swirski and Nahrendorf, 2018). Furthermore, one of the important characteristics of tissue resident macrophages is that they do not express the CCR2 on the surface, whereas circulating monocyte-derived macrophages express the CCR2 receptor. Thus, cardiac resident macrophages are denoted as CCR2- and circulating monocyte derived ones are denoted as CCR2+. In addition, the CCR2+ and CCR2- macrophages are also found in the adult human heart, and exhibit functions and localization that are compatible to the ones

found in mouse. These findings thus have potential translational implications (Bajpai *et al.*, 2019).

Once MI is established in mice, a significant number of cardiomyocytes start to perish in the infarct zone which secretes Death-Associated Molecular Patterns (DAMPs) that activate the surrounding resident macrophages in a paracrine manner. This process triggers the resident macrophages and cardiomyocytes to produce inflammatory cytokines and chemokines: IL-1, IL-6, TNF, CC-chemokine ligand 2 (CCL2), CXCL2, and CXCL5 (Bajpai *et al.*, 2019; Li et al., 2016). It also triggers cardiac fibroblasts to release haematopoietic growth factors, such as GM-CSF. This series of secretion and signalling lead to large-scale production and recruitment of circulating neutrophils and monocytes that are mainly derived from haematopoietic stem and progenitor cells (HSPCs) in the bone marrow and spleen (Swirski et al., 2009). Adrenergic signalling by the sympathetic nervous system stimulates the bone marrow, which is followed by subsequent activation of the spleen that induce extramedullary hematopoiesis (Dutta et al., 2012; Leuschner et al., 2012). Once these innate immune cells are produced, they enter the blood stream then reach the injury site and start to accumulate. They actively participate in an inflammatory cascade which initially starts by engulfing dying/dead cardiomyocytes which in turn generates inflammatory cytokines (e.g., IL-1, TNF, and IL-6) that amplify the inflammation by affecting leukocytes, endothelial cells, and cardiomyocytes (Frangogiannis et al., 2002). This phagocytic activity is mainly driven by the recruited neutrophils. As a part of the immediate response to the myocardial ischemic injury, endothelial cells within the infarct zone up-regulate adhesion molecules that mediate neutrophil extravasation (Nahrendorf *et al.*, 2007). However, the actions of the neutrophils can be somewhat non-specific, and lead to immunological misfiring aimed at myocytes that survived the ischemic injury. Thus, it is possible to state that

neutrophils can be damaging to the viable myocardium, which can undergo apoptosis and eventually be removed by macrophages (Swirski and Nahrendorf, 2013). The other rapid responder that gets recruited to the infarct zone are haematopoietically derived monocytes. The inflammatory chemokine, CCL2, that is secreted by dying cardiomyocytes and cardiac resident macrophages recruit the sub-type specific $Ly6C^{high}$ monocytes (Nahrendorf *et al.*, 2007). The 40% of infiltrating $Ly6C^{high}$ monocytes in the infarct originate from the spleen (Swirski *et al.*, 2009) which replaces the cardiac resident macrophages (Leuschner *et al.*, 2012). These recruited monocytes can undergo phenotypic conversion to macrophages which relays the further series of inflammation and LV remodelling processes (Dick et al., 2019; Honold and Nahrendorf, 2018). Therefore, these newly introduced monocyte-derived macrophages can self-maintain via local proliferation at the infarct zone over long periods of time (Hashimoto et al., 2013; Heidt *et al.*, 2014; Sager *et al.*, 2016; Scott et al., 2016). However, in addition to the phagocytosis and efferocytosis mediated by these macrophages, it is reported that they are actively involved in synthesis and secretion of molecules that establish the crosstalk with other cardiac cell types (Honold and Nahrendorf, 2018) (Figure. 22). The major molecules that are secreted by the monocyte derived macrophages are (1) TNF-α (2) TGF-β (3) MMPs (4) VEGF. TNF-α can also originate from cardiomyocytes and endothelial cells. The overall effect of TNF-α is to induce cardiomyocyte hypertrophy. TGF-β triggers conversion of cardiac fibroblasts to myofibroblasts which subsequently express α-smooth muscle actin and synthesize collagen that can be deposited to produce fibrotic scar. MMPs degrade the ECM via proteolytic enzymes that contribute to injured tissue remodelling. VEGF targets endothelial cells which promote angiogenesis (Frangogiannis, 2014; Honold and Nahrendorf, 2018; Lindsey, 2018; Nahrendorf *et al.*, 2007). Overall, it is possible to recognize that the activities of monocytes derived macrophages are not

just limited to phagocytosis and efferocytosis but rather they serve as a platform leading to additional adaptative LV remodelling.

Figure 22.

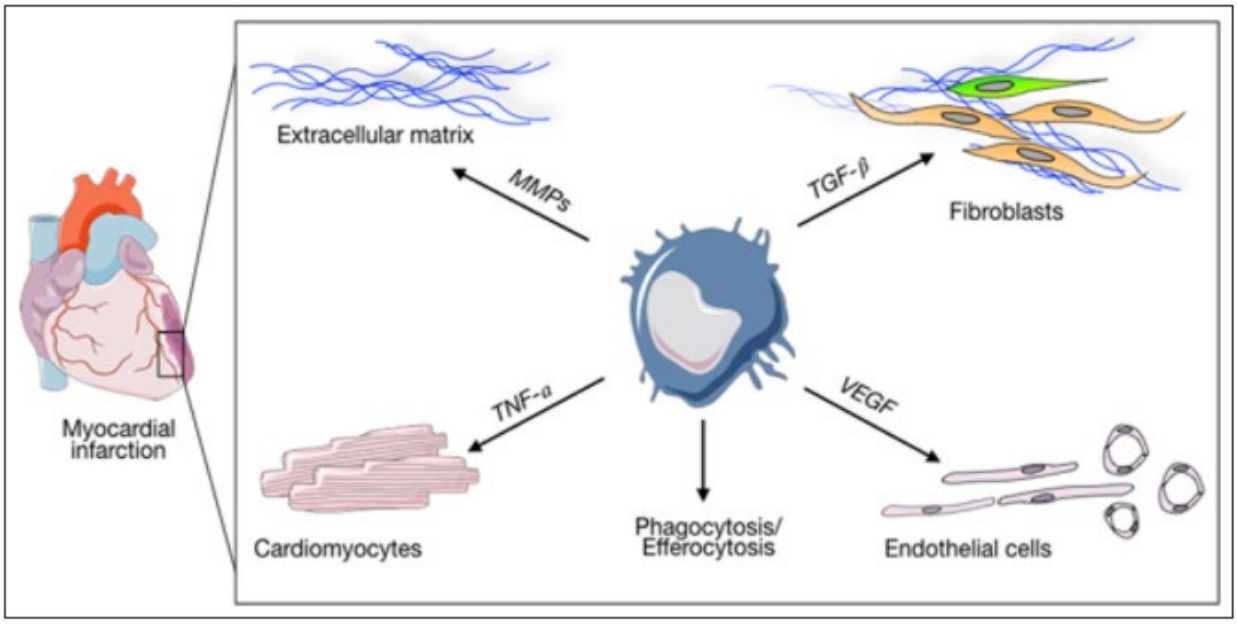

Figure 22. Macrophage mediators and crosstalk after myocardial infarction

Macrophages within the ischemic/infarcted zone (blue cell) release multiple mediators and participate in phagocytosis. TNF-α acts on cardiomyocytes and can induce hypertrophy and cell death. TGF-β induces conversion of fibroblasts to myofibroblasts that produce collagen necessary for scar formation. Proteolytic enzymes like matrix metalloproteinase (MMPs) contribute to tissue remodeling while VEGF acts on endothelial cells and stimulates angiogenesis.

[Taken from: Honold, L., and Nahrendorf, M. (2018). Resident and Monocyte-Derived Macrophages in Cardiovascular Disease. Circ Res *122*, 113-127.0.1161/circresaha.117.311071.]

The other subtype of haematopoietically derived monocyte is $Ly6C^{low}$ monocytes. As mentioned previously, the damaged tissue secrets the CCL2 that recruits the $Ly6C^{high}$ monocytes during the first several days post to the infarction. However, the damaged cardiomyocytes subsequently switch to CX3CL1-mediated recruitment of $Ly6C^{low}$ monocytes which partakes in the reparative phase of LV (Nahrendorf *et al.*, 2007). More specifically, the recruited $Ly6C^{high}$ monocytes have a life span of 20 hours, and they begin to differentiate into reparative $Ly6C^{low}$ monocytes (Courties et al., 2014; Hilgendorf *et al.*, 2014; Leuschner *et al.*, 2012). $Ly6C^{low}$ macrophages can persist for several weeks and renew partially by local proliferation (Hilgendorf *et al.*, 2014). However, the switching mechanism from $Ly6C^{high}$ to $Ly6C^{low}$ is not known and, the specific function of $Ly6C^{low}$ monocytes is not identified. However, with the basis of robust experimental evidence, there is no doubt that MI is an event that is associated with large-scale immune response, and it is mediated by multi-step processes that are highly timing dependent. This picture indicates that the timing of therapeutic interventions to mitigate MI is likely very important to maximize the beneficial effects and minimize the potential side-effects.

4.4 Cardiac Fibrosis is the major determinant of LV prognosis

A recent study reported by Densiet et al suggested that there is an important role played by pericardial cavity Gata6+ macrophages in the prevention of cardiac fibrosis (Deniset *et al.*, 2019). Gata6 is a transcription factor expressed by the pericardial fluid resident macrophages, but not expressed in the myocardial resident CCR2+ and CCR2- macrophages. Deniset et al. also reported that once the AMI is established in mice by surgically ligating the LAD coronary artery, the Gata6+ macrophages migrated from pericardial cavity into the infarct zone via a transmural pathway. This process was found to be distinct from other macrophages that are usually attracted

to the injury site via the circulation and endothelial extravasation (Deniset *et al.*, 2019). Furthermore, once the pericardial macrophages arrive in the myocardial space, the macrophages no longer express the Gata6 transcription factor and reduced the expansion of interstitial fibrosis into the peri-infarct/remote zone of myocardium (Deniset *et al.*, 2019). Therefore, from this experimental evidence, it is possible to recognize that migration of Gata6+ pericardial macrophages prevented the expansion of left ventricular fibrosis and improved overall cardiac function which was confirmed by measuring cardiac functional indicators such as EF, FS, ESPVR, EDPVR, etc.

However, there is another important aspect that needs to be recognized from the experiments reported by Deniset et al. As mentioned previously, the immunological response to ischemic myocardial injury is highly timing dependent. In other words, there is a series of events that occur in a chronological order. The cell sorting/flow cytometry experiments from the study by Deniset et al. demonstrated that there are certain distinct populations of immune cells present at different time points in the post-MI LV. The neutrophils and $Ly6C^{high}$ monocytes/macrophages showed a significant increase at ~3 days post-infarction and returned back to baseline levels at ~7 days post-infarction. However, $Ly6C^{low}$ macrophages displayed a decline at ~3 days post-injury and then increased to the baseline level at ~7 days post-injury (Figure. 23) (Deniset *et al.*, 2019). These observations provide more quantified information with regards to the activation and types of innate immune cells in the post-MI environment.

Figure 23.

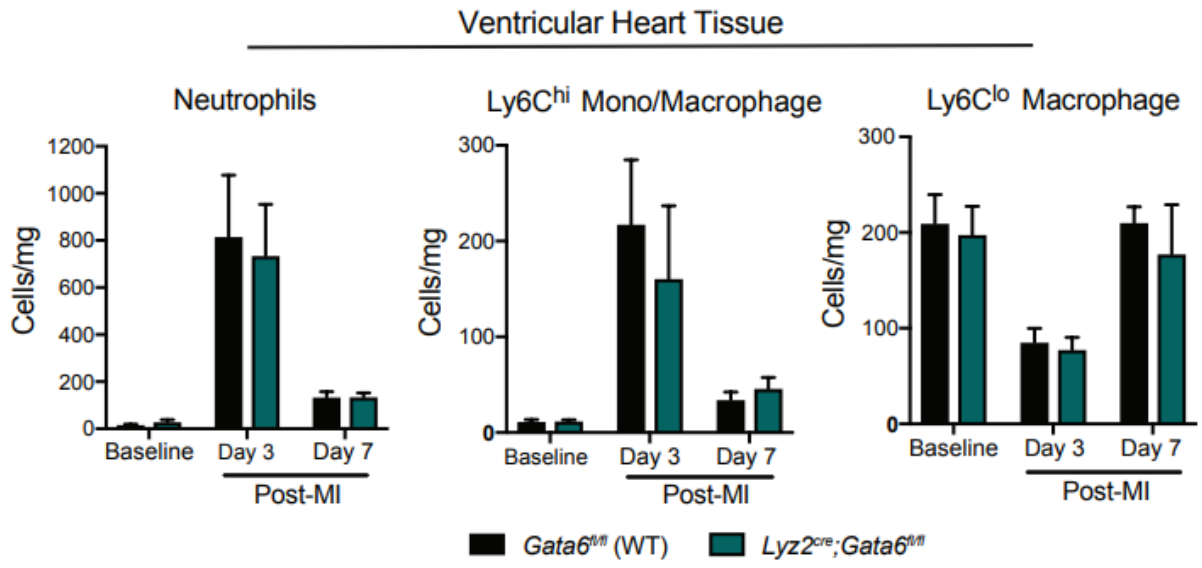

Figure 23. Pericardial and cardiac myeloid populations in $Lyz\ 2^{cre}$; $Gata6^{fl/fl}$ mice

Quantification of neutrophil, Ly6C^{hi}monocytes/macrophages, and Ly6C^{lo} macrophages in mouse ventricular tissue pre- and post-MI in Gata6$^{fl/fl}$ (WT) and Lyz 2^{cre-}; Gata6$^{fl/fl}$ mice. n=3-11 from at least 2 independent experiments per timepoint.

[Taken from: Deniset, J.F., Belke, D., Lee, W.Y., Jorch, S.K., Deppermann, C., Hassanabad, A.F., Turnbull, J.D., Teng, G., Rozich, I., Hudspeth, K., et al. (2019). Gata6(+) Pericardial Cavity Macrophages Relocate to the Injured Heart and Prevent Cardiac Fibrosis. Immunity *51*, 131-140.e135. 10.1016/j.immuni.2019.06.010.]

4.5 The timing of pharmacological intervention affects LV function in MI model mice

The experimental evidence indicates that post-infarction, LV healing is coordinated by multifactorial events. After MI, the innate immune cells are essential for tissue repair, but their oversupply and/or over-activity can be disadvantageous to the healing and can lead to HF (Swirski and Nahrendorf, 2013). Therefore, there needs to be a well-balanced supply and demand relationship of innate immunity to optimize the tissue healing. This also indicates that the beneficial effects of therapeutic intervention can be maximized if administered under the correct timing, which can augment the immune cells' ability to mediate healing processes but simultaneously, avoid the time window when activities of the neutrophils and monocytes are at their peak.

The above information represents an important variable that needs to be incorporated into the overall data interpretation of this project. As mentioned previously, the daily *in vivo* SKA-31 treatment started within ~48 hours post-surgery and lasted for ~6 weeks. With the *in vivo* drug treatment, it is important to consider the pharmacodynamics, which means, the drug would have systemic effects rather than limiting its impact to preferred sites, such as the vascular endothelium. Furthermore, with the robust experimental evidence reported by Deniset and colleagues, it is possible to recognize that there is a robust pro-inflammatory immune response in post-MI mice during first ~7 days driven by neutrophils and $Ly6C^{high}$ monocytes/macrophages. Based on this situation, there is an overlap between the timing of SKA-31 treatment and large-scale immune responses during the first ~7 days post-MI surgery. Therefore, it is possible to state that there could have been potential interactions between the blood plasma SKA-31 and significantly elevated level of neutrophils and $Ly6C^{high}$ monocytes/macrophages within the circulation. This situation is potentially important, as many immune cells express the KCa3.1

channel, a target for SKA-31. In addition, it is important to recognize that these immune cells reach the site of infarction via coronary circulation which subsequently extravasate between the coronary endothelial cells (Swirski and Nahrendorf, 2013) and as mentioned previously, one of the vascular beds that we envisioned would be affected by SKA-31 is coronary circulation. However, it is first important to review what are the potential molecular mechanisms that underlie this interaction between the SKA-31 and pro-inflammatory immune cells.

A variety of ion channels are expressed on lymphocytes and mediate many important physiological cell functions, such as gene expression, apoptosis, proliferation, development, and migration (Cahalan and Chandy, 2009). One of the most prominent activation signals that triggers physiological cell functions of lymphocytes is the entry of extracellular Ca^{2+}into the cytosolic space. This Ca^{2+}influx is often associated with initiation of intracellular signalling cascades that lead to gene expression, secretion, hyperplasia, etc. (Feske, 2007; Oh-hora, 2009). Therefore, the membrane potential (Vm) of lymphocytes is a major determinant that dictates Ca^{2+} entry. In non-excitable cells (e.g. immune cells, fibroblasts, endothelium, etc.), this external Ca^{2+} entry is augmented by the membrane hyperpolarization which increases the electric driving force and facilitates Ca^{2+} influx via receptor- and store-operated Ca^{2+}entry (SOCE) pathways (Mathew John *et al.*, 2018; Prakriya and Lewis, 2015; Soboloff et al., 2012). Therefore, the interplay among the ion channels that maintain Vm such as K^+, Na^+, and Cl^- channels are important. However, as hyperpolarization is a key process that determines the overall activities of immune cells, it is important to highlight the impact of K^+channels on immune cell physiology.

The best studied K^+ channels on lymphocytes are the voltage-activated K_v1.3 and the Ca^{2+}-activated K^+intermediate-conductance K_{Ca}3.1 channels which predominantly regulate

membrane potential (Feske et al., 2015). As the name suggests, the $K_v1.3$ channel is activated by membrane depolarization and once activated, it counteracts the depolarization by hyperpolarizing the membrane potential via K^+ efflux. This process establishes an electric driving force for the initial external Ca^{2+}entry which can form intracellular Ca^{2+}microdomains in vicinity of the plasma membrane (PM) and $K_{Ca}3.1$ channel (voltage-insensitive). This subsequently activates the $K_{Ca}3.1$ channel and promotes sustained Ca^{2+}influx (Feske *et al.*, 2015). Furthermore, to prevent the over-lasting hyperpolarization, there is Transient Receptor Potential Cation Channel Subfamily M, member 4 (TRPM4) expressed on the PM which is also a Ca^{2+}-activated monovalent cation channel that is highly permeable to Na^+ that depolarizes the Vm as a counteractive mechanism which prevents the excess Ca^{2+}-entry (Launay et al., 2004; Launay et al., 2002). These channels thus act in a physiologically coordinated manner that efficiently and safely mediates immune cell activation.

The major immune cell populations that increase significantly following an AMI in mice are neutrophils and $Ly6C^{high}$ monocytes/macrophages. These innate immune cells recognize the DAMPs generated by dying/dead cardiomyocytes via Toll-like receptors (TLRs) on its PM. Once they are activated, they express and secret pro-inflammatory cytokines that leads to further recruitment of neutrophils, macrophages, and dendritic cells (DCs). Ion channels are involved with this activation and migration pattern of immune cells. In macrophages and neutrophils, the intracellular $Ca^{2+}$is reported to play pivotal roles. In macrophages, intracellular Ca^{2+} regulates the production of TNF-α and nitric oxide (NO), phagocytosis (Chen et al., 1998; Watanabe et al., 1996) whereas in neutrophils, Ca^{2+} is associated with ROS generation (Zhang et al., 2014). Therefore, as introduced previously, membrane hyperpolarization mediated Ca^{2+}-entry can trigger activation of macrophages and neutrophils. In previous investigations, it has been

revealed and reported that monocytes and macrophages in rodents and humans express several types of K^+channels: $K_V1.3$, $K_V1.5$, $K_{Ca}1.1$, $K_{Ca}3.1$ and $K_{ir}2.1$ channels (Chung et al., 2002; DeCoursey et al., 1996; Gallin, 1984; Hanley et al., 2004; Nelson et al., 1992; Seydel et al., 2001; Vicente et al., 2003). The major function that are mediated by these K^+ channels are maintenance of resting Vm and establishing the platform for external Ca^{2+} entry. In human macrophages, there have been reports showing $K_{Ca}3.1$ channel presence on PM. They are activated by the Ca^{2+}influx via Calcium release activated channel (CRAC) via SOCE pathway. This allows prolonged Ca^{2+}signalling through hyperpolarization which facilitates store refilling (Gao et al., 2010b; Hanley *et al.*, 2004). Furthermore, with the presence of vascular injury and/or hypoxic events, ATP can be released from endothelial cells, red blood cells (RBCs) and platelets that can target P2Y receptors which stimulates a GPCR – G-protein – PLC - IP_3 evoked intracellular Ca^{2+} release pathway that activates the $CRAC$ channel (Procopio et al., 2021). Furthermore, it has been reported that $K_{Ca}3.1$ expression is commonly observed on macrophages that infiltrate atherosclerotic plaques, inflamed tissues such as inflammatory bowel disease (IBD) and vasculopathy (Chen et al., 2013; Strøbæk et al., 2013; Toyama et al., 2008).

Therefore, it is possible to state that under the circumstances of ischemic myocardial injury which was established in this project, there is a high possibility that recruited neutrophils and monocytes/macrophages would have $K_{Ca}3.1$ channel expression on the PM. Furthermore, the activation threshold of these $K_{Ca}3.1$ channels could have been enhanced in the presence of SKA-31. As explained previously, $K_{Ca}3.1$ channels have constitutively bound CaM on intracellular C-termini which acts as a Ca^{2+} sensor. Brown et al. revealed that SKA-31 binds to the CaM-BD/CaM interface on the C-termini by carrying out structure/function analyses and computational modeling of the $K_{Ca}3.1$ channel. The binding of SKA-31 would be expected to

sensitize the channel and increase the open probability in response to a stimulus (Brown et al., 2017). Thus, in the setting of robust inflammatory events such as AMI, SKA-31 could have potentiated the pro-inflammatory activities of innate immune cells. Moreover, another aspect that needs to be addressed is cardiac fibrosis that follows the myocardial inflammation. As mentioned previously, one of the molecules secreted by pro-inflammatory monocytes-derived macrophages is TGF-β which targets the cardiac fibroblasts. Once they are activated by TGF- β, these cells transdifferentiate into secretory myofibroblasts that mediate extracellular matrix deposition (Lighthouse and Small, 2016). Also, it is noteworthy that macrophages are in close proximity to the myofibroblasts within the myocardium (Frangogiannis et al., 2003). In previous investigations, $K_{Ca}3.1$ channels are reported to be expressed on fibroblasts of airway pathways and hepatic stellate cells that mediate tissue fibrosis (Roach and Bradding, 2020; Song et al., 2014; Van Der Velden et al., 2013). Therefore, it is possible to state that within the first 2 weeks, SKA-31 treatment in post-MI mice could have potentiated the pro-inflammatory responses within the LV along with increased progression of tissue fibrosis as evidenced by modestly elevated values of ESV and EDV in group 4 mice at 2-, 4-, and 6-weeks post-MI compared with group 3. Furthermore, it is important to recognize that $Ly6C^{high}$ monocytes have a life span of 20 hours within the infarct zone (Courties *et al.*, 2014; Deniset *et al.*, 2019; Hilgendorf *et al.*, 2014; Leuschner *et al.*, 2012) which largely overlaps with the pharmacokinetic profile of the SKA-31 (half life of ~12 h). Furthermore, Lee et al reported that there is also a significant elevation of monocytes and macrophages in the non-infarcted remote zone of myocardium after the onset of MI. PET/MRI imaging and flow cytometry approaches have revealed that recruitment of immune cells within the non-infarcted area of the myocardium was most abundant in the border zone. The population of monocytes/macrophages was increased by 66-fold in the

infarct and 9-fold in the remote zone on day 5 after MI. The population of $Ly6C^{high}$ monocytes within the remote zone subsequently reached a peak at day 10 after MI (Lee et al., 2012; Swirski and Nahrendorf, 2013). This experimental evidence suggests that these pro-inflammatory immune cells could be responsible for expansion of fibrotic scar into the remote zone. Correspondingly, the PSR staining that was carried out in this project reveal a noticeable increase in fibrosis within the mid-myocardium of group 4 compared to group 3. With the consideration of anatomical positioning of LAD ligation suture, the area distal to the stitch would inevitably have infarction/fibrosis. Thus, there is a comparable level of tissue fibrosis between groups 3 and group 4 within the apical myocardium. However, the noticeable difference in the extent of fibrosis within the mid-myocardium between these two groups could be explained by possibility that fibrotic scar had expanded from an original site within the LV apex. Therefore, in view of the experimental evidence provided by Lee et al and from this project, it is possible that SKA-31 treatment could have contributed to the expansion of fibrosis within the LV.

4.6 SKA-31 treatment did not significantly affect the cardiac electrophysiology.

The rhythmicity of heart is very important in terms of maintenance of overall cardiovascular homeostasis because it directly regulates the amount of blood being pumped and delivered during each heartbeat ($Cardiac\ Output = Heart\ Rate\ \times Stroke\ Volume$). Furthermore, the heart rate can vary under different metabolic demands and this dynamic physiology is coordinated by autonomic nerve innervation of the myocardium. This neurohumoral relationship that modifies the heart rate is coordinated by a complement of ion channels within the heart.

In this project, the heart rate (HR) was measured at 2-. 4- and 6-weeks post-infarction by both echocardiography and P-V loop analysis. As illustrated in Figure 17, it is apparent that there

is no significant impact mediated by SKA-31 treatment on HR in both sham and MI groups. However, to elucidate the reason why SKA-31 treatment did not have significant impact on overall heart rate and potentially cardiac electrophysiology, it is necessary to consider information with regards to $K_{Ca}2.x$ and $K_{Ca}3.1$ expression within the heart.

The $K_{Ca}2$ channels are reported to be expressed in the human and mouse atrial cells that showed apamin or dequalinium chloride sensitivity (Xu et al., 2003). The blockade of the putative $K_{Ca}2$ channel in the atrium delayed the late repolarization of the action potential that increased overall Action Potential Duration (APD). Furthermore, qRT-PCR analysis showed that the mRNA of $K_{Ca}2$ ($K_{Ca}2.1$ and $K_{Ca}2.2$) is expressed to a greater degree in mouse atria compared to ventricle, but $K_{Ca}2.3$ channels showed similar levels of mRNA expression in both regions (Tuteja et al., 2005). Other investigations have confirmed that K_{Ca} channels are expressed in atria and involved in atrial repolarization by demonstrating an increase in APD when cells were treated with BAPTA-AM, a Ca^{2+} chelator (Tuteja *et al.*, 2005). In addition, when rodent ventricular cardiomyocytes were pharmacologically treated with the KCa2 channel blocker apamin, it did not alter the AP shape and duration which further confirms that $K_{Ca}2$ channels are not predominantly expressed in mouse ventricle (Xu *et al.*, 2003). $K_{Ca}2$ channels are reported to be colocalized with voltage-gated Ca^{2+} channels in some tissues (Vandael et al., 2012) which suggests that channel activity may be more sensitive to the extracellular Ca^{2+} sources. In mouse atrial cells, $K_{Ca}2.2$ channels colocalize with L-type Ca^{2+} channels through α-actinin interactions and external calcium appears to be a major determinant of channel activation. This idea was supported by significantly reduced $K_{Ca}2.2$ current and shortened atrial APs in $Ca_v1.3$ null mice (Lu et al., 2007). Furthermore, in guinea pig ventricular cells, $K_{Ca}2$ channels are reported to be expressed on the inner membrane of mitochondria, as denoted by mK_{Ca}, which

was determined by single channel recordings from purified mitochondrial channels that showed Ca^{2+}-dependence and apamin-sensitivity (Stowe et al., 2013). In the same study, Stowe and colleagues demonstrated cardio-protective effects of a $K_{Ca}2/3$ channel opener (i.e. DCEBIO) in a model of ischemia reperfusion. When hearts were pre-treated with the K_{Ca} pharmacological opener, the LV exhibited better systolic pressure, coronary flow, and reduced infarct size, which was observed via isolated heart perfusion experiments. The authors suggested that this beneficial effect of mK_{Ca} activation is O_2^- dependent because the effect was reversed when heart was pre-treated together with an O_2^- dismutator compound (i.e. TBAP). Furthermore, in chronic Heart Failure with reduced Ejection Fraction (HFrEF), it is reported that the protein expression of $K_{Ca}2.3$ was increased in rabbit ventricle, whereas $K_{Ca}2.2$ was increased both in atria and ventricle (Chua et al., 2011). In another study with rabbit, isolated heart perfusion and patch clamp experiments revealed that there is an elevation of K_{Ca} channel expression in infarcted LV. The rabbit MI model was established by surgically ligating the LAD coronary artery via left thoracotomy. The isolated rabbit ventricular cells from the peri-infract zone displayed a larger apamin-sensitive current density than cardiomyocytes from the unaffected zone (Lee et al., 2013). This finding suggests that there is an alteration to the K_{Ca} channel expression and distribution pattern after the MI.

On the basis of experimental evidence, it is possible to recognize that $K_{Ca}2$ channels are mostly expressed in mammalian atria (Hancock et al., 2015; Reher et al., 2017; Shamsaldeen et al., 2019; Skibsbye et al., 2014; Tuteja *et al.*, 2005; Xu *et al.*, 2003). In contrast to this expression pattern of $K_{Ca}2$ channels, the $K_{Ca}3$ channels show a more diverse expression pattern. In adult mouse heart, the protein expression of $K_{Ca}3.1$ channels is observed in atrial appendages, ventricles, and in the sinoatrial node (Haron-Khun et al., 2017). In rats, the $K_{Ca}3.1$ channels are

expressed in the SAN, AVN and ventricles but less amount in the atria (Zhao et al., 2019). However, in previous investigations, the $K_{Ca}3.1$ channels in heart are also reported to play a role in the regulation of cardiac automaticity. The major electrophysiological events that dictate cardiac spontaneity and automaticity are diastolic depolarization or pacemaker depolarization. This pattern of a relatively more depolarized resting membrane potential (RMP) is mediated by a complement of ion channels: If, ICa,, $INCX$ and ICa,L ($Cav1.3$) (Baruscotti et al., 2010; Brown and Difrancesco, 1980; Groenke et al., 2013). Interestingly, Weisbrod et al reported that when human embryonic stem cell derived cardiomyocytes (hESC-CMs) are treated with $K_{Ca}3$ channel antagonists, it led to significant reduction of the diastolic pacemaker slope and essentially terminated the cardiac pacemaking activity (Weisbrod et al., 2013). Therefore, overall experimental evidence suggest that K_{Ca} channels may contribute to the repolarization phase of cardiac action potential in some species, which occurs during diastole and determines the firing of the next AP.

However, as evidenced by the heart rate data in this project, SKA-31 treatment did not have a significant impact on overall heart rate. The following suggestions could account for these observations: (1) a minimal dosage of SKA-31 was used in this project (2) the effects of isoflurane during the measurement (3) pharmacodynamics of SKA-31 on cardiomyocytes (4) relative minimal role of K_{Ca} channels on cardiac electrophysiology/pacing. In a previous investigation, Mishra and colleagues acutely administered a minimal dosage of SKA-31 (0.3 μM) to diabetic rat hearts and its corresponding control group using an *ex vivo* Langendorff perfused, isolated heart preparation (Mishra *et al.*, 2014) and did not detect changes in spontaneous heart rate. This evidence indicates that when heart is independent of autonomic nerve innervations and other potential neurohumoral interactions, acute SKA-31 treatment did

not impact the intrinsic myocardial heart rate. In other words, the SKA-31 treatment did not affect the K_{Ca} channels within the atria and ventricle with a minimal dosage. However, it is important to be aware of the potential impact of SKA-31 and comparable KCa channel activators on overall cardiac electrophysiology.

4.7 Limitations and future directions

In most scientific investigations, experimental design is one of the most important stages of the project because it directly impacts the ability of the investigator to evaluate the hypothesis. The experimental outline needs to be carefully created to prevent/minimize confounding variables. However, it is inevitable that there are always areas for improvement in most studies. Similarly, it is also important to consider the feasibility and cost-effectiveness of the experimental setup to undertake reasonable approaches.

In this project, male mice (12-15 weeks of age, C57B1/6 strain) were used to create the MI model and to assess cardiac function, the techniques of echocardiography, P-V loop analysis and histopathological analysis were implemented. These techniques are widely and routinely used in cardiac research (Lindsey *et al.*, 2018a; Lindsey *et al.*, 2018b; Pacher *et al.*, 2008). In addition, the extensive protocols that outline technical details for performing permanent occlusion MI surgery and transient occlusion MI injury in rodents are readily available (Michael et al., 1999; Nossuli et al., 2000; Wu et al., 2011; Zamilpa et al., 2013). Another strength of using rodent models is that it allows for higher throughput studies with a wide range of transgenic animals being available to study molecular mechanisms (Lindsey *et al.*, 2018a). However, rodents are reported to have relatively high surgical and postoperative mortality (Lindsey *et al.*, 2018a). To improve the survival of the animals, it is important to minimize the size of the thoracotomy and bleeding during the surgery. Furthermore, due to the surgical

approach to ligate the LAD coronary artery, it is very difficult to place suture at the same anatomical location across the group of animals which can lead to variability of the infarct size (Chen et al., 2017). It is also possible to miss the desired coronary artery during the ligation step of the surgery that leads to a failure to induce a bona fide MI injury. Therefore, thorough assessments to confirm successful induction of MI and the size of the infarct are very important. These steps of comprehensive confirmation were implemented in this project and, the infarct size variability was incorporated in the overall interpretation of the data. Nonetheless, to maximize the feasibility and utilization of the resources of well-established protocols, it was most appropriate to use a surgical method to establish a mouse model of MI in this project.

Furthermore, it is important to recognize the usage of isoflurane in this project. Isoflurane has been shown to cause moderate to severe cardio-depression (Hart et al., 2001; Matsuda et al., 2007; Szczesny et al., 2004). The major actions mediated by isoflurane are associated with chronotropic and inotropic decreases in cardiac function (Constantinides et al., 2016). This depression is mostly achieved by changes in autonomic tone which further impacts inward calcium transients and subsequent CICR events in excitation-contraction coupling of cardiomyocytes. The list of events reported to be mediated by isoflurane are (1) a decrease in HR due to its actions in the CNS and PNS (2) a decrease in inward Ca^{2+} transient by targeting L-type Ca^{2+}channels and a subsequent decrease in SR Ca^{2+} accumulation (3) changes in cardiac inotropy (Constantinides and Murphy, 2016). Furthermore, it is reported that isoflurane is a coronary artery vasodilator by targeting K_{atp} channels of coronary VSMCs and endothelium (Constantinides and Murphy, 2016). Thus, due to these effects of isoflurane on cardiovascular system, it is important to consider what are the potential impacts of such anesthetics in the functional measurements in this project. First, it is very important to review the pharmacokinetic

property of SKA-31. As mentioned previously, it is reported to have a half-life of ~12 hours in rodents. This property may be important because on the day of cardiac function measurements (echocardiography and P-V loop analysis), the animals did not receive SKA-31 treatment prior to the measurements. This indicates that the blood plasma level of SKA-31 would be minimal during exposure to the isoflurane which possibly avoided an interaction between the two molecules.

Furthermore, Lindsey et al have outlined 5 categories to consider when making choices regarding anesthetic usage: (1) ease of handling (2) amount of stress induced (3) ability to adjust level and duration (4) impact on BP, HR, cardiac function (5) recovery time. To fulfill most of these categories, isoflurane was the most ideal reagent to use in this project. The main benefit of using isoflurane was that it is inhalational, which means, it acts fast, and animals recover rapidly from the exposure. Also, it allows for prompt manipulation and monitoring of the isoflurane level. These conditions provided the most feasibility in terms of implementing the surgery, echocardiography and P-V loop analysis in the mice. Furthermore, as some of these techniques are very invasive, it was ethically and humanely reasonable to use isoflurane in this project. However, if there are anesthetic options available that can minimize the manipulation of autonomic tone and overall cardiovascular hemodynamics, it is important to objectively assess and decide their usage in future experiments with the condition that it can improve the overall quality and feasibility of the project. Nonetheless, it is very important to consider the potential impact of isoflurane on overall cardiac function to rigorously interpret the data.

In terms of future experiments, I suggest that it is important to look at what are the changes in the expression level of K_{Ca} channels after the onset of AMI in mice. The cell types that particularly require such evaluation are LV cardiomyocytes, vascular endothelium and

recruited monocytes, neutrophils, and macrophages. More specifically, it will be also informative to look at differential expression patterns of K_{Ca} channels in border and remote zone of the myocardium. I believe that the fundamental concept that needs to be highlighted to maximize the beneficial effects of SKA-31 is how to balance the effects of SKA-31 treatment on vascular endothelium to improve its health over its potential impacts on other cell types such as innate immune cells. Therefore, by evaluating the differential expression pattern of K_{Ca} channels on those cell types after MI could provide insight into how to use SKA-31, an enhancer of endothelial health, more effectively to promote myocardial tissue healing via enhancing coronary hemodynamics and reducing the amount of stress on remaining viable myocardium by improving the systemic circulation. However, as mentioned previously, the innate immune response to MI follows a temporal pattern. Thus, I suggest it will be reasonable to implement cell sorting/flow cytometry at certain time points after MI (e.g. 3 days, 5 days, 7 days and 10 days post-infarction) to obtain immune response profiles and explore the impact of SKA-31 administration on their activity by measuring K_{Ca} channel current by patch-clamp electrophysiology.

Also, a variety of genetically engineered knockout (KO) mice are readily available. Thus, by performing LAD coronary ligation surgery on K_{Ca} 2.x and K_{Ca}3.1 channel KO mice, one can possibly obtain more information with regards to the molecular mechanisms of SKA-31 in the setting of an acute MI.

Summary and Conclusions

In my study, I have investigated a novel strategy to mitigate MI by administering the K_{Ca} 2.x and K_{Ca}3.1 channel activator SKA-31 to male mice (12-15 weeks of age, C57B1/6 strain) following acute MI. The surgical approach to establish MI was successful and was confirmed by rigorous evaluation. The sham surgery mice (i.e. groups 1 and 2) in this project exhibited an EF

of ~45-50% and a FS of ~20-25%, with an ESV of ~40 µL and EDV of ~70 µL. On the other hand, mice subjected to MI surgery (i.e. groups 3 and 4) exhibited an EF of ~25-30% and FS of ~10-15%, with an ESV of ~70 µL and EDV of ~100 µL. The cardiac function and structure measurements were performed by echocardiography, P-V loop analysis and histological assessment of the heart.

From the data obtained by echocardiography and P-V loop analysis, it is clear that there was a significant decrease in LV systolic function in MI surgery mice, as evidenced by drops in EF and FS, which was accompanied with significant volume enlargement (increase in ESV and EDV). However, my data also indicate that SKA-31 treatment did not significantly affect the sham operated mice (groups 1 and group 2). The possible explanation for this trend is that SKA-31 was used at minimal dosage to sensitize the K_{Ca} 2.x and K_{Ca}3.1 channels and, the vessels of sham groups would be expected to have a relatively low degree of endothelial dysfunction. In other words, the vessels are already in a healthy state and did not require much improvement. Thus, SKA-31 treatment was not expected to induce significant changes in sham operated mice. However, as explained previously, the mice with MI injury displayed a significant drop in cardiac function. Interestingly, there is a trend of further exacerbation associated with SKA-31 treatment in MI group (group 4) compared to its MI control with vehicle treatment (group 3). Although none of the modest differences were statistically significant, I suggest that the interpretation of this trend needs to be done very carefully since myocardium undergoes multiple processes over the course of an acute MI and subsequent recovery phase. However, with the recent robust data published by Deniset, Swirski and Nahrendorff, it is possible to recognize that there are large-scale inflammatory processes associated with LV remodeling as a part of post-MI events. In addition, there are reports indicating K_{Ca}3.1 channel expression on monocytes,

macrophages, neutrophils, fibroblasts and myofibroblasts. Therefore, I suggest that such potential exacerbation mediated by SKA-31 may be associated with cardio-immunological events within the LV associated with infarction. Therefore, I suggest and emphasize that pharmacological intervention to mitigate the progression of MI requires consideration of timing and complex multifactorial events associated with post-MI remodelling.

References

Andersen, K., and Vik-Mo, H. (1982). Role of the Frank-Starling mechanism during maximal semisupine exercise after oral atenolol. Br Heart J *48*, 149-155. 10.1136/hrt.48.2.149.

Anderson, J.L., and Morrow, D.A. (2017). Acute Myocardial Infarction. N Engl J Med *376*, 2053-2064. 10.1056/NEJMra1606915.

Atkinson, N.S., Robertson, G.A., and Ganetzky, B. (1991). A component of calcium-activated potassium channels encoded by the Drosophila slo locus. Science *253*, 551-555. 10.1126/science.1857984.

Baan, J., van der Velde, E.T., de Bruin, H.G., Smeenk, G.J., Koops, J., van Dijk, A.D., Temmerman, D., Senden, J., and Buis, B. (1984). Continuous measurement of left ventricular volume in animals and humans by conductance catheter. Circulation *70*, 812-823. 10.1161/01.cir.70.5.812.

Bajpai, G., Bredemeyer, A., Li, W., Zaitsev, K., Koenig, A.L., Lokshina, I., Mohan, J., Ivey, B., Hsiao, H.M., Weinheimer, C., et al. (2019). Tissue Resident CCR2- and CCR2+ Cardiac Macrophages Differentially Orchestrate Monocyte Recruitment and Fate Specification Following Myocardial Injury. Circ Res *124*, 263-278. 10.1161/circresaha.118.314028.

Baruscotti, M., Barbuti, A., and Bucchi, A. (2010). The cardiac pacemaker current. J Mol Cell Cardiol *48*, 55-64. 10.1016/j.yjmcc.2009.06.019.

Brown, B.M., Shim, H., Zhang, M., Yarov-Yarovoy, V., and Wulff, H. (2017). Structural Determinants for the Selectivity of the Positive KCa3.1 Gating Modulator 5-Methylnaphtho[2,1-d]oxazol-2-amine (SKA-121). Mol Pharmacol *92*, 469-480. 10.1124/mol.117.109421.

Brown, H., and Difrancesco, D. (1980). Voltage-clamp investigations of membrane currents underlying pace-maker activity in rabbit sino-atrial node. J Physiol *308*, 331-351. 10.1113/jphysiol.1980.sp013474.

Burkhoff, D., Mirsky, I., and Suga, H. (2005). Assessment of systolic and diastolic ventricular properties via pressure-volume analysis: a guide for clinical, translational, and basic researchers. Am J Physiol Heart Circ Physiol *289*, H501-512. 10.1152/ajpheart.00138.2005.

Busse, R., Edwards, G., Félétou, M., Fleming, I., Vanhoutte, P.M., and Weston, A.H. (2002). EDHF: bringing the concepts together. Trends Pharmacol Sci *23*, 374-380. 10.1016/s0165-6147(02)02050-3.

Cahalan, M.D., and Chandy, K.G. (2009). The functional network of ion channels in T lymphocytes. Immunol Rev *231*, 59-87. 10.1111/j.1600-065X.2009.00816.x.

Chen, B.C., Chou, C.F., and Lin, W.W. (1998). Pyrimidinoceptor-mediated potentiation of inducible nitric-oxide synthase induction in J774 macrophages. Role of intracellular calcium. J Biol Chem *273*, 29754-29763. 10.1074/jbc.273.45.29754.

Chen, J., Ceholski, D.K., Liang, L., Fish, K., and Hajjar, R.J. (2017). Variability in coronary artery anatomy affects consistency of cardiac damage after myocardial infarction in mice. Am J Physiol Heart Circ Physiol *313*, H275-h282. 10.1152/ajpheart.00127.2017.

Chen, Y.J., Lam, J., Gregory, C.R., Schrepfer, S., and Wulff, H. (2013). The Ca^{2+}-activated K^{+} channel KCa3.1 as a potential new target for the prevention of allograft vasculopathy. PLoS One *8*, e81006. 10.1371/journal.pone.0081006.

Chua, S.K., Chang, P.C., Maruyama, M., Turker, I., Shinohara, T., Shen, M.J., Chen, Z., Shen, C., Rubart-von der Lohe, M., Lopshire, J.C., et al. (2011). Small-conductance calcium-activated potassium channel and recurrent ventricular fibrillation in failing rabbit ventricles. Circ Res *108*, 971-979. 10.1161/circresaha.110.238386.

Chung, I., Zelivyanskaya, M., and Gendelman, H.E. (2002). Mononuclear phagocyte biophysiology influences brain transendothelial and tissue migration: implication for HIV-1-associated dementia. J Neuroimmunol *122*, 40-54. 10.1016/s0165-5728(01)00462-3.

Constantinides, C., and Murphy, K. (2016). Molecular and Integrative Physiological Effects of Isoflurane Anesthesia: The Paradigm of Cardiovascular Studies in Rodents using Magnetic Resonance Imaging. Front Cardiovasc Med *3*, 23. 10.3389/fcvm.2016.00023.

Courties, G., Heidt, T., Sebas, M., Iwamoto, Y., Jeon, D., Truelove, J., Tricot, B., Wojtkiewicz, G., Dutta, P., Sager, H.B., et al. (2014). In vivo silencing of the transcription factor IRF5 reprograms the macrophage phenotype and improves infarct healing. J Am Coll Cardiol *63*, 1556-1566. 10.1016/j.jacc.2013.11.023.

Dalsgaard, T., Kroigaard, C., Misfeldt, M., Bek, T., and Simonsen, U. (2010). Openers of small conductance calcium-activated potassium channels selectively enhance NO-mediated bradykinin vasodilatation in porcine retinal arterioles. Br J Pharmacol *160*, 1496-1508. 10.1111/j.1476-5381.2010.00803.x.

Davis, M.J., and Hill, M.A. (1999). Signaling mechanisms underlying the vascular myogenic response. Physiol Rev *79*, 387-423. 10.1152/physrev.1999.79.2.387.

Deanfield, J.E., Halcox, J.P., and Rabelink, T.J. (2007). Endothelial function and dysfunction: testing and clinical relevance. Circulation *115*, 1285-1295. 10.1161/circulationaha.106.652859.

DeCoursey, T.E., Kim, S.Y., Silver, M.R., and Quandt, F.N. (1996). Ion channel expression in PMA-differentiated human THP-1 macrophages. J Membr Biol *152*, 141-157. 10.1007/s002329900093.

DeLeon-Pennell, K.Y., Meschiari, C.A., Jung, M., and Lindsey, M.L. (2017). Matrix Metalloproteinases in Myocardial Infarction and Heart Failure. Prog Mol Biol Transl Sci *147*, 75-100. 10.1016/bs.pmbts.2017.02.001.

Deniset, J.F., Belke, D., Lee, W.Y., Jorch, S.K., Deppermann, C., Hassanabad, A.F., Turnbull, J.D., Teng, G., Rozich, I., Hudspeth, K., et al. (2019). Gata6(+) Pericardial Cavity Macrophages Relocate to the Injured Heart and Prevent Cardiac Fibrosis. Immunity *51*, 131-140.e135. 10.1016/j.immuni.2019.06.010.

Dick, S.A., Macklin, J.A., Nejat, S., Momen, A., Clemente-Casares, X., Althagafi, M.G., Chen, J., Kantores, C., Hosseinzadeh, S., Aronoff, L., et al. (2019). Self-renewing resident cardiac macrophages limit adverse remodeling following myocardial infarction. Nat Immunol *20*, 29-39. 10.1038/s41590-018-0272-2.

Dutta, P., Courties, G., Wei, Y., Leuschner, F., Gorbatov, R., Robbins, C.S., Iwamoto, Y., Thompson, B., Carlson, A.L., Heidt, T., et al. (2012). Myocardial infarction accelerates atherosclerosis. Nature *487*, 325-329. 10.1038/nature11260.

Edwards, G., Félétou, M., and Weston, A.H. (2010). Endothelium-derived hyperpolarising factors and associated pathways: a synopsis. Pflugers Arch *459*, 863-879. 10.1007/s00424-010-0817-1.

Félétou, M. (2009). Calcium-activated potassium channels and endothelial dysfunction: therapeutic options? Br J Pharmacol *156*, 545-562. 10.1111/j.1476-5381.2009.00052.x.

Félétou, M., and Vanhoutte, P.M. (2006). Endothelium-derived hyperpolarizing factor: where are we now? Arterioscler Thromb Vasc Biol *26*, 1215-1225. 10.1161/01.ATV.0000217611.81085.c5.

Feske, S. (2007). Calcium signalling in lymphocyte activation and disease. Nat Rev Immunol *7*, 690-702. 10.1038/nri2152.

Feske, S., Wulff, H., and Skolnik, E.Y. (2015). Ion channels in innate and adaptive immunity. Annu Rev Immunol *33*, 291-353. 10.1146/annurev-immunol-032414-112212.

Frangogiannis, N.G. (2014). The inflammatory response in myocardial injury, repair, and remodelling. Nat Rev Cardiol *11*, 255-265. 10.1038/nrcardio.2014.28.

Frangogiannis, N.G., Dewald, O., Xia, Y., Ren, G., Haudek, S., Leucker, T., Kraemer, D., Taffet, G., Rollins, B.J., and Entman, M.L. (2007). Critical role of monocyte chemoattractant protein-1/CC chemokine ligand 2 in the pathogenesis of ischemic cardiomyopathy. Circulation *115*, 584-592. 10.1161/circulationaha.106.646091.

Frangogiannis, N.G., Mendoza, L.H., Ren, G., Akrivakis, S., Jackson, P.L., Michael, L.H., Smith, C.W., and Entman, M.L. (2003). MCSF expression is induced in healing myocardial infarcts and may regulate monocyte and endothelial cell phenotype. Am J Physiol Heart Circ Physiol *285*, H483-492. 10.1152/ajpheart.01016.2002.

Frangogiannis, N.G., Smith, C.W., and Entman, M.L. (2002). The inflammatory response in myocardial infarction. Cardiovasc Res *53*, 31-47. 10.1016/s0008-6363(01)00434-5.

Furchgott, R.F., and Zawadzki, J.V. (1980). The obligatory role of endothelial cells in the relaxation of arterial smooth muscle by acetylcholine. Nature *288*, 373-376. 10.1038/288373a0.

Gallin, E.K. (1984). Calcium- and voltage-activated potassium channels in human macrophages. Biophys J *46*, 821-825. 10.1016/s0006-3495(84)84080-1.

Gao, E., Lei, Y.H., Shang, X., Huang, Z.M., Zuo, L., Boucher, M., Fan, Q., Chuprun, J.K., Ma, X.L., and Koch, W.J. (2010a). A novel and efficient model of coronary artery ligation and myocardial infarction in the mouse. Circ Res *107*, 1445-1453. 10.1161/circresaha.110.223925.

Gao, X.M., Dart, A.M., Dewar, E., Jennings, G., and Du, X.J. (2000). Serial echocardiographic assessment of left ventricular dimensions and function after myocardial infarction in mice. Cardiovasc Res *45*, 330-338. 10.1016/s0008-6363(99)00274-6.

Gao, Y.D., Hanley, P.J., Rinné, S., Zuzarte, M., and Daut, J. (2010b). Calcium-activated K(+) channel (K(Ca)3.1) activity during Ca(2+) store depletion and store-operated Ca(2+) entry in human macrophages. Cell Calcium *48*, 19-27. 10.1016/j.ceca.2010.06.002.

Garcia, M., Mulvagh, S.L., Merz, C.N., Burning, J.E., Manson, J.E. (2016) Cardiovascular Disease in Women: Clinical Perspective. Circ Res *118*, 1273-1293. 10.1161/CIRCRESAHA. 116.307547

Gardos, G. (1958). The function of calcium in the potassium permeability of human erythrocytes. Biochim Biophys Acta *30*, 653-654. 10.1016/0006-3002(58)90124-0.

Givertz, M.M., and Mann, D.L. (2013). Epidemiology and natural history of recovery of left ventricular function in recent onset dilated cardiomyopathies. Curr Heart Fail Rep *10*, 321-330. 10.1007/s11897-013-0157-5.

Groenke, S., Larson, E.D., Alber, S., Zhang, R., Lamp, S.T., Ren, X., Nakano, H., Jordan, M.C., Karagueuzian, H.S., Roos, K.P., et al. (2013). Complete atrial-specific knockout of sodium-calcium exchange eliminates sinoatrial node pacemaker activity. PLoS One *8*, e81633. 10.1371/journal.pone.0081633.

Grundy, D. (2015). Principles and standards for reporting animal experiments in The Journal of Physiology and Experimental Physiology. J Physiol *593*, 2547-2549. 10.1113/jp270818.

Gschwend, S., Henning, R.H., Pinto, Y.M., de Zeeuw, D., van Gilst, W.H., and Buikema, H. (2003). Myogenic constriction is increased in mesenteric resistance arteries from rats with chronic heart failure: instantaneous counteraction by acute AT1 receptor blockade. Br J Pharmacol *139*, 1317-1325. 10.1038/sj.bjp.0705367.

Gupta A.K., Tomasoni D., Sidhu K., Metra M., and Ezekowitz J.A. (2021). Evidence-Based Management of Acute Heart Failure. Can J Cardiol *37*, 621-641. 10.1016/j.cjca.2021.01.002.

Hancock, J.M., Weatherall, K.L., Choisy, S.C., James, A.F., Hancox, J.C., and Marrion, N.V. (2015). Selective activation of heteromeric SK channels contributes to action potential repolarization in mouse atrial myocytes. Heart Rhythm *12*, 1003-1015. 10.1016/j.hrthm.2015.01.027.

Hanley, P.J., Musset, B., Renigunta, V., Limberg, S.H., Dalpke, A.H., Sus, R., Heeg, K.M., Preisig-Müller, R., and Daut, J. (2004). Extracellular ATP induces oscillations of intracellular Ca2+ and membrane potential and promotes transcription of IL-6 in macrophages. Proc Natl Acad Sci U S A *101*, 9479-9484. 10.1073/pnas.0400733101.

Haron-Khun, S., Weisbrod, D., Bueno, H., Yadin, D., Behar, J., Peretz, A., Binah, O., Hochhauser, E., Eldar, M., Yaniv, Y., et al. (2017). SK4 K(+) channels are therapeutic targets for the treatment of cardiac arrhythmias. EMBO Mol Med *9*, 415-429. 10.15252/emmm.201606937.

Hart, C.Y., Burnett, J.C., Jr., and Redfield, M.M. (2001). Effects of avertin versus xylazine-ketamine anesthesia on cardiac function in normal mice. Am J Physiol Heart Circ Physiol *281*, H1938-1945. 10.1152/ajpheart.2001.281.5.H1938.

Hasenau, A.L., Nielsen, G., Morisseau, C., Hammock, B.D., Wulff, H., and Köhler, R. (2011). Improvement of endothelium-dependent vasodilations by SKA-31 and SKA-20, activators of small- and intermediate-conductance Ca2+ -activated K+ -channels. Acta Physiol (Oxf) *203*, 117-126. 10.1111/j.1748-1716.2010.02240.x.

Hashimoto, D., Chow, A., Noizat, C., Teo, P., Beasley, M.B., Leboeuf, M., Becker, C.D., See, P., Price, J., Lucas, D., et al. (2013). Tissue-resident macrophages self-maintain locally throughout adult life with minimal contribution from circulating monocytes. Immunity *38*, 792-804. 10.1016/j.immuni.2013.04.004.

Heidt, T., Courties, G., Dutta, P., Sager, H.B., Sebas, M., Iwamoto, Y., Sun, Y., Da Silva, N., Panizzi, P., van der Laan, A.M., et al. (2014). Differential contribution of monocytes to heart macrophages in steady-state and after myocardial infarction. Circ Res *115*, 284-295. 10.1161/circresaha.115.303567.

Hilgendorf, I., Gerhardt, L.M., Tan, T.C., Winter, C., Holderried, T.A., Chousterman, B.G., Iwamoto, Y., Liao, R., Zirlik, A., Scherer-Crosbie, M., et al. (2014). Ly-6Chigh monocytes depend on Nr4a1 to balance both inflammatory and reparative phases in the infarcted myocardium. Circ Res *114*, 1611-1622. 10.1161/circresaha.114.303204.

Holt, D.B., Jr., and Pang, P.S. (2019). Vasodilator Therapies in the Treatment of Acute Heart Failure. Curr Heart Fail Rep *16*, 32-37. 10.1007/s11897-019-0421-4.

Honold, L., and Nahrendorf, M. (2018). Resident and Monocyte-Derived Macrophages in Cardiovascular Disease. Circ Res *122*, 113-127. 10.1161/circresaha.117.311071.

Ignarro, L.J., Buga, G.M., Wood, K.S., Byrns, R.E., and Chaudhuri, G. (1987a). Endothelium-derived relaxing factor produced and released from artery and vein is nitric oxide. Proc Natl Acad Sci U S A *84*, 9265-9269. 10.1073/pnas.84.24.9265.

Ignarro, L.J., Byrns, R.E., Buga, G.M., and Wood, K.S. (1987b). Endothelium-derived relaxing factor from pulmonary artery and vein possesses pharmacologic and chemical properties identical to those of nitric oxide radical. Circ Res *61*, 866-879. 10.1161/01.res.61.6.866.

Ishii, T.M., Silvia, C., Hirschberg, B., Bond, C.T., Adelman, J.P., and Maylie, J. (1997). A human intermediate conductance calcium-activated potassium channel. Proc Natl Acad Sci U S A *94*, 11651-11656. 10.1073/pnas.94.21.11651.

John, C.M., Khaddaj Mallat, R., Mishra, R.C., George, G., Singh, V., Turnbull, J.D., Umeshappa, C.S., Kendrick, D.J., Kim, T., Fauzi, F.M., et al. (2020). SKA-31, an activator of Ca(2+)-activated K(+) channels, improves cardiovascular function in aging. Pharmacol Res *151*, 104539. 10.1016/j.phrs.2019.104539.

Joiner, W.J., Wang, L.Y., Tang, M.D., and Kaczmarek, L.K. (1997). hSK4, a member of a novel subfamily of calcium-activated potassium channels. Proc Natl Acad Sci U S A *94*, 11013-11018. 10.1073/pnas.94.20.11013.

Jugdutt, B.I., Joljart, M.J., and Khan, M.I. (1996). Rate of collagen deposition during healing and ventricular remodeling after myocardial infarction in rat and dog models. Circulation *94*, 94-101. 10.1161/01.cir.94.1.94.

Keen, J.E., Khawaled, R., Farrens, D.L., Neelands, T., Rivard, A., Bond, C.T., Janowsky, A., Fakler, B., Adelman, J.P., and Maylie, J. (1999). Domains responsible for constitutive and Ca(2+)-dependent interactions between calmodulin and small conductance Ca(2+)-activated potassium channels. J Neurosci *19*, 8830-8838. 10.1523/jneurosci.19-20-08830.1999.

Khaddaj-Mallat, R., Mathew John, C., and Braun, A.P. (2018). SKA-31, an activator of endothelial Ca(2+)-activated K(+) channels evokes robust vasodilation in rat mesenteric arteries. Eur J Pharmacol *831*, 60-67. 10.1016/j.ejphar.2018.05.006.

Khaddaj Mallat, R., Mathew John, C., Mishra, R.C., Kendrick, D.J., and Braun, A.P. (2019). Pharmacological Targeting of KCa Channels to Improve Endothelial Function in the Spontaneously Hypertensive Rat. Int J Mol Sci *20*. 10.3390/ijms20143481.

Köhler, M., Hirschberg, B., Bond, C.T., Kinzie, J.M., Marrion, N.V., Maylie, J., and Adelman, J.P. (1996). Small-conductance, calcium-activated potassium channels from mammalian brain. Science *273*, 1709-1714. 10.1126/science.273.5282.1709.

Köhler, R., Oliván-Viguera, A., and Wulff, H. (2016). Endothelial Small- and Intermediate-Conductance K Channels and Endothelium-Dependent Hyperpolarization as Drug Targets in Cardiovascular Disease. Adv Pharmacol *77*, 65-104. 10.1016/bs.apha.2016.04.002.

Kübler, W., and Spieckermann, P.G. (1970). Regulation of glycolysis in the ischemic and the anoxic myocardium. J Mol Cell Cardiol *1*, 351-377. 10.1016/0022-2828(70)90034-9.

Kuriyama, H., and Suzuki, H. (1978). Electrical property and chemical sensitivity of vascular smooth muscles in normotensive and spontaneously hypersensitive rats. J Physiol *285*, 409-424. 10.1113/jphysiol.1978.sp012579.

Launay, P., Cheng, H., Srivatsan, S., Penner, R., Fleig, A., and Kinet, J.P. (2004). TRPM4 regulates calcium oscillations after T cell activation. Science *306*, 1374-1377. 10.1126/science.1098845.

Launay, P., Fleig, A., Perraud, A.L., Scharenberg, A.M., Penner, R., and Kinet, J.P. (2002). TRPM4 is a Ca2+-activated nonselective cation channel mediating cell membrane depolarization. Cell *109*, 397-407. 10.1016/s0092-8674(02)00719-5.

Ledoux, J., Gee, D.M., and Leblanc, N. (2003). Increased peripheral resistance in heart failure: new evidence suggests an alteration in vascular smooth muscle function. Br J Pharmacol *139*, 1245-1248. 10.1038/sj.bjp.0705366.

Lee, W.W., Marinelli, B., van der Laan, A.M., Sena, B.F., Gorbatov, R., Leuschner, F., Dutta, P., Iwamoto, Y., Ueno, T., Begieneman, M.P., et al. (2012). PET/MRI of inflammation in myocardial infarction. J Am Coll Cardiol *59*, 153-163. 10.1016/j.jacc.2011.08.066.

Lee, Y.S., Chang, P.C., Hsueh, C.H., Maruyama, M., Park, H.W., Rhee, K.S., Hsieh, Y.C., Shen, C., Weiss, J.N., Chen, Z., et al. (2013). Apamin-sensitive calcium-activated potassium currents in rabbit ventricles with chronic myocardial infarction. J Cardiovasc Electrophysiol *24*, 1144-1153. 10.1111/jce.12176.

Leite-Moreira, A.F. (2006). Current perspectives in diastolic dysfunction and diastolic heart failure. Heart *92*, 712-718. 10.1136/hrt.2005.062950.

Leuschner, F., Rauch, P.J., Ueno, T., Gorbatov, R., Marinelli, B., Lee, W.W., Dutta, P., Wei, Y., Robbins, C., Iwamoto, Y., et al. (2012). Rapid monocyte kinetics in acute myocardial

infarction are sustained by extramedullary monocytopoiesis. J Exp Med *209*, 123-137. 10.1084/jem.20111009.

Li, W., Hsiao, H.M., Higashikubo, R., Saunders, B.T., Bharat, A., Goldstein, D.R., Krupnick, A.S., Gelman, A.E., Lavine, K.J., and Kreisel, D. (2016). Heart-resident CCR2(+) macrophages promote neutrophil extravasation through TLR9/MyD88/CXCL5 signaling. JCI Insight *1*. 10.1172/jci.insight.87315.

Lighthouse, J.K., and Small, E.M. (2016). Transcriptional control of cardiac fibroblast plasticity. J Mol Cell Cardiol *91*, 52-60. 10.1016/j.yjmcc.2015.12.016.

Lindsey, M.L. (2018). Assigning matrix metalloproteinase roles in ischaemic cardiac remodelling. Nat Rev Cardiol *15*, 471-479. 10.1038/s41569-018-0022-z.

Lindsey, M.L., Bolli, R., Canty, J.M., Jr., Du, X.J., Frangogiannis, N.G., Frantz, S., Gourdie, R.G., Holmes, J.W., Jones, S.P., Kloner, R.A., et al. (2018a). Guidelines for experimental models of myocardial ischemia and infarction. Am J Physiol Heart Circ Physiol *314*, H812-h838. 10.1152/ajpheart.00335.2017.

Lindsey, M.L., Kassiri, Z., Virag, J.A.I., de Castro Brás, L.E., and Scherrer-Crosbie, M. (2018b). Guidelines for measuring cardiac physiology in mice. Am J Physiol Heart Circ Physiol *314*, H733-h752. 10.1152/ajpheart.00339.2017.

Lu, L., Zhang, Q., Timofeyev, V., Zhang, Z., Young, J.N., Shin, H.S., Knowlton, A.A., and Chiamvimonvat, N. (2007). Molecular coupling of a Ca2+-activated K+ channel to L-type Ca2+ channels via alpha-actinin2. Circ Res *100*, 112-120. 10.1161/01.Res.0000253095.44186.72.

Mach, F., Lovis, C., Gaspoz, J.M., Unger, P.F., Bouillie, M., Urban, P., and Rutishauser, W. (1997). C-reactive protein as a marker for acute coronary syndromes. Eur Heart J *18*, 1897-1902. 10.1093/oxfordjournals.eurheartj.a015198.

Mathew John, C., Khaddaj Mallat, R., George, G., Kim, T., Mishra, R.C., and Braun, A.P. (2018). Pharmacologic targeting of endothelial Ca(2+)-activated K(+) channels: A strategy to improve cardiovascular function. Channels (Austin) *12*, 126-136. 10.1080/19336950.2018.1454814.

Matsuda, Y., Ohsaka, K., Yamamoto, H., Jiyouraku, K., Natsume, K., Hirabayashi, S., Kounoike, M., and Inoue, M. (2007). NARCOBIT: a newly developed inhalational anesthesia system for mice. Exp Anim *56*, 131-137. 10.1538/expanim.56.131.

Meech, R.W., and Standen, N.B. (1974). Calcium-mediated potassium activation in Helix neurones. J Physiol *237*, 43p-44p.

Meera, P., Wallner, M., Song, M., and Toro, L. (1997). Large conductance voltage- and calcium-dependent K+ channel, a distinct member of voltage-dependent ion channels with seven N-terminal transmembrane segments (S0-S6), an extracellular N terminus,

and an intracellular (S9-S10) C terminus. Proc Natl Acad Sci U S A *94*, 14066-14071. 10.1073/pnas.94.25.14066.

Michael, L.H., Ballantyne, C.M., Zachariah, J.P., Gould, K.E., Pocius, J.S., Taffet, G.E., Hartley, C.J., Pham, T.T., Daniel, S.L., Funk, E., and Entman, M.L. (1999). Myocardial infarction and remodeling in mice: effect of reperfusion. Am J Physiol *277*, H660-668. 10.1152/ajpheart.1999.277.2.H660.

Mishra, R.C., Belke, D., Wulff, H., and Braun, A.P. (2013). SKA-31, a novel activator of SK(Ca) and IK(Ca) channels, increases coronary flow in male and female rat hearts. Cardiovasc Res *97*, 339-348. 10.1093/cvr/cvs326.

Mishra, R.C., Kyle, B.D., Kendrick, D.J., Svystonyuk, D., Kieser, T.M., Fedak, P.W.M., Wulff, H., and Braun, A.P. (2021). KCa channel activation normalizes endothelial function in Type 2 Diabetic resistance arteries by improving intracellular Ca(2+) mobilization. Metabolism *114*, 154390. 10.1016/j.metabol.2020.154390.

Mishra, R.C., Mitchell, J.R., Gibbons-Kroeker, C., Wulff, H., Belenkie, I., Tyberg, J.V., and Braun, A.P. (2016). A pharmacologic activator of endothelial KCa channels increases systemic conductance and reduces arterial pressure in an anesthetized pig model. Vascul Pharmacol *79*, 24-31. 10.1016/j.vph.2015.07.016.

Mishra, R.C., Wulff, H., Cole, W.C., and Braun, A.P. (2014). A pharmacologic activator of endothelial KCa channels enhances coronary flow in the hearts of type 2 diabetic rats. J Mol Cell Cardiol *72*, 364-373. 10.1016/j.yjmcc.2014.04.013.

Murray, C.J., Barber, R.M., Foreman, K.J., Abbasoglu Ozgoren, A., Abd-Allah, F., Abera, S.F., Aboyans, V., Abraham, J.P., Abubakar, I., Abu-Raddad, L.J., et al. (2015). Global, regional, and national disability-adjusted life years (DALYs) for 306 diseases and injuries and healthy life expectancy (HALE) for 188 countries, 1990-2013: quantifying the epidemiological transition. Lancet *386*, 2145-2191. 10.1016/s0140-6736(15)61340-x.

Murray, C.J., Vos, T., Lozano, R., Naghavi, M., Flaxman, A.D., Michaud, C., Ezzati, M., Shibuya, K., Salomon, J.A., Abdalla, S., et al. (2012). Disability-adjusted life years (DALYs) for 291 diseases and injuries in 21 regions, 1990-2010: a systematic analysis for the Global Burden of Disease Study 2010. Lancet *380*, 2197-2223. 10.1016/s0140-6736(12)61689-4.

Nahrendorf, M., Swirski, F.K., Aikawa, E., Stangenberg, L., Wurdinger, T., Figueiredo, J.L., Libby, P., Weissleder, R., and Pittet, M.J. (2007). The healing myocardium sequentially mobilizes two monocyte subsets with divergent and complementary functions. J Exp Med *204*, 3037-3047. 10.1084/jem.20070885.

Nelson, D.J., Jow, B., and Jow, F. (1992). Lipopolysaccharide induction of outward potassium current expression in human monocyte-derived macrophages: lack of correlation with secretion. J Membr Biol *125*, 207-218. 10.1007/bf00236434.

Nossuli, T.O., Lakshminarayanan, V., Baumgarten, G., Taffet, G.E., Ballantyne, C.M., Michael, L.H., and Entman, M.L. (2000). A chronic mouse model of myocardial ischemia-reperfusion: essential in cytokine studies. Am J Physiol Heart Circ Physiol *278*, H1049-1055. 10.1152/ajpheart.2000.278.4.H1049.

Oh-hora, M. (2009). Calcium signaling in the development and function of T-lineage cells. Immunol Rev *231*, 210-224. 10.1111/j.1600-065X.2009.00819.x.

Pacher, P., Bátkai, S., and Kunos, G. (2004). Haemodynamic profile and responsiveness to anandamide of TRPV1 receptor knock-out mice. J Physiol *558*, 647-657. 10.1113/jphysiol.2004.064824.

Pacher, P., Nagayama, T., Mukhopadhyay, P., Bátkai, S., and Kass, D.A. (2008). Measurement of cardiac function using pressure-volume conductance catheter technique in mice and rats. Nat Protoc *3*, 1422-1434. 10.1038/nprot.2008.138.

Palmer, R.M., Ferrige, A.G., and Moncada, S. (1987). Nitric oxide release accounts for the biological activity of endothelium-derived relaxing factor. Nature *327*, 524-526. 10.1038/327524a0.

Prakriya, M., and Lewis, R.S. (2015). Store-Operated Calcium Channels. Physiol Rev *95*, 1383-1436. 10.1152/physrev.00020.2014.

Procopio, M.C., Lauro, R., Nasso, C., Carerj, S., Squadrito, F., Bitto, A., Di Bella, G., Micari, A., Irrera, N., and Costa, F. (2021). Role of Adenosine and Purinergic Receptors in Myocardial Infarction: Focus on Different Signal Transduction Pathways. Biomedicines *9*. 10.3390/biomedicines9020204.

Reher, T.A., Wang, Z., Hsueh, C.H., Chang, P.C., Pan, Z., Kumar, M., Patel, J., Tan, J., Shen, C., Chen, Z., et al. (2017). Small-Conductance Calcium-Activated Potassium Current in Normal Rabbit Cardiac Purkinje Cells. J Am Heart Assoc *6*. 10.1161/jaha.117.005471.

Roach, K.M., and Bradding, P. (2020). Ca(2+) signalling in fibroblasts and the therapeutic potential of K(Ca)3.1 channel blockers in fibrotic diseases. Br J Pharmacol *177*, 1003-1024. 10.1111/bph.14939.

Sager, H.B., Hulsmans, M., Lavine, K.J., Moreira, M.B., Heidt, T., Courties, G., Sun, Y., Iwamoto, Y., Tricot, B., Khan, O.F., et al. (2016). Proliferation and Recruitment Contribute to Myocardial Macrophage Expansion in Chronic Heart Failure. Circ Res *119*, 853-864. 10.1161/circresaha.116.309001.

Sambuceti, G., Marzilli, M., Marraccini, P., Schneider-Eicke, J., Gliozheni, E., Parodi, O., and L'Abbate, A. (1997). Coronary vasoconstriction during myocardial ischemia induced by rises in metabolic demand in patients with coronary artery disease. Circulation *95*, 2652-2659. 10.1161/01.cir.95.12.2652.

Sankaranarayanan, A., Raman, G., Busch, C., Schultz, T., Zimin, P.I., Hoyer, J., Köhler, R., and Wulff, H. (2009). Naphtho[1,2-d]thiazol-2-ylamine (SKA-31), a new activator of KCa2 and KCa3.1 potassium channels, potentiates the endothelium-derived hyperpolarizing factor response and lowers blood pressure. Mol Pharmacol *75*, 281-295. 10.1124/mol.108.051425.

Schreiber, M., Yuan, A., and Salkoff, L. (1999). Transplantable sites confer calcium sensitivity to BK channels. Nat Neurosci *2*, 416-421. 10.1038/8077.

Scott, C.L., Zheng, F., De Baetselier, P., Martens, L., Saeys, Y., De Prijck, S., Lippens, S., Abels, C., Schoonooghe, S., Raes, G., et al. (2016). Bone marrow-derived monocytes give rise to self-renewing and fully differentiated Kupffer cells. Nat Commun *7*, 10321. 10.1038/ncomms10321.

Seydel, U., Scheel, O., Müller, M., Brandenburg, K., and Blunck, R. (2001). A K+ channel is involved in LPS signaling. J Endotoxin Res *7*, 243-247.

Shamsaldeen, Y.A., Culliford, L., Clout, M., James, A.F., Ascione, R., Hancox, J.C., and Marrion, N.V. (2019). Role of SK channel activation in determining the action potential configuration in freshly isolated human atrial myocytes from the SKArF study. Biochem Biophys Res Commun *512*, 684-690. 10.1016/j.bbrc.2019.03.074.

Sheng, J.Z., Ella, S., Davis, M.J., Hill, M.A., and Braun, A.P. (2009). Openers of SKCa and IKCa channels enhance agonist-evoked endothelial nitric oxide synthesis and arteriolar vasodilation. Faseb j *23*, 1138-1145. 10.1096/fj.08-120451.

Shioura, K.M., Geenen, D.L., and Goldspink, P.H. (2007). Assessment of cardiac function with the pressure-volume conductance system following myocardial infarction in mice. Am J Physiol Heart Circ Physiol *293*, H2870-2877. 10.1152/ajpheart.00585.2007.

Skibsbye, L., Poulet, C., Diness, J.G., Bentzen, B.H., Yuan, L., Kappert, U., Matschke, K., Wettwer, E., Ravens, U., Grunnet, M., et al. (2014). Small-conductance calcium-activated potassium (SK) channels contribute to action potential repolarization in human atria. Cardiovasc Res *103*, 156-167. 10.1093/cvr/cvu121.

Soboloff, J., Rothberg, B.S., Madesh, M., and Gill, D.L. (2012). STIM proteins: dynamic calcium signal transducers. Nat Rev Mol Cell Biol *13*, 549-565. 10.1038/nrm3414.

Song, Y., Zhan, L., Yu, M., Huang, C., Meng, X., Ma, T., Zhang, L., and Li, J. (2014). TRPV4 channel inhibits TGF-β1-induced proliferation of hepatic stellate cells. PLoS One *9*, e101179. 10.1371/journal.pone.0101179.

Stowe, D.F., Gadicherla, A.K., Zhou, Y., Aldakkak, M., Cheng, Q., Kwok, W.M., Jiang, M.T., Heisner, J.S., Yang, M., and Camara, A.K. (2013). Protection against cardiac injury by small Ca(2+)-sensitive K(+) channels identified in guinea pig cardiac inner mitochondrial membrane. Biochim Biophys Acta *1828*, 427-442. 10.1016/j.bbamem.2012.08.031.

Strøbæk, D., Brown, D.T., Jenkins, D.P., Chen, Y.J., Coleman, N., Ando, Y., Chiu, P., Jørgensen, S., Demnitz, J., Wulff, H., and Christophersen, P. (2013). NS6180, a new K(Ca) 3.1 channel inhibitor prevents T-cell activation and inflammation in a rat model of inflammatory bowel disease. Br J Pharmacol *168*, 432-444. 10.1111/j.1476-5381.2012.02143.x.

Swirski, F.K., and Nahrendorf, M. (2013). Leukocyte behavior in atherosclerosis, myocardial infarction, and heart failure. Science *339*, 161-166. 10.1126/science.1230719.

Swirski, F.K., and Nahrendorf, M. (2018). Cardioimmunology: the immune system in cardiac homeostasis and disease. Nat Rev Immunol *18*, 733-744. 10.1038/s41577-018-0065-8.

Swirski, F.K., Nahrendorf, M., Etzrodt, M., Wildgruber, M., Cortez-Retamozo, V., Panizzi, P., Figueiredo, J.L., Kohler, R.H., Chudnovskiy, A., Waterman, P., et al. (2009). Identification of splenic reservoir monocytes and their deployment to inflammatory sites. Science *325*, 612-616. 10.1126/science.1175202.

Szczesny, G., Veihelmann, A., Massberg, S., Nolte, D., and Messmer, K. (2004). Long-term anaesthesia using inhalatory isoflurane in different strains of mice-the haemodynamic effects. Lab Anim *38*, 64-69. 10.1258/00236770460734416.

Toyama, K., Wulff, H., Chandy, K.G., Azam, P., Raman, G., Saito, T., Fujiwara, Y., Mattson, D.L., Das, S., Melvin, J.E., et al. (2008). The intermediate-conductance calcium-activated potassium channel KCa3.1 contributes to atherogenesis in mice and humans. J Clin Invest *118*, 3025-3037. 10.1172/jci30836.

Tran, D.T., Welsh, R.C., Ohinmaa, A., Thanh, N.X., Bagai, A., and Kaul, P. (2017). Quality of Acute Myocardial Infarction Care in Canada: A 10-Year Review of 30-Day In-Hospital Mortality and 30-Day Hospital Readmission. Can J Cardiol *33*, 1319-1326. 10.1016/j.cjca.2017.06.014.

Tuteja, D., Xu, D., Timofeyev, V., Lu, L., Sharma, D., Zhang, Z., Xu, Y., Nie, L., Vázquez, A.E., Young, J.N., et al. (2005). Differential expression of small-conductance Ca2+-activated K+ channels SK1, SK2, and SK3 in mouse atrial and ventricular myocytes. Am J Physiol Heart Circ Physiol *289*, H2714-2723. 10.1152/ajpheart.00534.2005.

Tzahor, E., and Poss, K.D. (2017). Cardiac regeneration strategies: Staying young at heart. Science *356*, 1035-1039. 10.1126/science.aam5894.

Van Der Velden, J., Sum, G., Barker, D., Koumoundouros, E., Barcham, G., Wulff, H., Castle, N., Bradding, P., and Snibson, K. (2013). K(Ca)3.1 channel-blockade attenuates airway pathophysiology in a sheep model of chronic asthma. PLoS One *8*, e66886. 10.1371/journal.pone.0066886.

Vandael, D.H., Zuccotti, A., Striessnig, J., and Carbone, E. (2012). Ca(V)1.3-driven SK channel activation regulates pacemaking and spike frequency adaptation in mouse chromaffin cells. J Neurosci *32*, 16345-16359. 10.1523/jneurosci.3715-12.2012.

Vanhoutte, P.M., Shimokawa, H., Feletou, M., and Tang, E.H. (2017). Endothelial dysfunction and vascular disease - a 30th anniversary update. Acta Physiol (Oxf) *219*, 22-96. 10.1111/apha.12646.

Vergara, C., Latorre, R., Marrion, N.V., and Adelman, J.P. (1998). Calcium-activated potassium channels. Curr Opin Neurobiol *8*, 321-329. 10.1016/s0959-4388(98)80056-1.

Vicente, R., Escalada, A., Coma, M., Fuster, G., Sánchez-Tilló, E., López-Iglesias, C., Soler, C., Solsona, C., Celada, A., and Felipe, A. (2003). Differential voltage-dependent K+ channel responses during proliferation and activation in macrophages. J Biol Chem *278*, 46307-46320. 10.1074/jbc.M304388200.

Virani, S.S., Alonso, A., Benjamin, E.J., Bittencourt, M.S., Callaway, C.W., Carson, A.P., Chamberlain, A.M., Chang, A.R., Cheng, S., Delling, F.N., et al. (2020). Heart Disease and Stroke Statistics-2020 Update: A Report From the American Heart Association. Circulation *141*, e139-e596. 10.1161/cir.0000000000000757.

Watanabe, N., Suzuki, J., and Kobayashi, Y. (1996). Role of calcium in tumor necrosis factor-alpha production by activated macrophages. J Biochem *120*, 1190-1195. 10.1093/oxfordjournals.jbchem.a021540.

Weisbrod, D., Peretz, A., Ziskind, A., Menaker, N., Oz, S., Barad, L., Eliyahu, S., Itskovitz-Eldor, J., Dascal, N., Khananshvili, D., et al. (2013). SK4 Ca2+ activated K+ channel is a critical player in cardiac pacemaker derived from human embryonic stem cells. Proc Natl Acad Sci U S A *110*, E1685-1694. 10.1073/pnas.1221022110.

Wu, Y., Yin, X., Wijaya, C., Huang, M.H., and McConnell, B.K. (2011). Acute myocardial infarction in rats. J Vis Exp. 10.3791/2464.

Xu, Y., Tuteja, D., Zhang, Z., Xu, D., Zhang, Y., Rodriguez, J., Nie, L., Tuxson, H.R., Young, J.N., Glatter, K.A., et al. (2003). Molecular identification and functional roles of a Ca(2+)-activated K+ channel in human and mouse hearts. J Biol Chem *278*, 49085-49094. 10.1074/jbc.M307508200.

Zamilpa, R., Zhang, J., Chiao, Y.A., de Castro Brás, L.E., Halade, G.V., Ma, Y., Hacker, S.O., and Lindsey, M.L. (2013). Cardiac wound healing post-myocardial infarction: a novel method to target extracellular matrix remodeling in the left ventricle. Methods Mol Biol *1037*, 313-324. 10.1007/978-1-62703-505-7_18.

Zhang, H., Clemens, R.A., Liu, F., Hu, Y., Baba, Y., Theodore, P., Kurosaki, T., and Lowell, C.A. (2014). STIM1 calcium sensor is required for activation of the phagocyte oxidase during inflammation and host defense. Blood *123*, 2238-2249. 10.1182/blood-2012-08-450403.

Zhao, H., Yang, M., Wang, F., Yang, A., Zhao, Q., Wang, X., Tang, Y., Wang, T., and Huang, C. (2019). Overexpression of the medium-conductance calcium-activated potassium channel (SK4) and the HCN2 channel to generate a biological pacemaker. Mol Med Rep *20*, 3406-3414. 10.3892/mmr.2019.10591.

Appendix

Figure S1.

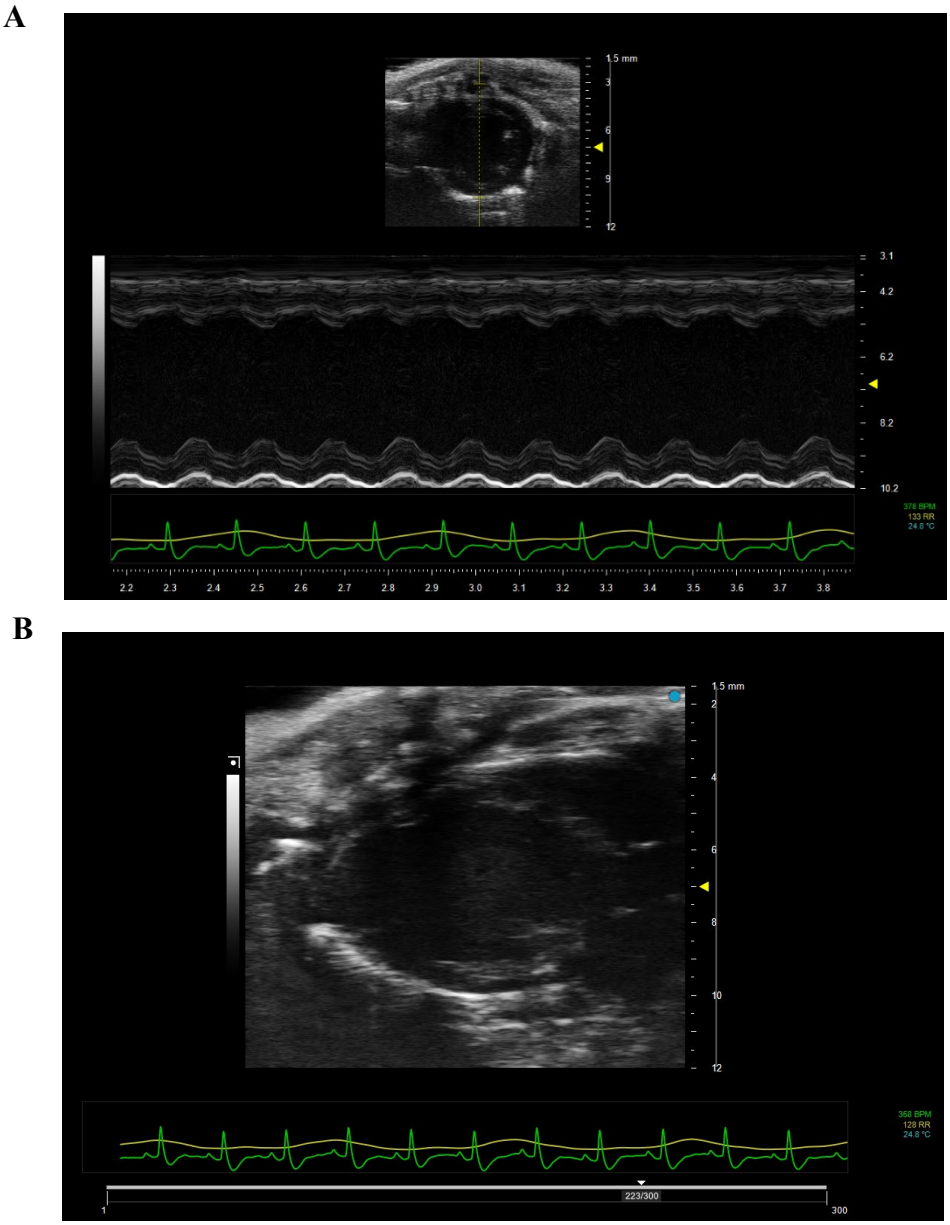

Sham + Vehicle
[2 weeks]

Figure S1. [Echocardiography] Group 1: Sham + Vehicle. These representative images were taken at 2 weeks following sham surgery. **[A]** Short axis view illustrates clean patterns of anterior and posterior side of left ventricular wall. Also, the accompanying ECG (lower trace) is normal with clear layout of the PQRST complex. **[B]** Long axis view illustrates relatively uniform layout of myocardium from base to apex. The images were taken prior to the P wave of ECG.

Figure S2.

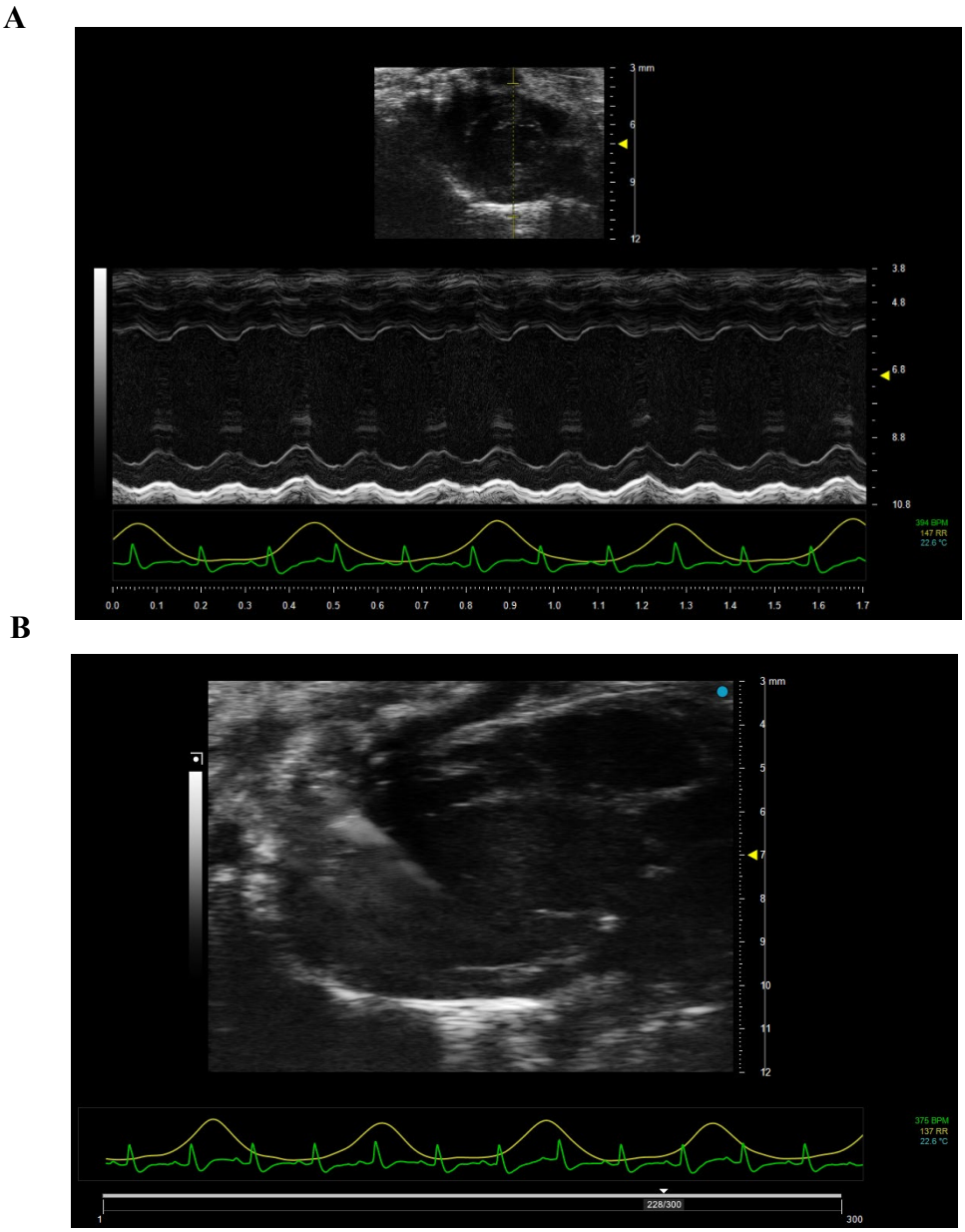

Figure S2. [Echocardiography] Group 2: Sham + SKA-31. Representative images were taken at 2 weeks following sham surgery. **[A]** Short axis view illustrates clean patterns of anterior and posterior side of left ventricular wall. Also, the accompanying ECG (lower trace) is normal with clear layout of the PQRST complex. **[B]** Long axis view illustrates relatively uniform layout of myocardium from base to apex. The images were taken prior to the P wave of ECG.

Figure S3.

A

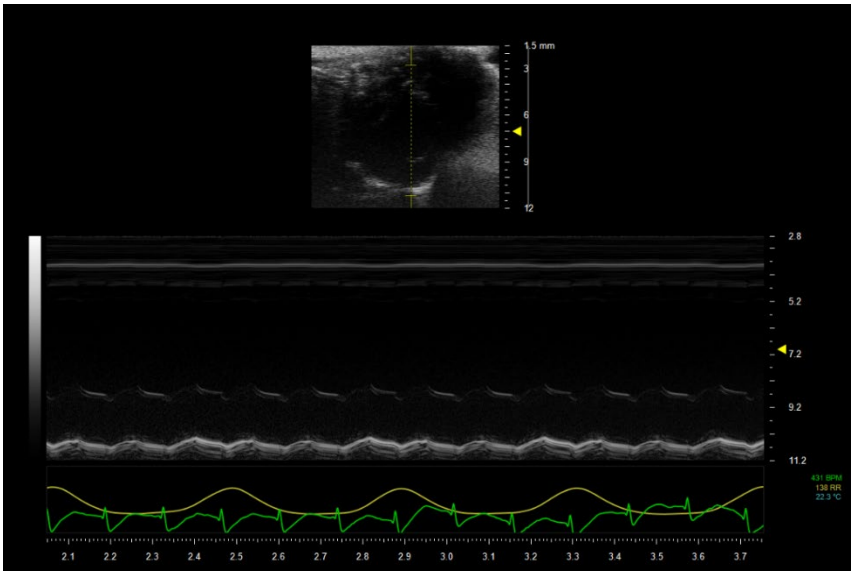

B

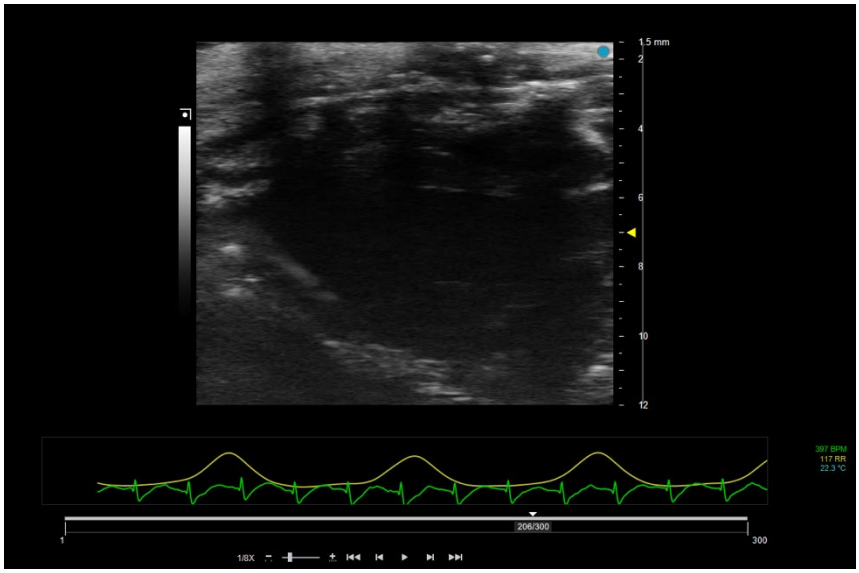

MI + Vehicle
[2 weeks]

Figure S3. [Echocardiography] Group 3: MI + Vehicle. These representative images were taken at 2 weeks following MI surgery. **[A]** Short axis view illustrates relatively reduced anterior wall thickness at both systole and diastole. Also, the accompanying ECG (lower trace) depicts ST-segment elevation. **[B]** Long axis view illustrates thinning/absence of the apical myocardium, implying no muscle movement. The images were taken prior to the P wave of ECG.

Figure S4.

A

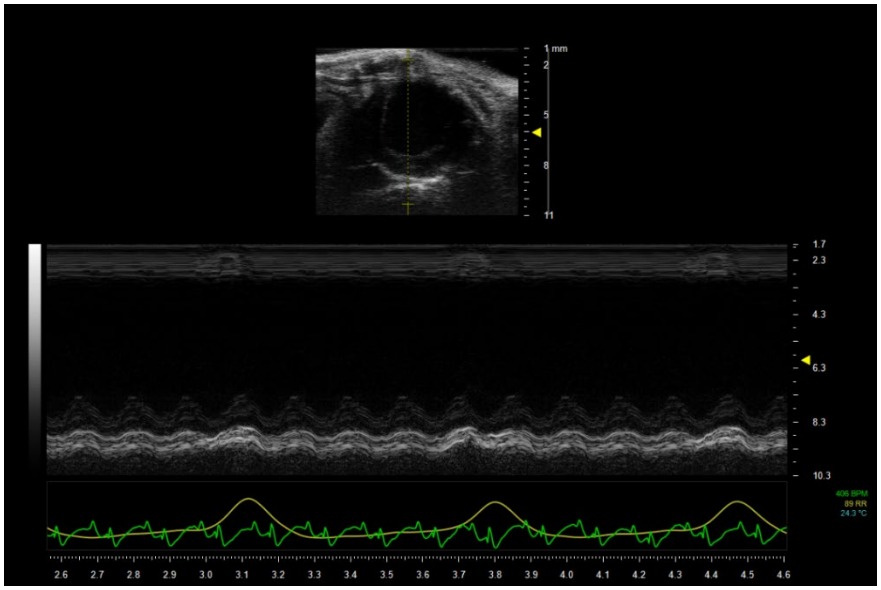

B

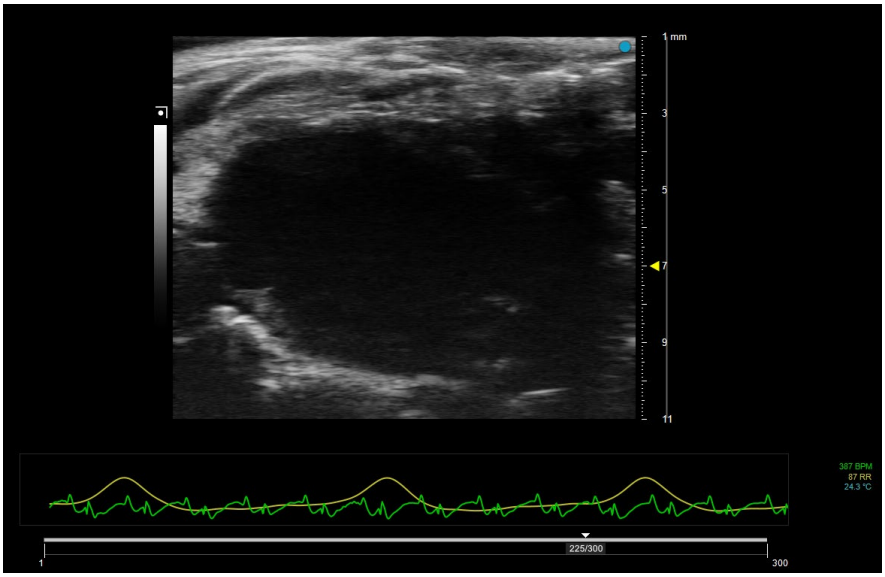

MI + SKA-31
[2 weeks]

Figure S4. [Echocardiography] Group 4: MI + SKA-31. Representative images were taken at 2 weeks following MI surgery. **[A]** Short axis view illustrates relatively reduced anterior wall thickness at both systole and diastole. Also, the accompanying ECG (lower trace) depicts abnormal QRS complex with ST-segment elevation. **[B]** Long axis view illustrates thinning/absence of the apical myocardium, implying no muscle movement. The images were taken prior to the P wave of ECG.

Figure S5.

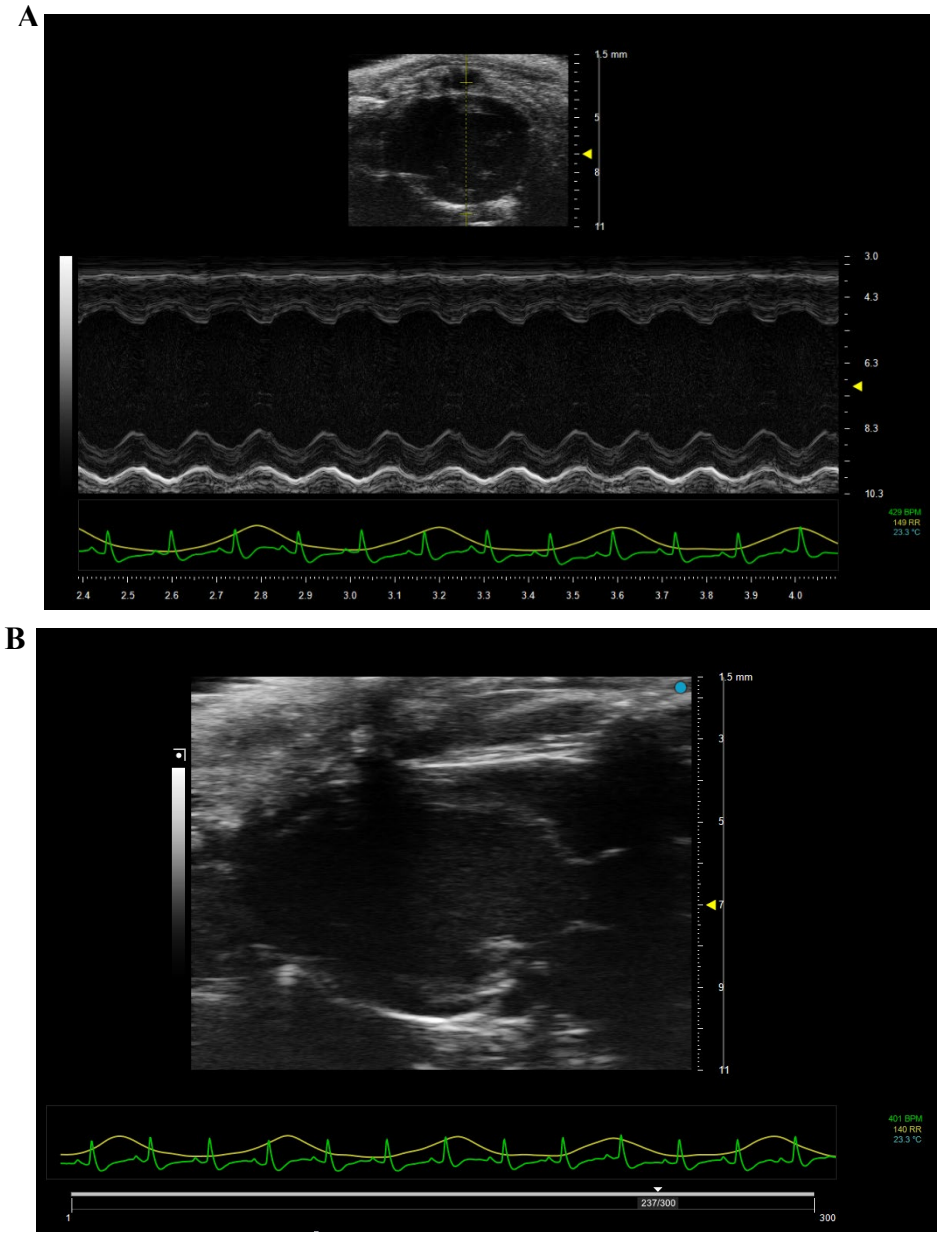

Sham + Vehicle
[4 weeks]

Figure S5. [Echocardiography] Group 1: Sham + Vehicle. These representative images were taken at 4 weeks following sham surgery. **[A]** Short axis view illustrates clean patterns of anterior and posterior side of left ventricular wall. Also, the accompanying ECG (lower trace) is normal with clear layout of the PQRST complex. **[B]** Long axis view illustrates relatively uniform layout of myocardium from base to apex. The images were taken prior to the P wave of ECG.

Figure S6.

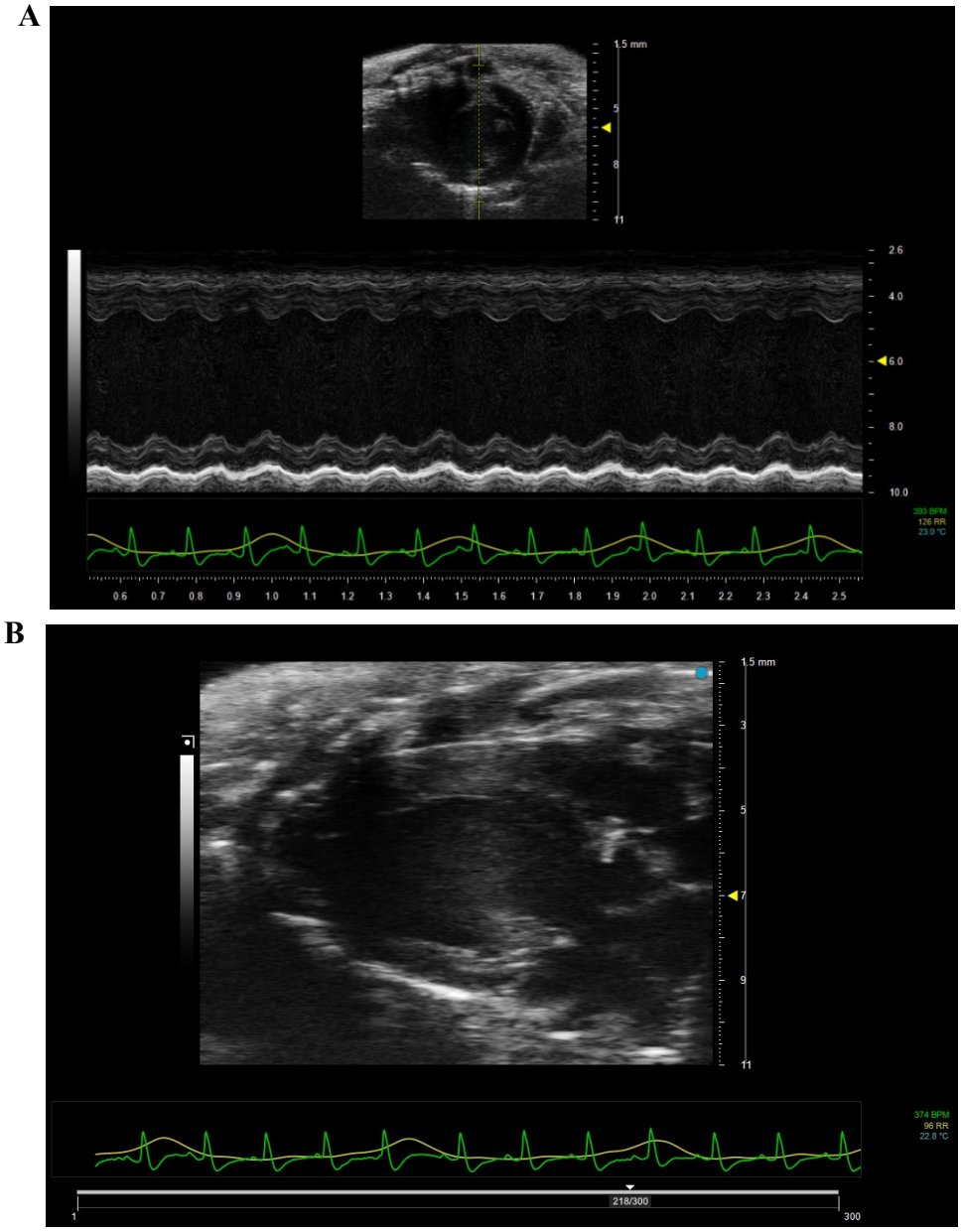

Sham + SKA-31
[4 weeks]

Figure S6 [Echocardiography] Group 2: Sham + SKA-31. Representative images were taken at 4 weeks following sham surgery. **[A]** Short axis view illustrates clean patterns of anterior and posterior side of left ventricular wall. Also, the accompanying ECG (lower trace) is normal with clear layout of the PQRST complex. **[B]** Long axis view illustrates relatively uniform layout of myocardium from base to apex. The images were taken prior to the P wave of ECG.

Figure S7.

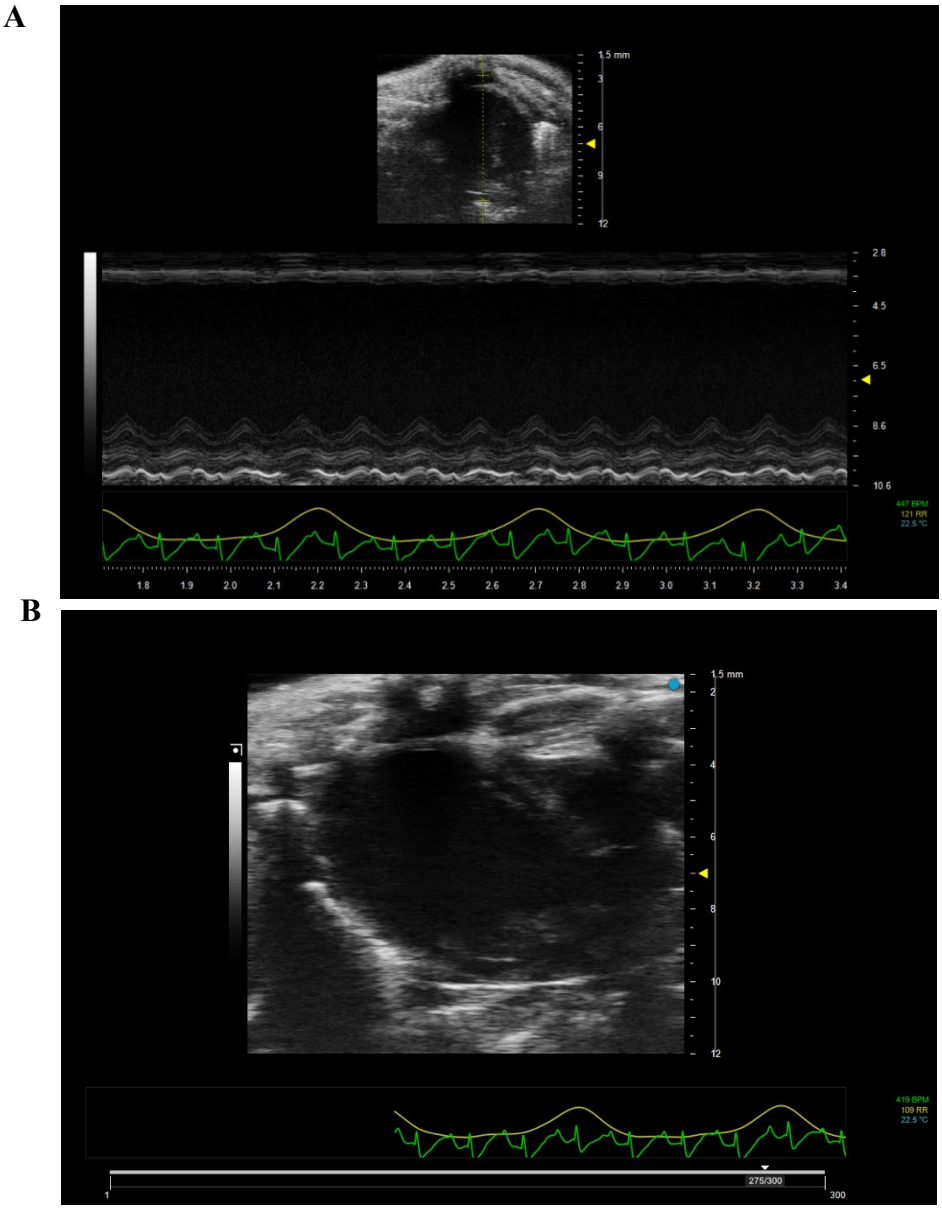

Figure S7. [Echocardiography] Group 3: MI + Vehicle. These representative images were taken at 4 weeks following MI surgery. **[A]** Short axis view illustrates relatively reduced anterior wall thickness at both systole and diastole. Also, the accompanying ECG (lower trace) depicts ST-segment elevation. **[B]** Long axis view illustrates thinning/absence of the apical myocardium, implying no muscle movement. The images were taken prior to the P wave of ECG.

Figure S8.

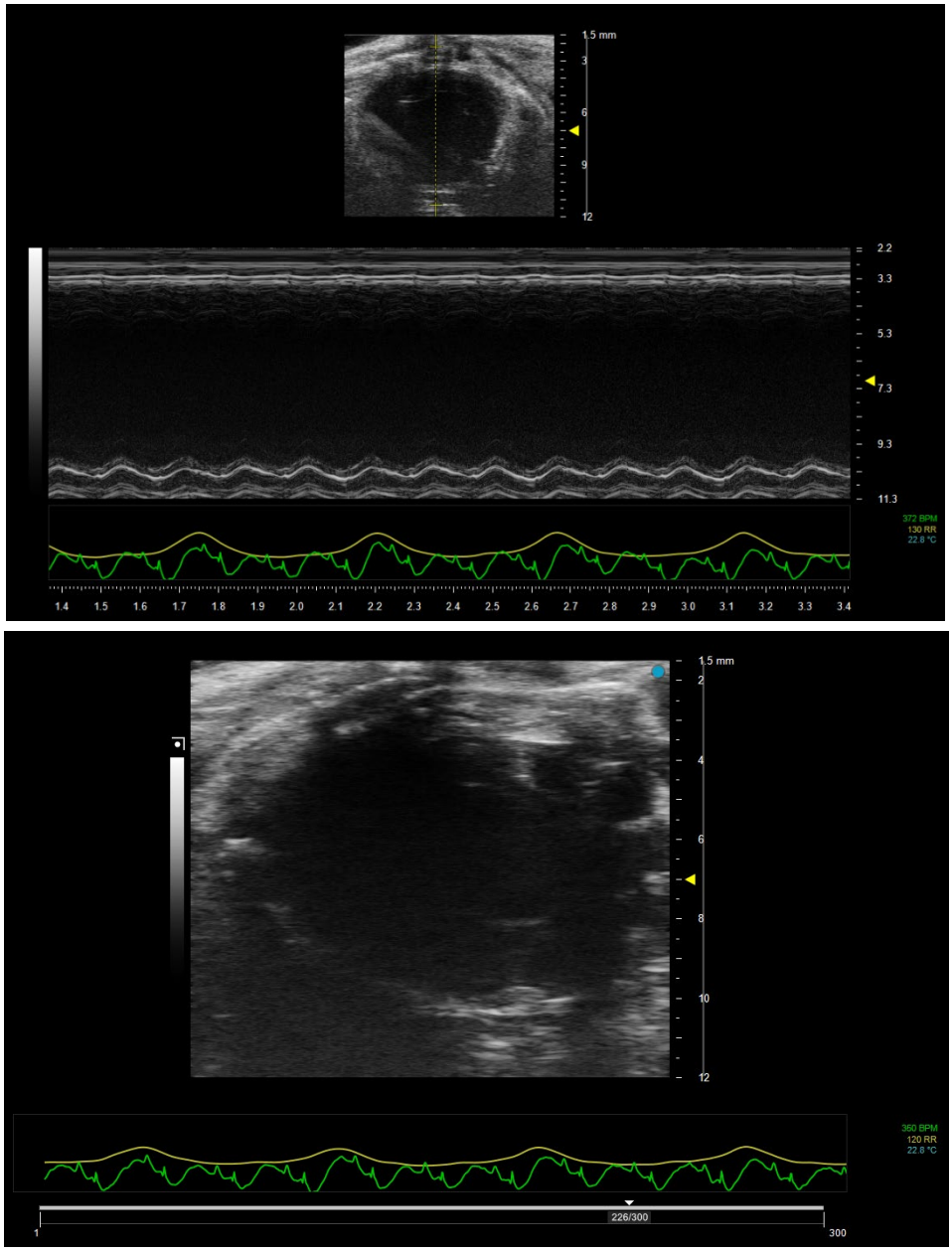

MI + SKA-31
[4 weeks]

Figure S8 [Echocardiography] Group 4: Sham + SKA-31. These representative images were taken at 4 weeks following sham surgery. **[A]** Short axis view illustrates clean patterns of anterior and posterior side of left ventricular wall. Also, the accompanying ECG (lower trace) is normal with clear layout of the PQRST complex. **[B]** Long axis view illustrates relatively uniform layout of myocardium from base to apex. The images were taken prior to the P wave of ECG.

Figure S9.

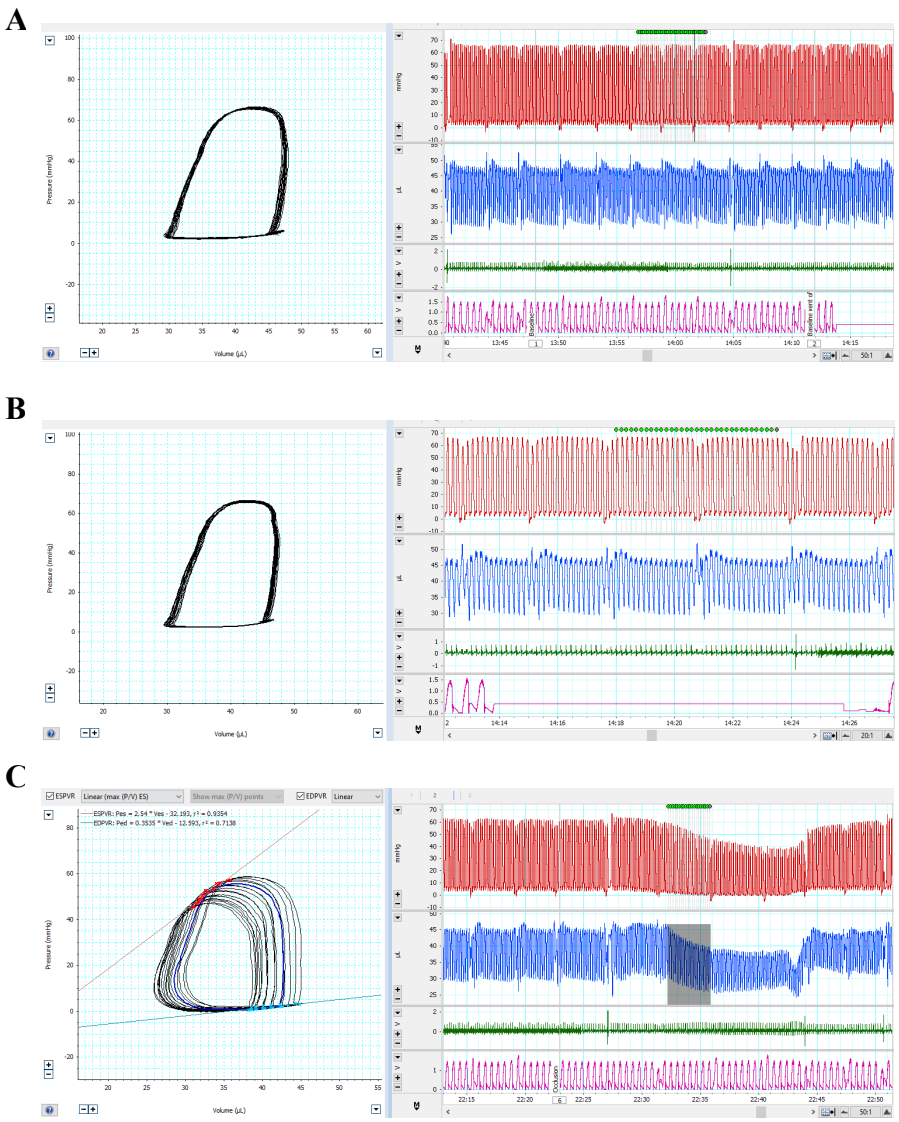

Figure S9. [P-V Loop Analysis] Group 1: Sham + Vehicle. Baseline measurements of cardiac performance obtained from P-V loop analysis. In these representative screen capture plots, the red trace in the top panel indicates left ventricular (LV) pressure, the blue trace below indicates LV volume, the green trace indicates ECG and the pink trace indicates ventilatory activity. **[A]** The baseline measurements of cardiac performance with the ventilator on. **[B]** The baseline measurements with ventilator off as indicated by the flat pink line. **[C]** Load-independent measurement of ESPVR and EDPVR following occlusion of the abdominal vena cava. The specific region of data where both pressure and volume drop imultaneously, as indicated by the shading in the panel, was selected for the measurement.

Figure S10.

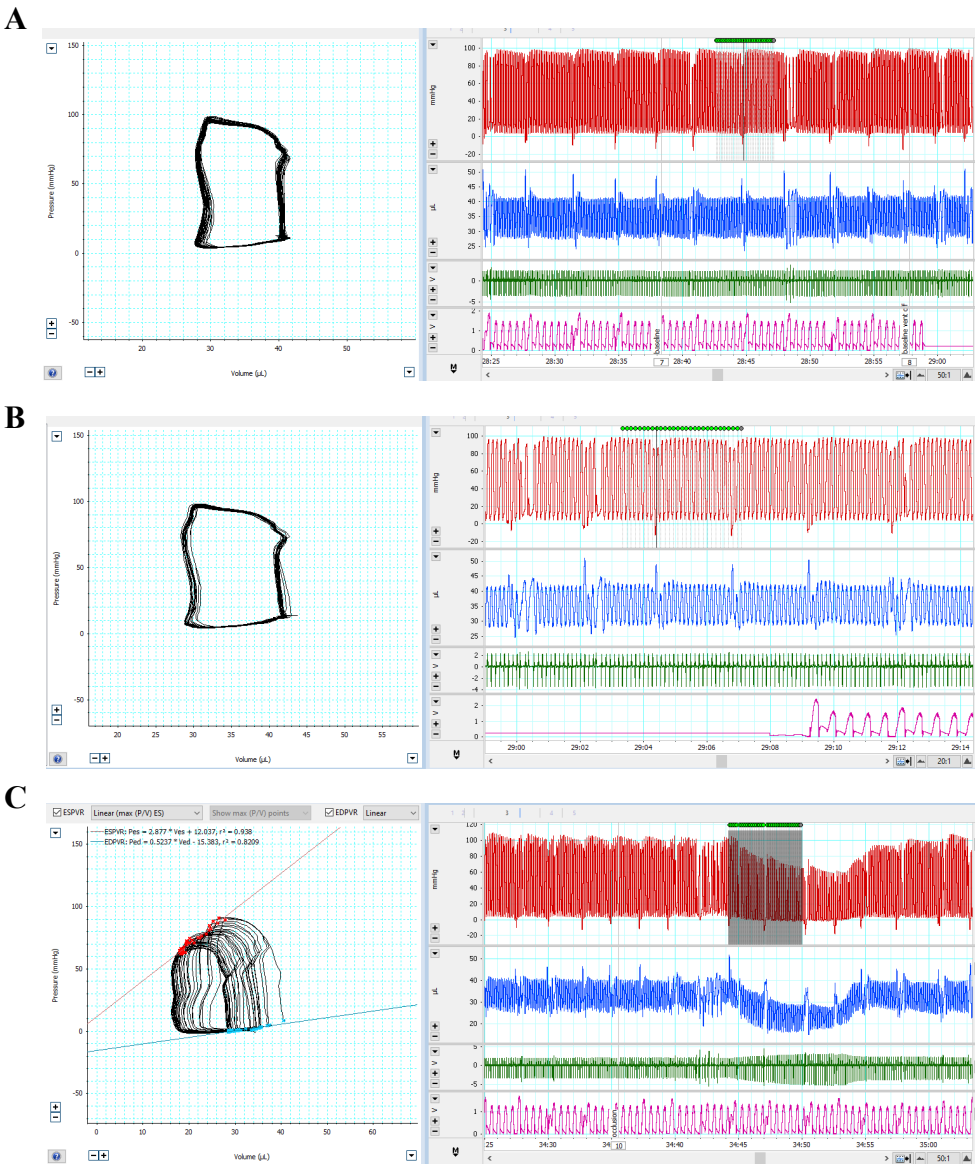

Sham + SKA-31
[6 weeks]

Figure S10. [P-V Loop Analysis] Group 2: Sham + SKA-31. Baseline measurements of cardiac performance obtained from P-V loop analysis. In these representative screen capture plots, the red trace in the top panel indicates left ventricular (LV) pressure, the blue trace below indicates LV volume, the green trace indicates ECG and the pink trace indicates ventilatory activity. **[A]** The baseline measurements of cardiac performance with the ventilator on. **[B]** The baseline measurements with ventilator off as indicated by the flat pink line. **[C]** Load-independent measurement of ESPVR and EDPVR following occlusion of the abdominal vena cava. The specific region of data where both pressure and volume drop imultaneously, as indicated by the shading in the panel, was selected for the measurement.

Figure S11.

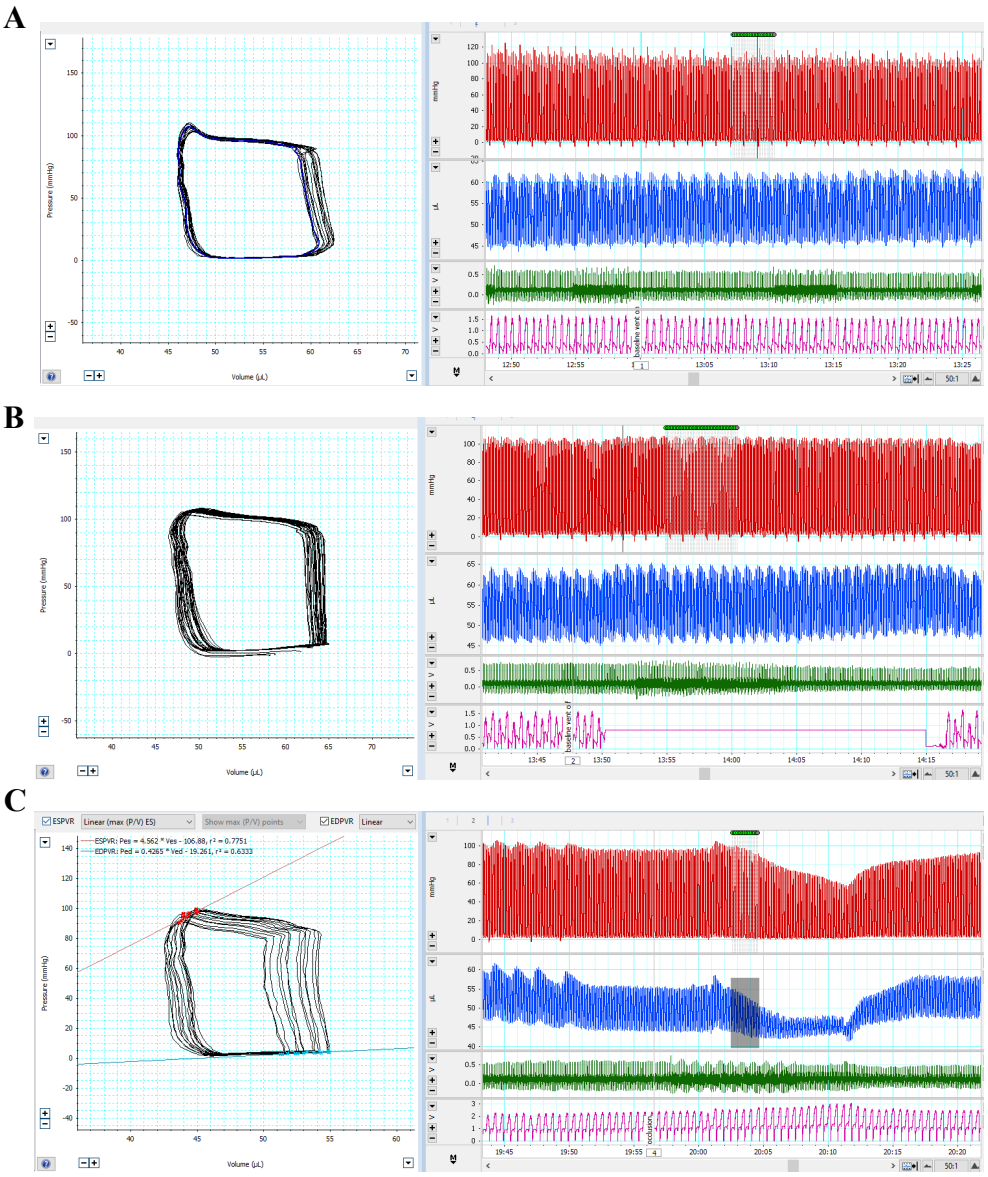

MI + Vehicle
[6 weeks]

Figure S11. [P-V Loop Analysis] Group 3: MI + Vehicle. Baseline measurements of cardiac performance obtained from P-V loop analysis. In these representative screen capture plots, the red trace in the top panel indicates left ventricular (LV) pressure, the blue trace below indicates LV volume, the green trace indicates ECG and the pink trace indicates ventilatory activity. **[A]** The baseline measurements of cardiac performance with the ventilator on. **[B]** The baseline measurements with ventilator off as indicated by the flat pink line. **[C]** Load-independent measurement of ESPVR and EDPVR following occlusion of the abdominal vena cava. The specific region of data where both pressure and volume drop imultaneously, as indicated by the shading in the panel, was selected for the measurement.

Figure S12.

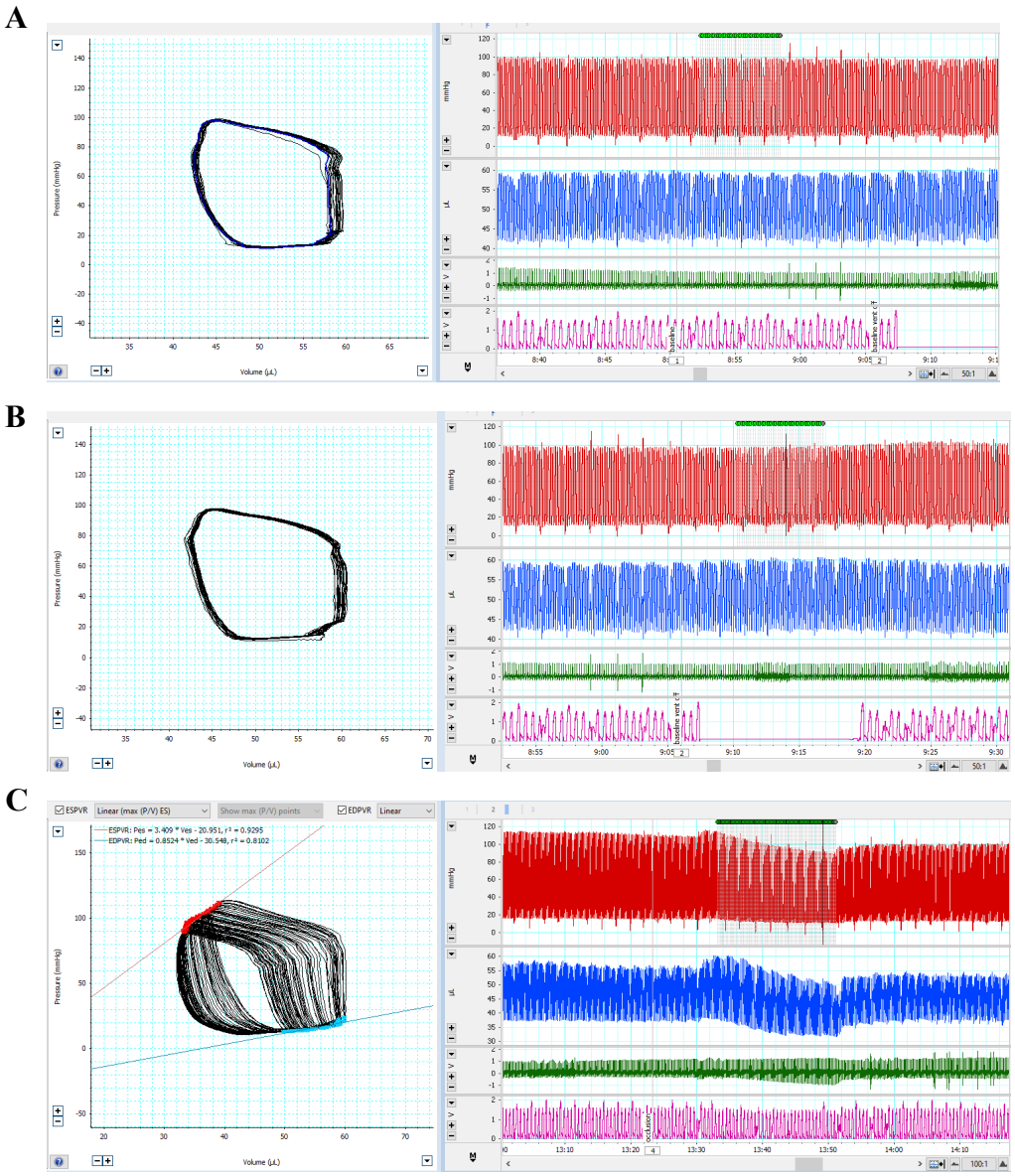

Figure S12. [P-V Loop Analysis] Group 4: MI + SKA-31. Baseline measurements of cardiac performance obtained from P-V loop analysis. In these representative screen capture plots, the red trace in the top panel indicates left ventricular (LV) pressure, the blue trace below indicates LV volume, the green trace indicates ECG and the pink trace indicates ventilatory activity. **[A]** The baseline measurements of cardiac performance with the ventilator on. **[B]** The baseline measurements with ventilator off as indicated by the flat pink line. **[C]** Load-independent measurement of ESPVR and EDPVR following occlusion of the abdominal vena cava. The specific region of data where both pressure and volume drop imultaneously, as indicated by the shading in the panel, was selected for the measurement.

Figure S13.

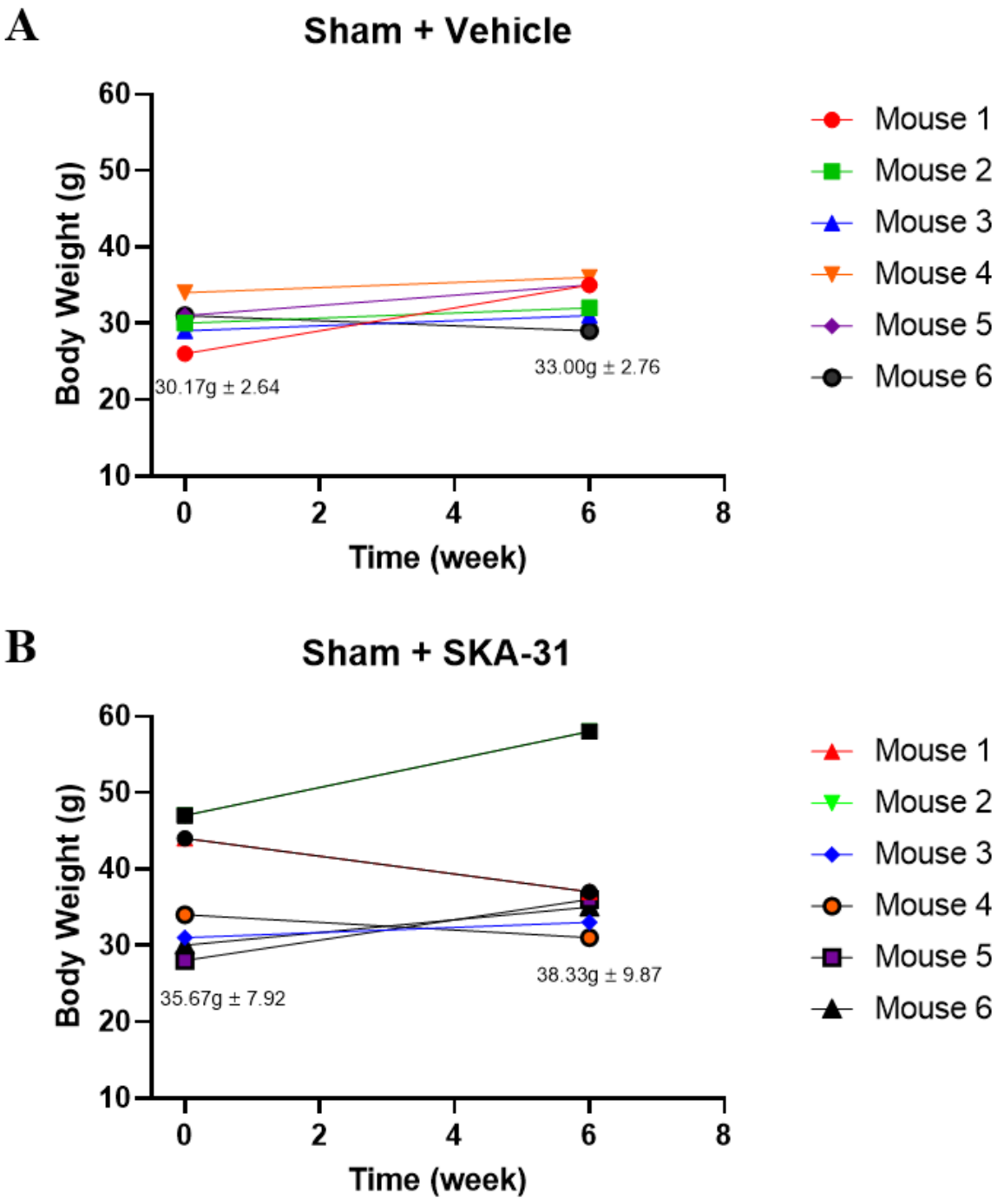

Figure S13. Weights of animals that received a sham surgery operation followed by either **[A]** vehicle or **[B]** SKA-31 treatment. Weight measurements were taken at 2 different time points: (1) prior to the surgery: week 0 (2) at the time of sacrifice (post to the P-V loop analysis): week 6. Data represented as mean ± SD, n = 6. No statistically significant difference in body weight changes in each group was detected. $p>0.05$.

Figure S14.

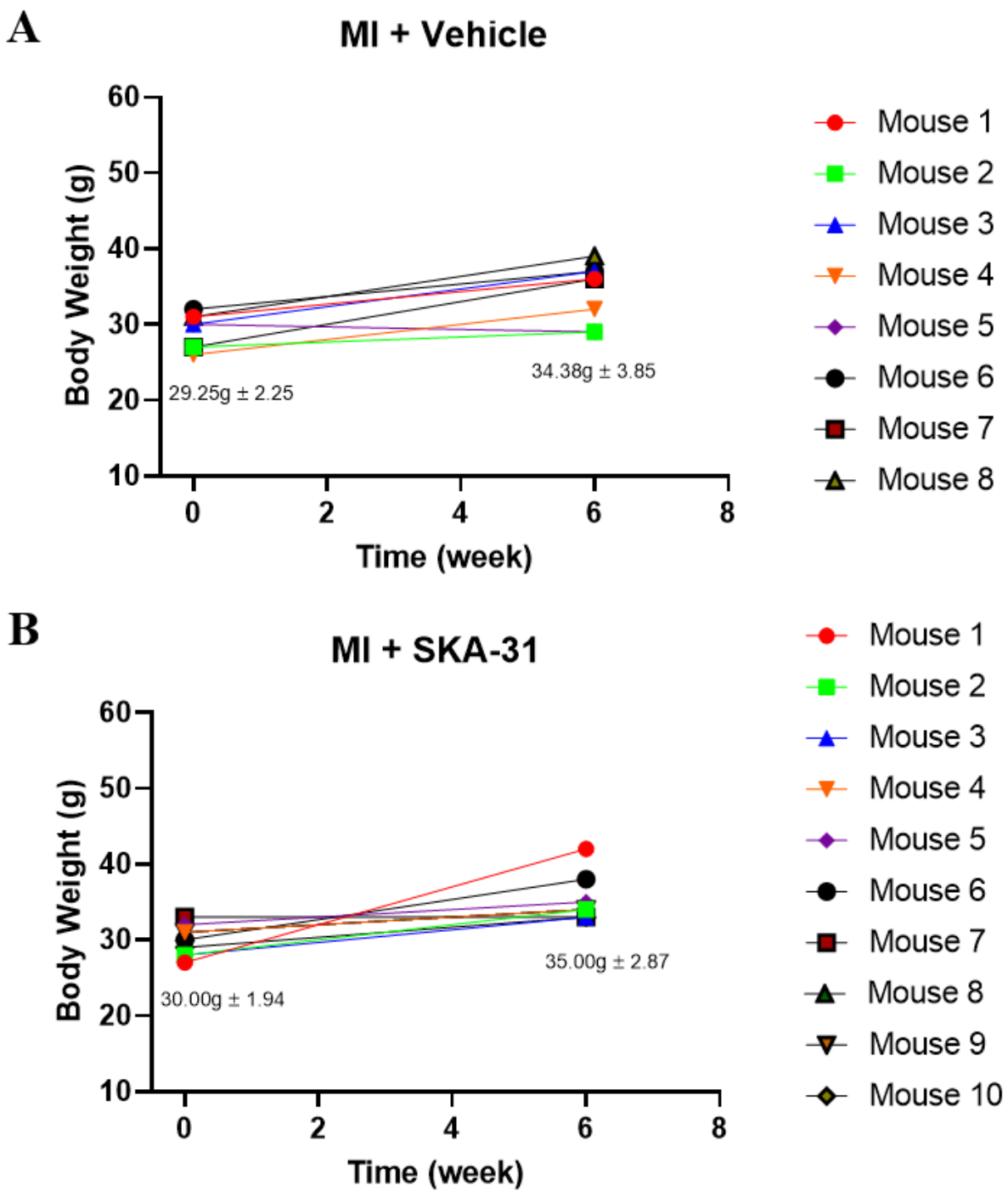

Figure S14. Weights of animals that received a MI surgery operation followed by either **[A]** vehicle or **[B]** SKA-31 treatment. Weight measurements were taken at 2 different time points: (1) prior to the surgery: week 0 (2) at the time of sacrifice (post to the P-V loop analysis): week 6. Data represented as mean ± SD, n = 6-10. No statistically significant difference in body weight changes in each group was detected. $p>0.05$.